University of Nebraska - Lincoln
DigitalCommons@University of Nebraska - Lincoln

Public Access Theses and Dissertations from the College of Education and Human Sciences

Education and Human Sciences, College of (CEHS)

Spring 2016

Hemodynamic Changes in Cortical Sensorimotor Systems Following Hand and Orofacial Motor Tasks and Pulsed Cutaneous Stimulation

Austin Oder Rosner
University of Nebraska-Lincoln, aoder@huskers.unl.edu

Follow this and additional works at: http://digitalcommons.unl.edu/cehsdiss

 Part of the Communication Sciences and Disorders Commons

Rosner, Austin Oder, "Hemodynamic Changes in Cortical Sensorimotor Systems Following Hand and Orofacial Motor Tasks and Pulsed Cutaneous Stimulation" (2016). *Public Access Theses and Dissertations from the College of Education and Human Sciences*. 256.
http://digitalcommons.unl.edu/cehsdiss/256

This Article is brought to you for free and open access by the Education and Human Sciences, College of (CEHS) at DigitalCommons@University of Nebraska - Lincoln. It has been accepted for inclusion in Public Access Theses and Dissertations from the College of Education and Human Sciences by an authorized administrator of DigitalCommons@University of Nebraska - Lincoln.

HEMODYNAMIC CHANGES IN CORTICAL SENSORIMOTOR SYSTEMS FOLLOWING HAND AND OROFACIAL MOTOR TASKS AND PULSED CUTANEOUS STIMULATION

by

Austin Oder Rosner

A DISSERTATION

Presented to the Faculty of

The Graduate College at the University of Nebraska

In Partial Fulfillment of Requirements

For the Degree of Doctor of Philosophy

Major: Interdepartmental Area of Human Sciences

(Communication Disorders)

Under the Supervision of Professor Steven M. Barlow

Lincoln, Nebraska

January, 2016

HEMODYNAMIC CHANGES IN CORTICAL SENSORIMOTOR SYSTEMS FOLLOWING HAND AND OROFACIAL MOTOR TASKS AND PULSED CUTANEOUS STIMULATION

Austin Oder Rosner, Ph.D.

University of Nebraska, 2016

Advisor: Steven M. Barlow

The integrity of the cerebral cortex can be assessed by measuring its responsiveness to repetitive sensory stimulation and voluntary motor activity. This neurophysiologic feature is called neural adaptation, and is thought to enhance learning and detection of environmental stimuli. The adaptation of hemodynamic responses to motor and sensory experiences in hand and face are of particular interest—as these are structures used in human communication—and proper delivery of oxy-hemoglobin to primary motor (M1) and somatosensory (S1) cortices is essential for functional cortical activation.

The objective of this study was to examine the hemodynamic differences between hand and face cortical representations during motor and passive somatosensory conditions, as measured with functional near-infrared spectroscopy (fNIRS).

The study design included 22 neurotypical adults, ages 19-30, and 11 neurotypical children, ages 6-13. Anatomical MRI localized each individual's M1 and S1. fNIRS determined relative levels of oxy- and deoxy-hemoglobin during the stimulus conditions. Motor tasks consisted of repetitive squeezing on a grip force strain gage, and repetition of bilabial compressions on a lip force strain gage. Somatosensory stimulation with a

Galileo™ tactile stimulus stimulator occurred through pneumatic TAC-Cells placed on the glabrous right hand and lower face near right oral angle.

Results from healthy participants (N=22 adults, mean age 23.16 ± 1.76; N=11 children, mean age 10.05 ± 2.76) revealed significant oxygenation differences across stimulus conditions in respective cortical regions. Overall, children exhibited greater mean cortical oxygen concentration levels and more variability than adults, with adults displaying more typical patterns of neural activation following each stimulus condition.

The precise delivery of natural, pneumatic stimulation as well as functionally relevant and measurable motor tasks, allowed for a novel examination of hemodynamic changes in somatosensory and motor cortices using fNIRS technology. These data present a picture of normal physiologic connectivity and function across a wide range of ages, which provides a broader view of how the healthy cerebral cortex operates in terms of neuronal responses to specific types of stimuli, neurovascular coupling, and cerebral oxygenation.

Acknowledgements

This study was funded, in part, by the Barkley Trust Foundation at the University of Nebraska-Lincoln. First, I would like to thank my advisor, Dr. Steven M. Barlow, for providing support, encouragement, mentorship, and friendship throughout my graduate school career. He has continually inspired me to work hard, be confident in my abilities, never shy away from a challenge, and when something fails: try and try again. His mentoring style has fostered immense personal and professional growth and independence, for which I will be forever grateful. I would also like to thank my dissertation committee members: Drs. Julie Honaker, Angela Dietsch, and Max Kurz for their insight and support throughout this project.

I would like to thank the MRI technologists at the Center for Brain, Biology and Behavior, Joanne Murray and Kerry Hartz, both of whom were instrumental in collecting the imaging data for this project. I would also like to thank those in the Communication Neuroscience Laboratories (CNL) who assisted with data collection and processing, especially Brianna Jallo and Grace Wilder. A special thanks to my primary research assistant and friend Chelsey Krug, who was my photo model, guinea pig, and go-to person throughout this entire study.

I would also like to thank the other CNL members, both at the University of Kansas and the University of Nebraska, for providing encouragement, laughter, and the occasional tough love needed to persevere in the pursuit of my PhD. Thank you to my dear friend Caitlin Imgrund, whose positivity and encouragement made the CNL at KU a more vibrant and cheerful environment in which to work. Thank you to Hyuntaek Oh for

his help with *all* things engineering, and for being a genuine and supportive friend. Finally, a very special thank you to my lab mate/roommate/friend Rebecca Custead. Thank you for always making me see the bright side of situations, for believing in me in when I struggled to believe in myself, and for being a constant friend and support system before, during, and after our move to Nebraska.

Lastly, I would like to thank my family for providing help in so many other ways. Thank you to my brother, Dillon, for always being proud of me, for making me laugh until I cry, and for showing me what it means to truly enjoy life. To my parents, thank you for believing in me, nurturing me, and above all loving me. You have always been actively engaged in my life (our daily phone calls are invaluable to me), you have encouraged me to never give up (even when I thought I wanted to), and you have never doubted my ability to achieve my life goals, all of which I am forever grateful. I am the person I am today because of you two, and I strive to make you proud in everything that I do. To my husband, Bryan, thank you for being my best friend and biggest supporter. I know it was not ideal to spend our first year and a half of marriage living apart, but you always supported my goals and remained a fundamental source of strength. Thank you for your patience, understanding, levity, and unwavering love and commitment. I am so grateful to have you as my partner in this journey of life.

Table of Contents

List of Figures

List of Tables

Abbreviation Key

α-MN..... Alpha motor neuron

γ-MN..... Gamma motor neuron

BOLD..... Blood-oxygen-level dependent

CBF..... Cerebral blood flow

$CMRO_2$ ..... Cerebral metabolic rate of oxygenation

CN..... Cranial nerve

CNS..... Central nervous system

CPG..... Central pattern generator

CT ..... Computed tomography

CW..... Continuous waveform

DTI..... Diffusion tensor imaging

EEG..... Electroencephalography

ECG..... Electrocardiogram

FA ..... Fast adapting

FF ..... Fast fatiguing motor units

FFT..... Fast Fourier Transform

fMRI..... Functional magnetic resonance imaging

fNIRS ..... Functional near-infrared spectroscopy

FR..... Fast fatigue-resistant motor units

HbO..... Oxygenated hemoglobin, or oxyhemoglobin

HbR..... Deoxygenated hemoglobin, or deoxyhemoglobin

HbT ..... Total hemoglobin

HRF ..... Hemodynamic response function

MNI ..... Montreal Neurological Institute

MRI ..... Magnetic resonance imaging

MRS ..... Magnetic resonance spectroscopy

M1 ..... Primary motor cortex

NIRS ..... Near-infrared spectroscopy

PCA ..... Principal components analysis

PET ..... Positron emission tomography

PNS ..... Peripheral nervous system

PPC ..... Posterior parietal cortex

rCBF ..... Regional cerebral blood flow

S ..... Slow motor units

SA ..... Slow adapting

SMA ..... Supplementary motor area

S1 ..... Primary somatosensory cortex

S2 ..... Secondary somatosensory cortex

TE ..... Echo time

TMS ..... Transcranial magnetic stimulation

TR ..... Repetition time

CHAPTER ONE: INTRODUCTION

Specific Aims

The proposed research examined the hemodynamic changes and adaptation patterns in different cortical locations during motor and somatosensory experiences in the face and hand in healthy adults and children. Motor tasks consisted of functionally relevant activities, while somatosensory stimulation consisted of biphasic pneumotactile pulses delivered via a Galileo™ somatosensory stimulator. Relative amounts of oxy- and deoxy-hemoglobin in cerebral cortex were measured using functional near-infrared spectroscopy (fNIRS).

Specific Aim #1:

To examine the hemodynamic differences between hand and face cortical representations during passive somatosensory conditions, as measured with fNIRS. Stimulation was delivered via a 3 cell tactile stimulator (Galileo™, Epic Medical Concepts & Innovations, Mission, Kansas) programmed to generate a biphasic pneumatic pulse train (-80 to 140 cmH_2O, 50-ms pulse width, 9 ms rise/fall time) applied through TAC-Cells (6 mm ID) placed on the glabrous right hand and lower face near right oral angle. Repeating pulse trains were delivered continuously at 2 Hz for 20 seconds followed by 20 second rest periods. It was hypothesized that this form of punctate tactile stimulation would produce patterns of hemodynamic adaptation in corresponding contralateral somatosensory cortex areas, and that the hemodynamic responses would differ across hand and face areas during stimulation due to differences in regional

arterial/venous anatomy, cortical vascular beds, extent and orientation of somatotopy, task dynamics, and mechanoreceptor typing in hand and face.

Specific Aim #2:

To examine the hemodynamic differences between hand and face cortical representations during motor tasks, as measured with fNIRS. The two motor conditions consisted of a repetitive hand grip on a grip force strain gage, and repetition of bilabial compressions on a lip compression force strain gage, each at 2 Hz, for 20 seconds followed by 20 second rest periods. It was hypothesized that hemodynamic responses would be significantly elevated and distributed over additional cortical areas during motor tasks, beyond that of the pure somatosensory conditions, due to the fact that both primary motor and somatosensory cortices are co-activated during motor activity. The force dynamics associated with a skilled motor task may elevate heart rate, therefore increasing overall blood flow. It was also hypothesized that the hemodynamic responses would differ across and hand and face areas during respective motor activities due to differences in regional arterial/venous anatomy, cortical vascular beds, extent and orientation of somatotopy, task dynamics, and mechanoreceptor typing in hand and face. Findings could provide further support for combining motor and sensory tasks in rehabilitation and prohabilitation therapies, as this could potentially drive more neural circuits with a greater intensity and increase oxygen levels in the cortex.

Specific Aim #3:

To examine developmental changes in patterns of cortical adaptation and hemodynamic responses to somatosensory stimulation and voluntary motor activity in pediatric (age 6-13 years) and adult participants (age 19-30 years), in an effort to provide a preliminary cross-sectional picture of normal physiologic connectivity and function in children and adults. It was hypothesized that age-related differences would be observed, and as children develop, cortical adaptation to the pulsed somatosensory stimulus occurs more rapidly, and hemodynamic responses become more adult-like. These data provide a broader look at how the healthy cerebral cortex functions in the presence of repetitive somatosensory and motor activity, which will inform future neurodiagnostic and neurotherapeutic applications in disordered populations.

Background, Significance, and Rationale

The human brain contains a vastly complex network of neural connections, which are necessary to perform life-sustaining functions such as managing complicated sensory input from the environment, controlling and fine tuning the movements of the body, and performing a wide variety of high-level cognitive processes. Individuals with aberrancies in connectivity (due to disease, disorder, trauma, etc.) can experience a loss in any or all of these domains, making communication and other daily activities particularly challenging. Because sensory and motor experiences are especially crucial for shaping and reorganizing these neural circuits (Buonomano & Merzenich, 1998; Hebb, 1947, 1949), non-invasive experience-dependent therapies have immense clinical potential in a variety of patient populations.

Fundamentals of Sensory and Motor Mechanisms

To fully appreciate the complexity of the mammalian nervous system, one must consider both peripheral and central components. Each division contains motor and sensory axons that relay information between the two. The following sections will provide an in depth description of the anatomy and physiology of sensory and motor systems among the peripheral nervous system (PNS) and central nervous system (CNS), and how these systems differ when examining different body parts (limbs versus head/neck). A solid understanding of how these mechanisms function in healthy individuals is necessary before one can investigate disordered populations.

Peripheral and Central Somatosensory Physiology

Human skin contains a number of specialized nerve endings responsible for relaying different types of cutaneous information to the brain: nociceptors for pain, thermoreceptors for temperature, and mechanoreceptors for mechanical strains or deformations of tissue (i.e., stretch, pressure, vibration, etc.). For the purposes of the current project, as well as future therapeutic strategies, mechanoreceptors and the processing of tactile information will be considered in further detail. The areas of the body with the greatest innervation density of mechanoreceptors, and therefore the areas with the most refined tactile acuity, include the hand and orofacial tissues, as these areas are most commonly used to manipulate objects and interact with the surrounding world.

Mechanoreceptors are subdivided based on two physiologic features: the rate of adaptation of their firing rate to novel, sustained stimuli (fast versus slow), and the size of

their receptive fields in the skin (small versus large). Each type of mechanoreceptor is individually tuned to specific qualities or characteristics of the tactile world (Abraira & Ginty, 2013). Fast adapting (FA) mechanoreceptors (sometimes also called rapidly adapting [RA] mechanoreceptors) respond best to rapidly changing stimuli or objects moving across the skin, while slowly adapting (SA) mechanoreceptors maintain their firing rate during sustained force or stretch. Type I mechanoreceptors have very small receptive fields (2-8 mm diameter), are typically very dense around the tips of the fingers (Johansson & Vallbo, 1983) and transitional zone of the lip (Barlow, 1987; Edin et al., 1992; Johansson et al., 1988a; Nordin & Hagbarth, 1989), and are especially sensitive to detecting fine form and texture of objects. Type II mechanoreceptors are fewer in number and have much larger receptive fields. The specifics in location and physiology of type II receptors vary across the body, as all mechanoreceptors are found in the hand, while not all are found in the face—FA type II mechanoreceptors are not present in orofacial regions (see below).

Each type of mechanoreceptor terminates in morphologically-specific nerve endings, and has a "best frequency" of stimulation to which each responds (Toma & Nakajima, 1995). Meissner corpuscles (FA I) have a best response frequency of 30-40 Hz. Pacinian corpuscles (FA II) have a best frequency at 250 Hz, and are not found in the face (Johansson et al., 1988a; Nordin & Hagbarth, 1989), making the orofacial region insensitive to high frequency vibratory stimulus and mechanical transients (Trulsson & Essick, 2004). Merkel cells (SA I) have a best frequency between 5 and 15 Hz. And Ruffini endings (SA II) have a best frequency of 0-10 Hz. Figure 1.1 shows the general shape of each mechanoreceptor type and their respective receptive fields on the hand,

innervation density (in cm^2), and their adaptation profile given a step increase in force (modified from Vallbo & Johansson, 1984; Trulsson & Essick, 2004). Innervation density varies across orofacial regions, as Meissner corpuscles dominate the tongue tip providing extremely high tactile acuity, and SA mechanoreceptors (Merkel cells and Ruffini endings) dominate facial skin, lip vermillion, and oral mucosa making these areas particularly well suited to encode the typically low frequency (<20 Hz) orofacial kinematics (Andreatta & Barlow, 2003; Trulsson & Essick, 1997; Trulsson & Johansson, 2002).

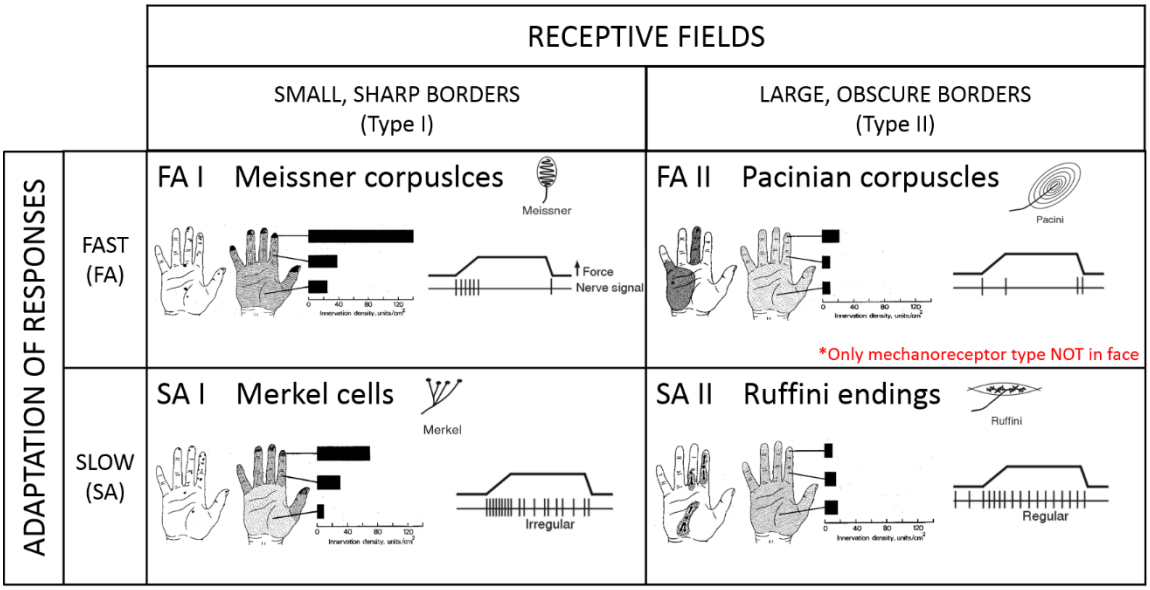

Figure 1.1. Classification of cutaneous mechanoreceptors based on receptive field properties and adaptation of responses. Also shown are examples of the shape of each mechanoreceptor, the location and innervation density within the hand, and characteristic spiking activity given a ramp and hold skin indentation force (modified from Vallbo & Johansson, 1984; Trulsson & Essick, 2004).

In order for these mechanoreceptors to relay touch information to the CNS, they must act as transducers and convert mechanical stimulus energy (force) into electrical energy/current flow in a process known as mechanotransduction. Upon mechanical stimulation, specific ion channels are opened allowing an influx and efflux of ions at the receptor membranes. This change in membrane voltage (known as receptor potential), causes the cell to depolarize and, given that the receptor potential is amplified enough, generates an action potential (French, 1992; Gardner & Martin, 2000). Action potentials are then carried from the receptors in the PNS to the CNS via different types of afferent axons. These sensory axons are characterized by their degree of myelination, which is a main determinant of conduction velocity. Table 1.1 provides a list of the types of afferent axons, the primary receptor organ from which they carry signals, the average diameter of the axons, and the conduction velocity (adapted from McGlone & Reilly, 2010). Aβ fibers carry afferent information from mechanoreceptors to the CNS. These pathways differ between the hand and face.

Hand

Somatosensory information from the hand travels along myelinated Aβ axons, passes through the dorsal root ganglion in the PNS (the cell body of the first order neuron is located here), and enters the CNS through the dorsal horn of the spinal cord. The axons ascend ipsilaterally through the dorsal columns of the spinal cord and synapse on second order neurons of the nucleus cuneatus (information from legs and trunk synapse on the nucleus gracilis) in the medulla. These second order neurons then decussate across midline in the medulla, ascend along the medial lemniscus, and synapse on third

order neurons in the ventral posterolateral nucleus of the thalamus. In the final leg of this pathway, third order neurons travel through the posterior limb of the internal capsule and synapse on neurons in the somatotopically organized somatosensory cortex in the contralateral hemisphere.

Table 1.1. List of sensory afferent fiber types, their size, conduction velocity, and the type of receptor end organ they innervate (adapted from McGlone & Reilly, 2010; Chudler, 2014).

Sensory afferent nerves			
Class	**Modality**	**Axon diameter (µm)**	**Conduction velocity (m/s)**
Myelinated			
Aα	Proprioceptors from muscles/tendons	13-20	80-120
Aβ	Low-threshold mechanoreceptors	6-12	35-75
Aδ	Cold thermoreceptors, nociceptors	1-5	5-35
Unmyelinated			
C	Heat thermoreceptors, nociceptors	0.2-1.5	0.5-2

Face

Tactile information from the orofacial region is relayed to the CNS in a homologous manner as the hand; however, because cranial nerves innervate the head and

neck (as opposed to spinal nerves throughout the rest of the body), this pathway does not involve ascension through the spinal cord. The cranial nerve that provides somatic sensation for the face is cranial nerve five (CN V), the trigeminal nerve. CN V contains three branches that innervate the face: the ophthalmic nerve (V1) carries somatosensory information from the scalp, forehead, eyelids, nose, nasal mucosa and frontal sinuses; the maxillary nerve (V2) carries somatosensory information from the lower eyelid and cheek, upper lip, and upper portions of the oral cavity; the mandibular nerve (V3) is a mixed nerve, in that it carries somatosensory information from the lower lip, chin, jaw, parts of the ear, and anterior 2/3 of the tongue, as well as motor signals to the muscles of mastication and a few muscles of the palate, inner ear and upper neck (Saper, 2000). Somatosensory signals travel from orofacial mechanoreceptors via Aβ axons in trigeminal sensory nerves, and converge on the trigeminal ganglion (the cell body of the first order neuron is located here; homologous to the dorsal root ganglion of spinal nerves) before entering the CNS at the level of the pons. Upon entry of the brainstem at the level of the pons, the axons synapse on second order neurons in the chief sensory trigeminal nucleus. Most second order afferents will decussate immediately in the pons and ascend through the ventral trigeminothalamic tract, synapsing on third order neurons in the ventral posteromedial nucleus of the thalamus. These third order neurons then travel through the posterior limb of the internal capsule and synapse on cells in the somatotopically organized somatosensory cortex in the contralateral hemisphere (Kaas et al., 1984; Lenz et al., 1988).

Cortical Somatosensory Networks

Neural representations of the body in the primary somatosensory cortex of humans were first mapped by Penfield and Rasmussen (1950). This map, called the sensory homunculus, reflects differences in innervation density across different areas of the body. For example, densely innervated areas of the body, like the fingertips/hands and orofacial regions, have high cortical magnification factors (the ratio of the representation area in somatosensory cortex to the area of innervated skin) while less densely innervated areas of the body, like the trunk and legs, have lower cortical magnification factors (Toda & Taoka, 2004). The somatosensory cortical network consists of three major divisions: primary somatosensory cortex (S1), secondary somatosensory cortex (S2), and the posterior parietal cortex (PPC).

S1 is comprised of four distinct cytoarchitectonic regions along the postcentral gyrus: Brodmann's areas 3a, 3b, 1, and 2. Each area contains a complete homuncular map (Kaas et al., 1979; 1981), however each represents different types of afferent inputs. Area 3a receives kinesthetic and proprioceptive information from muscles and joint receptors. Areas 3b and 1 receive cutaneous afferents from mechanoreceptors in the skin (SA receptor information mainly in 3b, FA receptor information mainly in 1). It is believed that area 2 receives pressure information from deep skin receptors, but also integrates proprioceptive, kinematic, and cutaneous information (Hsiao, 2008; Kandel, 2000).

S2, located in the parietal operculum (ceiling of the lateral sulcus), is generally thought to include parts of Brodmann's areas 40 and 43. Though not nearly as fine-grained as S1, a somatotopic body map also exists within S2 of monkeys (Burton et al., 1995; Krubitzer et al., 1995) and humans (Disbrow et al., 2000; Ruben et al., 2001).

Strong connectivity exists between S1 and S2, and much research has shown that tactile information is processed serially from S1 to S2 (Hu et al., 2013; Inui et al., 2004; Pons et al., 1992), as S2 is thought to perform higher-order functions related to touch processing, such as sensorimotor integration, integrating tactile information from both halves of the body, attention, memory, and learning (Chen et al., 2009; Dijkerman & de Haan, 2007; Garcia-Larrea et al., 1995). A study by Hu and colleagues (2012) used electroencephalography (EEG) to determine processing latencies in the somatosensory system. This study determined that electrical stimulation of the hand was processed from thalamus to contralateral S1, then from contralateral S1 to bilateral S2, and from contralateral S2 to ipsilateral S2. However, a few studies using focal, non-invasive tactile/vibratory stimuli (Bardouille & Ross, 2008; Popescu et al., 2013; Venkatesan et al., 2014) have been unable to evoke consistent activation of S2, suggesting that S2 may only be activated under certain somatosensory conditions.

PPC lies just posterior to the postcentral gyrus (S1), is comprised of Brodmann's areas 5 and 7, and has been found to play a role in proprioceptive and multimodal sensory integration (Arezzo et al., 1981; Gobbele et al., 2003; Hyvarinen, 1982; Mountacastle et al., 1975; Sack, 2009) as well as a wide range of motor and cognitive tasks (Constantinidis et al., 2013). Several studies have shown PPC to be activated in humans during passive tactile stimulation of the hand (Bardouille & Ross, 2008; Popescu et al., 2013), but not of the face (Venkatesan et al., 2014). Both S2 and PPC have dense connectivity with S1, however the information flow among cortices related to tactile processing is not well understood. Undoubtedly, S2 and PPC have much more complex physiological properties than S1, and it is possible that many of their roles overlap.

Peripheral and Central Motor Physiology

Peripheral nerves not only carry afferent signals from the PNS to the CNS, as previously discussed, but they can also carry efferent signals from the CNS to the PNS to initiate muscle contraction and produce movements. All spinal nerves are mixed, in that they carry both motor and sensory signals to and from the body below the head and neck, whereas cranial nerves innervating the head and neck can be purely sensory in nature, purely motoric in nature, or both. Regardless of the level upon exiting the CNS, alpha motor neurons in the periphery share the same basic structure and function. Lower motor neurons required for voluntary movement—located in either the ventral horn of the spinal cord (and exit via spinal nerves) or the basal plate of the brainstem (and exit via cranial nerves)—are classified by the muscle fiber type they innervate: *alpha motor neurons* (α-MNs) innervate extrafusal muscle fibers (make up striated skeletal muscle), and *gamma motor neurons* (γ-MNs) innervate intrafusal muscle fibers (make up muscle spindles, which lie in the belly of skeletal muscles and provide proprioceptive information about the change of muscle length).

Interestingly, during mammalian development a motor neuron synapses with many muscle fibers, and each muscle fiber receives many different axon terminals; however with maturation, eventually each muscle fiber forms a synapse with a terminal from a single parent α-MN (Rothwell, 1994). This entire structure—the α-MN axon, synaptic terminal branches, and the set of muscle fibers they innervate—is called a motor unit (Liddell & Sherrington, 1925). The number of muscle fibers innervated by a single α-MN varies across different types of muscles. For example, small extraocular muscles

may have an innervation ratio of 5 muscle fibers to1 α-MN, whereas large postural muscles may have an innervation ration of 2000:1 (Rothwell, 1994). Motor units are classified physiologically by the contractile speed of their muscle fibers following a single stimulus to the motor neuron axon, also known as the twitch test. Slow units (S; sometimes referred to as Type 1 units) are generally associated with smaller α-MNs, have a slower conduction velocity, are extremely resistant to fatigue, and relax at a slower rate than their faster counterparts. Fast units are further subdivided into two types: fast fatigue-resistant (FR) and fast fatiguing (FF; sometimes referred to as Type 2a and 2b, respectively). Both types of fast motor units have large α-MNs, fast conduction velocities, relatively short contraction times, but differ on how sensitive they are to fatigue (Burke et al., 1971; 1973).

Rothwell (1994) states that "the advantage of having the subgroups is that the total range of operation of the muscle is extended beyond that of any single unit type. The relative number of each unit can give distinctive properties to whole muscles which makes them suitable for different kinds of movements" (p. 41). Muscle fiber types do display a certain degree of plasticity, as trained athletes show a distribution of muscle fiber types appropriate for their sport. For example, marathon runners have a greater number of fatigue resistant (S and FR) fiber types, while sprinters have more fast fiber types (FF and FR). Certain muscle groups also contain a predominant type of motor unit that are more specific to their function. In particular, body parts designed for quick, precise movements, like the eyes, are dominated by fast motor units, whereas postural muscles in the back are dominated by slow motor units (Purves et al., 2001). Several orofacial muscles have been shown to contain a high proportion of fast fiber types, while

the masseter (a large jaw closing muscle) contains a majority of slow fibers (Stål, 1994). While these examples of clear distinctions in motor unit distribution do exist in humans, most muscles in the body extend along a continuum of slow to fast motor unit types (Burke & Tsairis, 1974; Garnett et al., 1979; McDonagh et al., 1980; Romaiguère et al., 1989; Van Cutsem et al., 1997). Motor units in the hand have not been found to cluster into the classical physiologic types (Bigland-Ritchie et al., 1998; Duchateau & Enoka, 2011).

While large α-MNs and their motor units (often clinically just called "lower motor neurons") represent the output through which all motor behavior (reflexive or voluntary) must be expressed (Rothwell, 1994), smaller γ-MNs are involved in the stretch reflex, the contraction of muscle elicited by a stretch, as well as in stiffness regulation. As previously mentioned, γ-MNs innervate the intrafusal muscle fibers that comprise muscle spindles, the sensory receptors that provide the CNS with information about changes in muscle length. γ-MNs do not directly make adjustments to muscle (which is the role of α-MNs), but rather cause strong contractions of the intrafusal fibers. In this way, the contraction of intrafusal fibers significantly influences sensory afferents that ultimately provide α-MNs with the information they need to make changes in skeletal muscle contractions (see Figure 1.2).

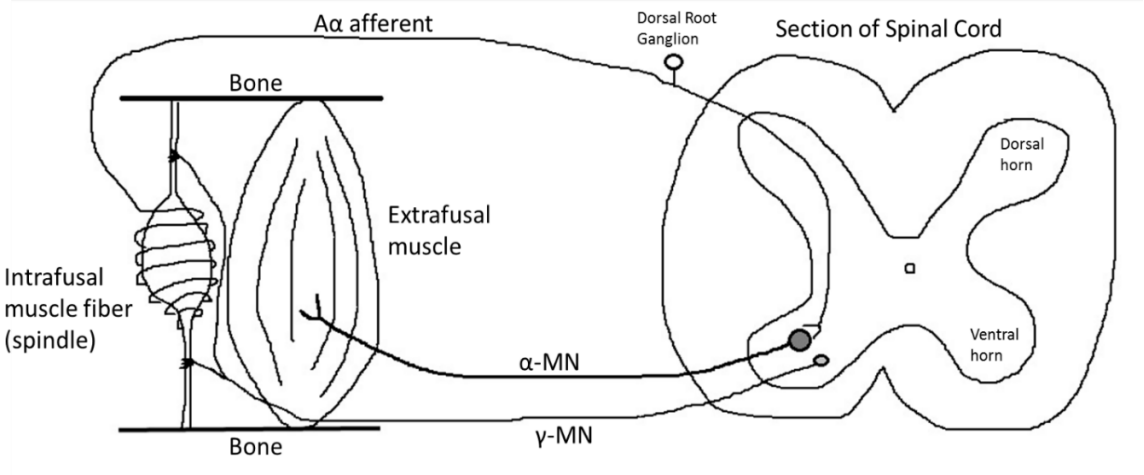

Figure 1.2. Synaptic effects of muscle spindle afferents on motor neurons (adapted from Rothwell, 1994).

As a general rule, smaller muscles tend to have a greater density of muscle spindles than larger muscles, suggesting that more spindle afferents are functionally necessary for smaller muscles involved in fine motor control or manipulation of objects (Barker, 1974; Brooks, 1986; Matthews, 1972; Peck et al., 1984; Richmond & Abrahams, 1975). In fact, muscles with the greatest density of spindles include the extraocular, hand, and neck muscles (Gordon & Ghez, 1991). Vallbo & Wessberg (1998) determined that human hand movements requiring higher precision resulted in stronger γ-MN activity, indicating that as α-MN activity in the parent muscle increased so did intrafusal γ-MN activity (referred to as "α-γ coactivation"). Interestingly, the face is one of the most sensitive areas of the body yet facial muscles contain no muscle spindles (Lovell et al., 1977; Voss, 1956). Perhaps the high density of mechanoreceptors (particularly pseudo-Ruffini endings) in the orofacial region provides the required sensory feedback to fine tune motor movements of facial structures in place of muscle spindles (Barlow,

1987; Barlow, 1998). It is also important to note that muscle spindles are disproportionately greater in number among antigravity muscles (biceps > triceps, quadriceps > hamstrings), as they play a key role in maintaining the body in an upright position and opposing external loads placed upon the body by gravitational pull (Eyzaguirre & Fidone, 1975).

Hand

The muscular anatomy of the hand, wrist, and forearm consists of approximately 30 dedicated muscles (Flanagan & Johansson, 2002) and is innervated by branches from 3 major nerves: the radial, median, and ulnar nerves. These nerves (among others) run in a network of nerve fibers running from the spinal cord called the brachial plexus, which carries fibers from the ventral roots of spinal nerves C5-T1 (Schuenke et al., 2010). During voluntary movement, motor signals are sent from neurons in the cortex to make powerful and direct connections with α-MNs in the ventral horn of the spinal cord at the level of these spinal segments. This major motor pathway is aptly named the corticospinal tract, and will be discussed in more detail in the section on motor cortical networks.

Face

The human face is made up of many muscles, some predominantly for facial expression, and others for speech and deglutition (e.g., chewing, sucking, etc.). The majority of facial muscles are innervated by the motor branches of cranial nerve seven (CN VII), the facial nerve, while the muscles of mastication are innervated by the

maxillary branch of the trigeminal nerve (CN V), and tongue muscles are innervated by cranial nerve twelve (CN XII), the hypoglossal nerve. During voluntary movement, such as those related to facial expression and speech gestures, signals from motor cortex are sent to α-MNs of motor nuclei at different levels in the brainstem (CN V in mid pons, VII at the pontomedullary junction, and XII at the pyramids of the medulla) (Ghez & Krakauer, 2000; Saper, 2000). This major motor pathway is called the corticobulbar tract, and will be discussed in further detail in the following section. It is important to note that rhythmic orofacial activities such as sucking and chewing are under the control of brainstem internuncial circuits known as central pattern generators (CPGs) (Barlow & Estep, 2006; Barlow, Lund, Estep, Kolta, 2010).

Cortical Motor Networks

Similar to the somatosensory cortex, primary motor cortex is also somatotopically mapped onto a motor homunculus, in that body parts requiring a high degree of motor control (namely, muscles of the hand and face) also have a high cortical magnification factor (Penfield & Rasmussen, 1950). Unlike the somatosensory cortical network though, the processing sequence in the motor system is essentially opposite, in that motor planning and programming presumably takes place in motor association areas before projecting to primary motor cortex and ultimately to descending pathways (particularly, corticospinal and corticobulbar) that project to the muscles required to execute the motor task. The motor system consists of many components, and their coordinated activity is necessary to produce controlled voluntary movements. Within the cerebral cortex several subdivisions of motor areas exist: the primary motor cortex (Brodmann's area 4),

premotor cortex (Brodmann's areas 6 and 8), and the supplementary motor area (SMA; medial surface of Brodmann's area 6). Before sending signals via motor neurons to execute muscle activity, these cortical motor areas receive input from other cortical and subcortical sources, namely motor nuclei in thalamus (relay information from cerebellum and basal ganglia, which is discussed in the following paragraph), S1 and PPC (provide information about ongoing motor movements), and prefrontal cortex (involved in motor planning) (Saper et al., 2000).

Other structures involved in coordinating and refining motor activity include the basal ganglia and the cerebellum. The basal ganglia are believed to work as a gating mechanism for the motor system, as they have been shown to inhibit competing motor mechanisms, and removal of this inhibition allows a motor system to proceed with its desired activity (Mink, 1996). By opening and closing the "gate", the basal ganglia pathways may be involved in modulating parameters of movement (Contreras-Vidal & Stelmach, 1996; Chakravarthy et al., 2010). The cerebellum receives sensory signals from a variety of peripheral receptors (somatosensory, visual, auditory, vestibular) as well as the cerebral cortex via brainstem relay neurons, and integrates the information to coordinate muscle activity, producing smoother voluntary movements (Fetz, 2006). Figure 1.3 provides a schematic model of all the major motor centers and their connections to one another. It is clear that these areas are heavily interconnected, and function as a series of circuits rather than in isolation to produce well-coordinated and efficient motor movements.

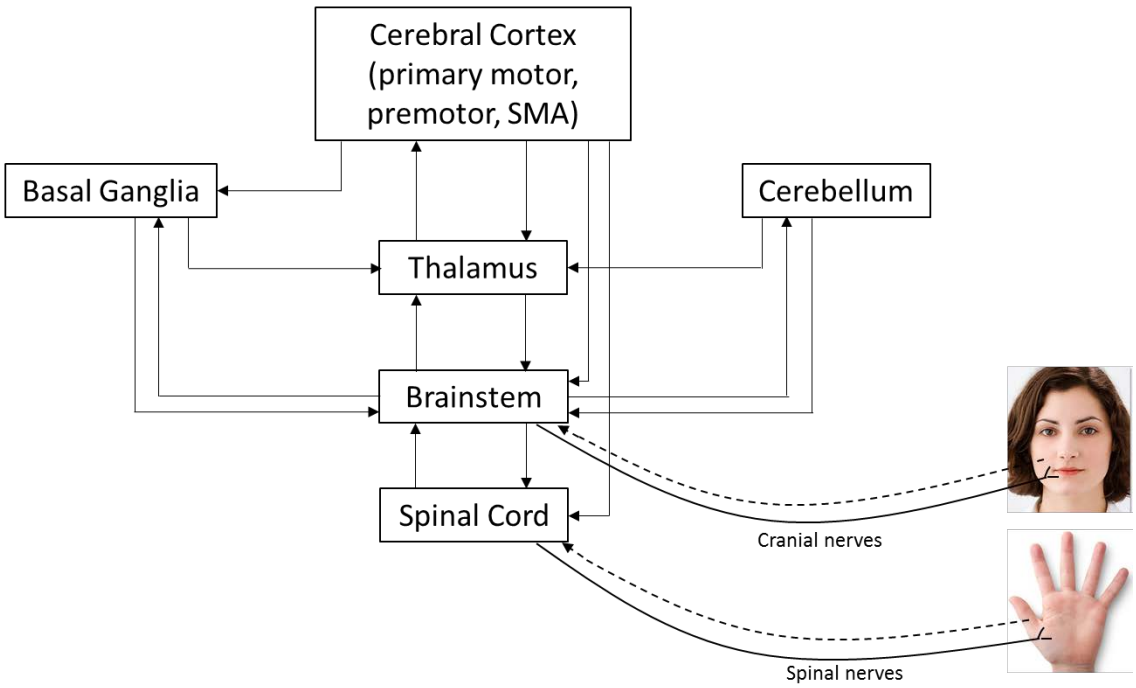

Figure 1.3. Connectivity of major motor centers in the CNS, and their connection with human hand and face (modified from Fetz, 2006).

Once a motor command is planned and programmed, it is sent to motor neuron pools within brainstem or spinal cord nuclei via corticobulbar or corticospinal fibers, respectively. These are the primary pathways underlying voluntary movement. Both types of descending fibers (often clinically referred to as “upper motor neurons”) typically originate in primary motor cortex (though some do originate in premotor areas) and send projections together through the internal capsule. Beyond this point they begin to differentiate. Most corticobulbar fibers have bilateral innervation of motor neurons in the brainstem, meaning they receive an approximately equal amount of projections from both contralateral and ipsilateral hemispheres (albeit, slightly greater connectivity is seen contralaterally). The only exceptions to this rule are the facial nerve (CN VII) nuclei that

innervate muscles of the lower 2/3 of the face and the hypoglossal nerve (CN XII), which receive primarily contralateral corticobulbar projections (Ghez & Krakauer, 2000). Corticospinal fibers continue to descend through the midbrain, decussate at the pyramids of the medulla, and finally descend contralaterally to the appropriate motor nuclei within the spinal cord. Approximately 90% of corticospinal fibers cross at the pyramidal decussation, making motor activity below the head and neck under the control of the contralateral motor cortex (Young, Young, & Tolbert, 2008). The remaining 10% of corticospinal fibers decussate at the segmental level to the ventral horn.

Changes in Sensory and Motor Systems during Development

Though much of the development of central and peripheral components of motor and somatosensory systems occurs *in utero*, human infants are not born with adult-like structure and functioning of these systems. In fact, these pathways are physically shaped, modified, and refined by network dynamics as a result of sensory experiences and activity-dependent mechanisms throughout life (Catalano & Shatz, 1998; Katz & Shatz, 1996; Penn & Shatz, 1999). More specifically, the period directly after birth and throughout early childhood (and even adolescence) is especially important in terms of sensory and motor experiences, as Toga and colleagues (2006) suggest that "much of the potential and many of the vulnerabilities of the brain might, in part, depend on the first two decades of life" (p. 148).

Because clinical examinations of sensory and motor systems can be difficult with children, nerve conduction studies can be particularly informative about the maturation of the nervous system (Thomas & Lambert, 1960). The speed with which motor and

sensory signals are transmitted between the PNS and CNS relies heavily on the degree of axonal myelination. During the first 2-3 years of life, myelination proceeds rapidly, first in the PNS, then in the spinal cord, and finally in the brain (Holland et al., 1986). As myelination progresses in the brain, conduction speeds increase approximately 100 fold (Toga et al., 2006). Generally, phylogenetically older cortical areas—those responsible for more "primitive" or basic functions, such as processing sensory and motor activity—are myelinated earlier in development than those responsible for more higher order cognitive functions (Toga et al., 2006; Yakovlev & Lecours, 1967). Interestingly, though white matter volumes increase over the first 2 decades of life, gray matter volumes (neuronal cell bodies) start to decrease beginning at 4-8 years of age in parietal and primary sensorimotor regions (Gogtay et al., 2004; Jernigan & Tallal, 1990), showing more adult-like gray matter structure. This loss in gray matter has been suggested to be due to synaptic pruning during adolescence (Bourgeois et al., 1994; Huttenlocher, 1994; Rakic, 1996), as well as the fact that the advancement of white matter may overtake the overall rate of brain expansion, causing a progressive reduction of gray matter appearing on magnetic resonance imaging (MRI) (Jernigan & Tallal, 1990; Paus, 2005). Therefore, age-related changes during the first 10 years of life may be more closely related to the development of synaptic efficacy (synaptogenesis), rather than progression of myelination (Nezu et al., 1997).

Peripheral and central components of somatosensory and motor pathways have been assessed in past studies via electrical stimulation (with needle and/or surface electrodes) and transcranial magnetic stimulation (TMS). A cross-sectional study by Eyre and colleagues (1991) examined peripheral and central conduction times in both

somatosensory and motor pathways across a wide range of ages (32 weeks gestation to 55 years) using these stimulation techniques. These researchers found that during the first 2 years of life, central conduction times in both somatosensory and motor pathways decreased rapidly (most likely due to the rapid myelination occurring in the brain), then remained constant at adult-like values. Peripheral conduction times also decreased early in life for both pathways, then gradually increased with age starting at 5 years due to increasing limb length (this study investigated pathways in the arm). Another study by Barlow and colleagues (1993) used punctate mechanical inputs to the perioral region to map the speed of facial reflexes across a wide range of ages, from infancy to adulthood. Similar to findings in the limb, conduction velocity in sensory and motor pathways of the lower face increases with maturation, particularly over the first year of life, and remain in a transitory state until approximately 11 or 12 years of age when the craniofacial structures attain 90% of adult scale. Other studies have shown that central motor conduction times decrease in a semi-linear fashion from 2 years until age 13, when the corticospinal pathway is "electrophysiologically complete" (Nezu et al., 1997). One major limitation of these types of studies is the stimulation methods used (excluding Barlow et al., (1993) who used mechanical tactile stimuli). Though electrical stimulation and TMS are valuable and objective methods of studying peripheral and central responses, these modalities are not natural (and can be invasive), and do not necessarily mimic functional behavior. The rationale for the motor activities and somatosensory stimulation methods used in the current study will be discussed in further detail in another section.

Adaptation & Neural Plasticity

One way to get a glimpse of "the brain at work" is by examining the neuronal and vascular responses to external stimuli (Villringer & Dirnagl, 1995). To this end, we can assess and characterize the integrity of sensory and motor cortices by measuring their hemodynamic responsiveness to repetitive stimulation. The physiologic phenomenon known as adaptation is the process in which neuronal responses decrease when a repeated/prolonged stimulus is presented. Therefore, each response of an activated neuron depends on its previous history of activity, and thus neural responses reflect the current state of synaptic activity within the context of the previous synaptic activity (Abbott et al., 1997). Neuronal responses can also reflect the current cellular state of the cell membrane within the context of previous action potential firing or electrotonic spread of voltage gradients. This dynamic process occurs ubiquitously across all sensory modalities in their respective areas of the brain, including auditory cortex (Shu et al., 1993; Ulanovsky et al., 2004), somatosensory cortex (Ahissar et al., 2000; Hellweg et al., 1977; Popescu et al., 2013; Venkatesan et al., 2010, 2014), visual cortex (Carandini & Ferster, 1997; Gutnisky & Dragoi, 2008; Muller et al., 1999; Ohzawa et al., 1982), and olfactory cortical areas (Wilson, 1998). Adaptation (also sometimes referred to in the literature as synaptic depression, or short-term depression) occurs in sensory systems as a means of maximizing and making more efficient and accurate the neural coding of behaviorally relevant afferent information (Abbott et al., 1997; Cortes et al., 2012; Kohn, 2007; Schwartz et al., 2007; Webber & Stanley, 2006). It also adjusts the dynamic range of the sensory system in order to enhance its ability to gather information about the sensory environment (Keidel et al., 1961). While adaptation effects can occur early in

sensory processing (i.e., at receptors in the periphery), it is generally thought to occur at more central levels (Webster, 2012; Zaidi et al., 2012). Furthermore, it is thought to occur more so cortically than subcortically due to the delays resulting from central integration, as cortical adaptation is greater, more rapid, and more stimulus specific than adaptation seen in the thalamus (Chung et al., 2002). A significant amount of sensory adaptation research has been conducted in the visual system, and less so in somatosensory systems. While somatosensory adaptation has been studied in animals and humans, experiments vary tremendously in the type, duration, amplitude, and frequency of the stimulation used, and the location of stimulation on the body.

According to Kohn (2007), adaptation is of particular interest in sensory systems for two reasons: due to the rapidity of its occurrence, it contributes to moment-to-moment sensory processing; and it can be used to study functional plasticity. Many physiological benefits of adaptation have been suggested, including maximizing information transmission (Brenner et al., 2000), improving detectability or discriminability of novel or rare stimuli by suppressing neural responses to persistent environmental stimuli (thereby enhancing novel input) (Dragoi et al., 2002; Hosoya et al., 2005; Sharpee et al., 2006; Ulanovsky et al., 2003), and facilitating short-term (Abbott et al., 1997) and long-term neural plasticity (Greenlee et al., 1991). As sensory and motor areas of the brain are highly interconnected, all of the benefits of sensory adaptation are crucially important for motor learning as well, both in developing systems and systems relearning motor skills during rehabilitation (due to stroke, brain injury, disease, etc.). By examining sensory adaptation patterns (across all sensory modalities) in a variety of human populations (healthy, disordered, young, old, etc.) we are able to more comprehensively understand

fundamental sensory processes, and how these processes may play a role in sensorimotor integration, functional motor behaviors, and neuroplasticity.

As the brain is ever-changing due to experience-dependent mechanisms, the somatosensory and motor representations are especially important since they occupy much of the mammalian brain (Kaas, 1991), and such changes in these representations may be correlated with functional improvements in sensory and motor skills. Adaptation plays an important role in moment-to-moment sensory processing (Kohn, 2007) as well as promoting synaptic efficiency, which ultimately enhances sensorimotor integration and motor functioning. Decades of research have shown that somatosensory input plays a significant role in acquiring motor skills (Asanuma & Pavlides, 1997), as well as inducing excitability (Hamdy et al., 1998) and plastic changes in both somatosensory and motor cortices (i.e., cross-system plasticity; for review see Luft et al., 2002). In fact, cortical networks can undergo significant alterations in functional connectivity (i.e., synaptic plasticity) due to continuous stimulation and long-term adaptation, which physiologically underlies cortical map reorganization (Buonomano & Merzenich, 1998). Animal studies have demonstrated that short-term changes in somatosensory input or motor output can result in long-term reorganization of somatosensory (Wang et al., 1995; Jenkins et al., 1990) and motor (Adkins et al., 2006; Kleim et al., 1998; Nudo et al., 1996; 1997) cortices, respectively. Human studies have found similar cortical reorganization effects following short-term somatosensory (Godde et al., 2003) and motor (Classen et al., 1998) stimulation, demonstrating the dynamic nature of sensorimotor cortical areas and the impact behavioral experiences can have on neuroplasticity. While these changes can occur across the lifespan, they may be more pronounced during development, and

more specifically during critical periods. Using experience-dependent adaptation paradigms to study functional plasticity, we may gain valuable knowledge that can be used to better inform intervention strategies with a variety of different patient populations. For example, such interventions could ultimately provide the necessary experiences to place a child at risk for developmental disorder on a more "normal" trajectory or keep them on this trajectory (Nelson, 1999), or rehabilitate an adult with sensory and/or motor dysfunction.

According to Nelson (1999), experience induces changes in the brain via three mechanisms: *anatomically* (i.e., existing neurons exhibit axonal growth, dendritic sprouting, and modify synaptic connections), *neurochemically* (i.e., existing neurons increase/decrease synthesis and release of neurotransmitters), and *metabolically* (i.e., fluctuations in glucose or oxygen consumption due to experience). Due to the nature of these changes, as well as the invasiveness of certain procedures used to study these changes, research with living humans is limited to relatively non-invasive procedures that make assumptions about the underlying biological processes involved in alterations in the brain. Some neuroimaging techniques are used to study anatomical changes in the brain, such as computed tomography (CT) and structural magnetic resonance imaging (MRI). Diffusion tensor imaging (DTI; an MRI technique) maps the diffusion patterns of molecules (primarily water) to reveal microscopic details about tissue architecture. Microdialysis is a technique used to directly study changes in the extracellular chemical environment of the human brain; however, the invasiveness of inserting a needle probe into brain tissues is not often feasible, and other indirect methods of studying neurochemical changes, such as positron emission tomography (PET) imaging and

magnetic resonance spectroscopy (MRS), are typically used in lieu of microdialysis. Techniques used to study metabolic changes in the human brain include PET, blood-oxygen-level dependent (BOLD) functional MRI (fMRI) and near-infrared spectroscopy (NIRS), to name a few (more on these techniques in the following section). Through the use of these neuroimaging methods (and many others), we are now able to make assumptions about the underlying anatomy and physiology of the human brain across the lifespan without having to wait to examine the brain post mortem, and can view functional changes in the brain during specific sensorimotor or cognitive tasks (i.e., the brain at work).

Using NIRS to Study Brain Activation

As mentioned in the previous section, there are many ways in which to directly and indirectly study the brain. Each technique has its advantages and disadvantages, and some are more appropriate for answering particular research questions than others. Of particular interest to this study is the way in which functional changes occur in hand and face cortical sensorimotor areas following repetitive somatosensory stimulation and voluntary motor activity, therefore techniques examining blood flow and metabolic changes during brain activation are most appropriate to address the specific aims. In general, as a stimulus evokes a neural response in certain areas of the brain, a local increase in cortical blood flow accompanies it in order to deliver energy to the activated neurons (in the form of oxygen and glucose). This relationship is known as neurovascular coupling, which is responsible for generating the hemodynamic response, and is the basis of many neuroimaging techniques, such as fMRI, PET, and optical

imaging (i.e., NIRS). Because PET requires an invasive injection of a radioactive tracer and has relatively low spatial resolution, it is not always feasible for human studies (Villringer, 1997). Though fMRI and NIRS use different means to monitor regional changes in cortical tissue oxygenation (magnetic fields and near-infrared light, respectively), previous studies have shown that fMRI and NIRS agree quite well on measurements of cortical oxygenation changes (Kleinschmidt et al., 1996; Mehagnoul-Shipper et al., 2002; Sassaroli et al., 2005; Toronov et al., 2001). Due to the unrestrictive and portable nature of NIRS, and the comparatively less expensive equipment than in MRI, NIRS (or functional NIRS [fNIRS]) will be used in the current study to examine hemodynamic changes and adaptation in sensorimotor cortices following repetitive somatosensory stimulation and voluntary motor activity.

Neurophysiological Basis of NIRS

NIRS, a popular optical imaging technique, uses near-infrared light (wavelengths of approximately 800 to 2500 nm) to penetrate a medium (e.g. human tissue), and measures the absorption (or scattering) of light photons that pass through that medium—for reference, the visible part of the electromagnetic spectrum ranges from ~400 nm (blue/violet) to ~700 nm (red). NIR light is absorbed by some chromophores (molecules responsible for color) in mediums and reflected by others. In the human body, blood carries the chromophore hemoglobin (red blood cell protein that transports oxygen), which can either be bound or unbound to oxygen molecules (referred to as oxyhemoglobin [HbO] and deoxyhemoglobin [HbR], respectively). While both types of hemoglobin are strong absorbers of light, each one exhibits different absorption spectra

for NIR light, which is why 2 different wavelengths of light are typically projected into the medium to measure changes of the two chromophores. 690 nm (more sensitive to HbR) and 830 nm (more sensitive to HbO) have been suggested as optimal wavelengths in NIRS research (Boas et al., 2004; Sato et al., 2004; Strangman et al., 2003; Yamashita et al., 2001). The attenuation of photon absorption can then be used to calculate the relative concentration of oxygen being brought to the tissue via hemoglobin in the blood. This conversion of photon attenuation into hemoglobin oxygenation changes follows the Beer-Lambert law, which states that the transmission of light through a substance or medium depends on the absorption coefficient of the substance and the distance the light travels through the substance (Kocsis et al., 2006). Human brain tissues (meninges, gray matter), skin, and bone are comparatively transparent to light within 600-1000 nm range (often called the NIR spectral window, or optical window) (Ferrari & Quaresima, 2012), allowing for maximum depth of penetration of NIR light through tissue. Light of these wavelengths can penetrate several centimeters and still be detected (Strangman et al., 2002a). In order to emit NIR light into a medium and receive the amount of photons not absorbed by a chromophore (here hemoglobin, though water, fat, and melanin are also chromophores that absorb NIR light in the human body, to a much lesser degree), a source-detector pair of optical electrodes, or “optodes”, is used.

The source-detector optode pair used in NIRS consists of a laser diode and/or light emitting diode (source) and a photon detecting sensor that carries the NIR light reflected back from the tissues (detector). The distance between source and detector will determine the depth at which the light will penetrate the tissue, and based on physical models of light propagation and scattering we are able to determine which region of

tissue it has most likely come through. In general, light travels through what is known as the "photon banana" (Figure 1.4), where photons are more likely to pass through more central regions of the banana (darker red) than outer regions (lighter pink), therefore measurement sensitivity can be addressed accordingly. In the figure, location 1 is in the main light path, therefore hemoglobin within this location would be more easily detected, as opposed to hemoglobin in location 2. The optimal source-detector distance for measuring cortical surface hemoglobin changes has been estimated to be 3 cm in adults (Obata et al., 2003; Okada & Delpy, 2003; Sato et al., 2006; Watanabe et al., 1996), though this distance may vary depending on NIR light intensity and wavelength, cortical region of interest, and age of the subject (i.e., smaller distance used in small children) (Ferrari & Quaresima, 2012).

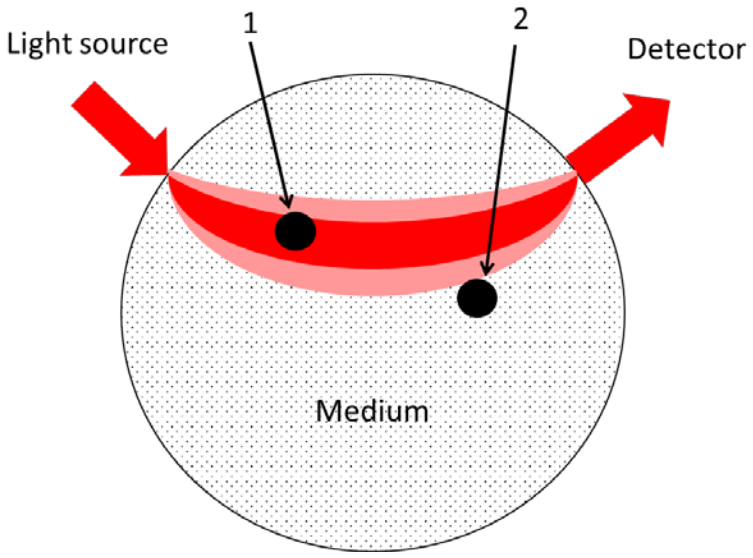

Figure 1.4. The "photon banana". Photons are more likely to pass through central regions of the banana (darker red) than outer regions (lighter pink), making signals from location 1 more easily detected (adapted from http://www.nirx.net/principles-of-optical-tomography).

As previously mentioned, the hemodynamic response occurs as a result of neurovascular coupling, the relationship between local neural activity (and thus cerebral energy metabolism) and the resultant changes in regional cerebral blood flow (rCBF) (van Essen et al., 2001). With these changes in rCBF also come changes in cerebral blood oxygenation. Activated neurons consume and metabolize oxygen at an increased rate (as compared to "resting state" neurons), meaning tissue oxygenation decreases during functional activity, therefore requiring an increased delivery of oxygen supply in the blood (Ances et al., 2001; Enager et al., 2009; Offenhauser et al., 2005; Thompson et al., 2003). Though a tight coupling exists between neural and vascular mechanisms, there is still much debate as to whether this relationship is completely linear. Logothetis and colleagues (2001) found that sustained visual stimulation evoked spike rate (output signal) adaptation effects in visual cortex neurons, but local field potentials (a reflection of synaptic activity [input signals]) more linearly correlated with the hemodynamic response. Contrary to these findings, Devor and colleagues (2003) found a strong nonlinear relationship between electrophysiological measure and hemodynamics, as the hemodynamic response continued to grow beyond that of the electrical activity. Other studies demonstrate both linear and nonlinear aspects (Obrig et al., 2002; Sheth et al., 2004), as the hemodynamic response may be linear over only a narrow range of neural activity, more specifically later in cortical neural responses (>30 ms) (Ou et al., 2009). More research in the area of neurovascular coupling is warranted. Perhaps multimodal imaging approaches paired with more complex experimental designs can provide a more in depth look at these physiological mechanisms.

Hemodynamic Changes in Neighboring Areas following Activation – Cortical Steal

At any given time, spontaneous variations are occurring in the vascular bed in different parts of the body in response to changes in local requirements. This shifting of blood from tissue to tissue changes the way in which blood volume is distributed, and thus the distribution of hemoglobin (both oxygenated and deoxygenated). In 1947, DeBakey and colleagues examined this effect in peripheral body parts (fingers, toes, pinnae), and termed it the "borrowing-lending hemodynamic phenomenon", or "hemometakinesia", where activated areas requiring an increase in blood volume essentially borrow it from a neighboring area, causing a simultaneous decrease in blood volume in that region. More recently this phenomenon has come to be called "vascular steal", and more specific to the brain "cortical steal". Characterized by a negative hemodynamic response, this has been noted to occur in areas adjacent to the activated area in human visual cortex using fMRI (Shmuel et al., 2002), and in rodent somatosensory cortex using fMRI (Boorman et al., 2010) and optical imaging (Kennerley et al., 2012). Similar results using NIRS have shown reductions in HbO and HbR in somatosensory cortex following hand grasping (Lu et al., 2013), and reductions in HbO and HbR in sensorimotor cortex following vibratory and median nerve somatosensory stimulation (Obrig et al., 1996). While there are controversial findings, it is certainly worth noting that this phenomenon has been observed across peripheral and central nervous system tissues, and can be detected by oxygenation changes in the hemodynamic response.

Developmental Changes seen in Cortical Hemodynamics

Because NIRS is non-invasive and does not require subjects to enter a scanner bore (as in MRI), it is often more desirable than other neuroimaging methods for use in children (Wartenburger et al., 2007 used NIRS in 4 year olds). In fact, NIRS is gaining popularity for use in newborns and infants, though there is still little information regarding brain metabolism and functional activation in these young populations (and in school-aged children) as compared to adults (Roche-Labarbe et al., 2014). Most recent research looking at hemodynamics in infants and children has used fMRI, though it is common to use light anesthesia in younger children undergoing MRI scanning, which could ultimately affect findings. Conflicting reports have been found across a wide range of developmental ages, and it is difficult to compare fMRI findings with so much variability in stimulus paradigms. A study by Marcar et al. (2004) compared the BOLD response between a group of younger children (<5 years old) and older children (>5 years old) following visual stimulation. The authors found that though the amplitude of the BOLD response did not differ between groups, younger children exhibit greater cerebral metabolic rate of oxygenation ($CMRO_2$) (which is associated with cortical processing) than older children, and suggest that $CMRO_2$ plays a more important role in the BOLD signal than does the vascular response (i.e., cerebral blood flow [CBF]; though this study did not directly measure CBF). Another set of experiments by Moses and colleagues (2014a; 2014b) measured both the BOLD response and CBF in children 8 years of age, 12 years of age, and adults following auditory and motor stimulation (finger tapping). These authors also found no significant differences in the amplitude of BOLD responses, but did find that the younger children exhibited greater CBF during auditory stimulation,

and both child groups exhibited greater CBF during motor tasks than adults. Because CBF directly influences the relative amount of HbO and HbR in the brain, these authors suggest that cerebrovascular dynamics influence the BOLD signal more so in immature systems. Further studies using more robust stimulus paradigms across a wider range of ages will be helpful to elucidate these hemodynamic differences during cortical maturation.

Rationale and Overall Purpose of the Study

The proposed study investigated the hemodynamic effects of repetitive somatosensory stimulation and voluntary motor activity of the face and hand in corresponding cortical areas. The type of pneumatic somatosensory stimulation used in this study produces a rapid and localized deflection of the skin and represents a natural form of stimulation compared to electrical stimulation. The forms of voluntary motor activity—repeated bilabial compressions for lower face, repeated grip force squeeze for hand, both at 10% maximum voluntary contraction level—represent functionally relevant motor activities (speech and hand grip), which may have therapeutic implications for individuals experiencing motor deficits. The hand and lower face were chosen as the body structures to investigate because they are most commonly used in human communication (speech, facial expression, writing, sign language, etc.), and each has an elaborate central representation for skilled sensorimotor activities. Finally, fNIRS was chosen as the imaging modality to assess the hemodynamic response due to its non-invasiveness, ease of use with subjects of all ages, portability, relatively low cost (as compared to fMRI), good temporal and reasonable spatial sensitivity, and ability to

examine specific and subtle changes in oxygenation levels in hemoglobin at the level of the cortex. Anatomical MRI scans were obtained in order to locate sensorimotor cortices on each participant, and ensure accurate fNIRS probe placement on the scalp.

This study was also designed to investigate age-related changes in sensorimotor cortical hemodynamics, with the hope of gaining insight into the changes in neuronal processing of somatosensory and motor information resulting from cortical maturation. To this end, healthy children (ages 6-13 years) and adults (19-30 years) were studied in an effort to examine developmental changes in cortical activation patterns, thus providing a longitudinal view of normal physiologic connectivity and function. The results could have implications for the development of new assessments and therapeutic strategies, as these normative data may be used for comparison to how sensorimotor systems may function in disordered populations across a developmental timeline.

CHAPTER TWO: METHODS

Participants

Child (ages 6-13 years; N=11; 8 females) and adult (ages 19-30 years; N=22; 17 females) participants were recruited by word of mouth and posted advertisements (approved by the University of Nebraska Institutional Review Board [IRB]). Tables 2.1 and 2.2 provide demographic data and direction of hemodynamic responses for children and adults, respectively.

Table 2.1. Participant information for children.

Subject ID	Sex	Age at Testing (years)	HRF Face Motor	HRF Face Sensory	HRF Hand Motor	HRF Hand Sensory
C01	F	7.99	NEG	NEG	NEG	NEG
C02	F	12.75	NEG	NEG	NEG	NEG
C03	M	13.07	NEG	POS	POS	NEG
C04	F	13.07	NEG	POS	n/a	POS
C05	F	7.51	n/a	NEG	n/a	POS
C06	F	12.24	POS	NEG	POS	NEG
C07	M	10.11	NEG	NEG	n/a	NEG
C08	M	12.29	POS	NEG	POS	NEG
C09	F	6.25	POS	POS	POS	POS
C10	F	6.28	n/a	POS	n/a	NEG
C11	F	8.95	NEG	NEG	NEG	POS
MEAN		10.05				
SD		2.76				

Table 2.2. Participant information for adults.

Subject ID	Sex	Age at Testing (years)	HRF Face Motor	HRF Face Sensory	HRF Hand Motor	HRF Hand Sensory
N01	M	19.30	POS	NEG	POS	POS
N02	M	23.45	NEG	POS	NEG	NEG
N03	F	20.04	NEG	NEG	POS	POS
N04	F	23.18	NEG	NEG	NEG	NEG
N05	M	23.73	POS	NEG	POS	NEG
N06	F	23.85	POS	NEG	POS	POS
N07	F	27.76	POS	POS	POS	POS
N08	F	22.52	NEG	POS	NEG	POS
N09	F	23.32	POS	POS	POS	POS
N10	F	23.69	NEG	NEG	POS	NEG
N11	F	23.20	POS	POS	NEG	POS
N12	M	20.31	POS	NEG	POS	POS
N13	F	24.93	POS	NEG	POS	NEG
N14	F	22.36	POS	POS	NEG	NEG
N15	F	22.82	POS	POS	POS	NEG
N16	F	23.73	POS	NEG	POS	NEG
N17	F	23.54	POS	POS	POS	POS
N18	F	24.60	n/a	NEG	POS	NEG
N19	F	23.47	NEG	POS	POS	NEG
N20	F	23.64	POS	POS	POS	NEG
N21	M	24.18	POS	NEG	NEG	NEG
N22	F	21.98	NEG	NEG	POS	NEG
MEAN		23.16				
SD		1.76				

Human Subjects Review

This research project was approved on 4/4/2014 by the University of Nebraska IRB for the Protection of Human Subjects (IRB Number: 20140414252EP, Project ID:

14252). The primary investigator and associated research staff have completed the required CITI biomedical training modules on responsible research and protection of human subjects.

Inclusion Criteria

Children: healthy, typically-developing (i.e., no concerns from a family practitioner or pediatrician), right-handed, no history of neurological insult or disease, in good health at the time of testing. Adults: healthy, right-handed, no history of neurological insult or disease. All participants had to be eligible for MRI scanning.

Exclusion Criteria

All subjects: medications required for attentional deficits, previous history of somatosensory or motor deficits. Each subject also completed an MRI screening form (see Appendix A) prior to participation. This form was reviewed by the MRI technician to determine eligibility for MR scanning (i.e., no metal implants, surgical staples, hearing aids, etc.). There was no exclusion based on gender, race, or ethnicity.

Informed Consent

As per inclusion criteria, all subjects were asked to confirm his/her right handedness. For children, parents were asked to complete a questionnaire prior to study enrollment to determine if their child was eligible for participation (child's handedness was confirmed with both the parent and child). On the day of testing, signed consent was obtained from the guardian, and verbal assent and signed consent was obtained from the

child before beginning any procedures. For adults, on the day of testing, signed consent was obtained from the participant before beginning any procedures. Adult participants and parents were also made aware of the evolving incidental findings policy at the Center for Brain, Biology and Behavior (CB3), and once the university IRB approved an informed consent addendum, adult participants and parents provided signed consent. Any incidental findings that occurred throughout this study were reported according to the current CB3 policy.

Equipment

Siemens Skyra 3.0 Tesla MRI Scanner: A standard 3.0 T MRI scanner was used to acquire structural images from all subjects. A FLASH spoiled gradient echo scanning sequence was used to acquire a T1-weighted 3D image of each individual participant's head (TR=20 ms, TE = 4.92 ms, matrix = 512 × 512, flip angle = 25°, voxel size 0.5 × 0.5 × 1 mm, 192 sagittal slices; Figure 2.1). Vitamin-E capsules were taped to 3 landmarks on the scalp based on the international 10-20 system (Jasper, 1958): the nasion (Nz), vertex (Cz), and inion (Iz). Two other vitamin-E capsules were placed where the short separation optodes on the fNIRS probe were located, in an effort to align the central row of optodes along the central sulcus.

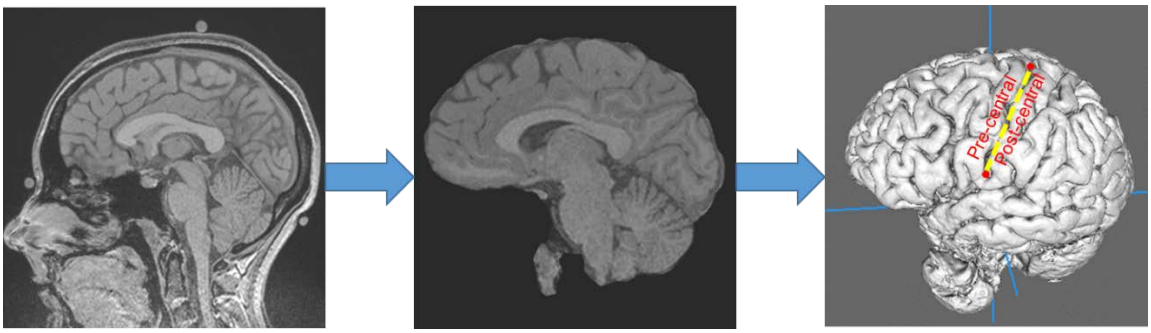

Figure 2.1. T1-weighted MRI image and 3D surface projection performed in Mango. Images were used to determine the location of pre- and post-central gyri, which determined the placement of the fNIRS probe array on the scalp. Vitamin-E capsules are seen on Nz, Cz, and Iz in the first image. The two red dots in the surface rendering correspond to the location of the two short separation optodes on the fNIRS probe.

TechEn Continuous Waveform (CW6) NIRS System: A 16-channel NIRS system from TechEn with 16 source-detector pairs was used to measure hemodynamic activity. This device consists of a PC with a monitor for displaying and manipulating recorded data, control card with 3 control LEDs/USB/up to 8 BNC auxiliary channels, 16 laser source emitters, 16 detector receivers, fiber optical laser source bifurcated cables (for the 2 different wavelengths of light), fiber bundle detector cables, and plastic optodes (Figure 2.2). Each end of a laser bifurcated fiber cable attaches to 2 sources of different wavelengths (e.g., laser A1 emits 690 nm light, laser A2 emits 830 nm light), and both are recorded by detector optodes near the light-emitting optode. The recorded signals are used to calculate the hemodynamic response in the tissues penetrated by the lasers, and both HbO (more sensitive at 830 nm) and HbR (more sensitive at 690 nm) are displayed

in real time with a sampling rate of 50 Hz (see Figure 2.3 for example of real time data using a simple probe).

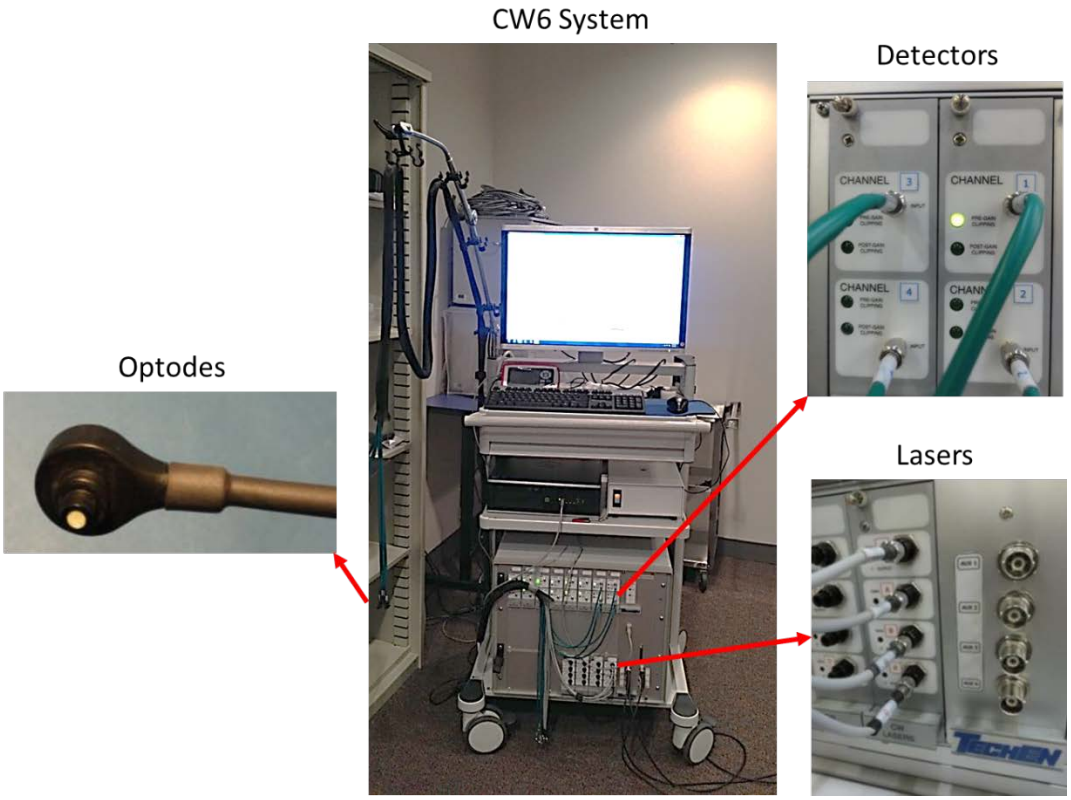

Figure 2.2 TechEn CW6 instrument.

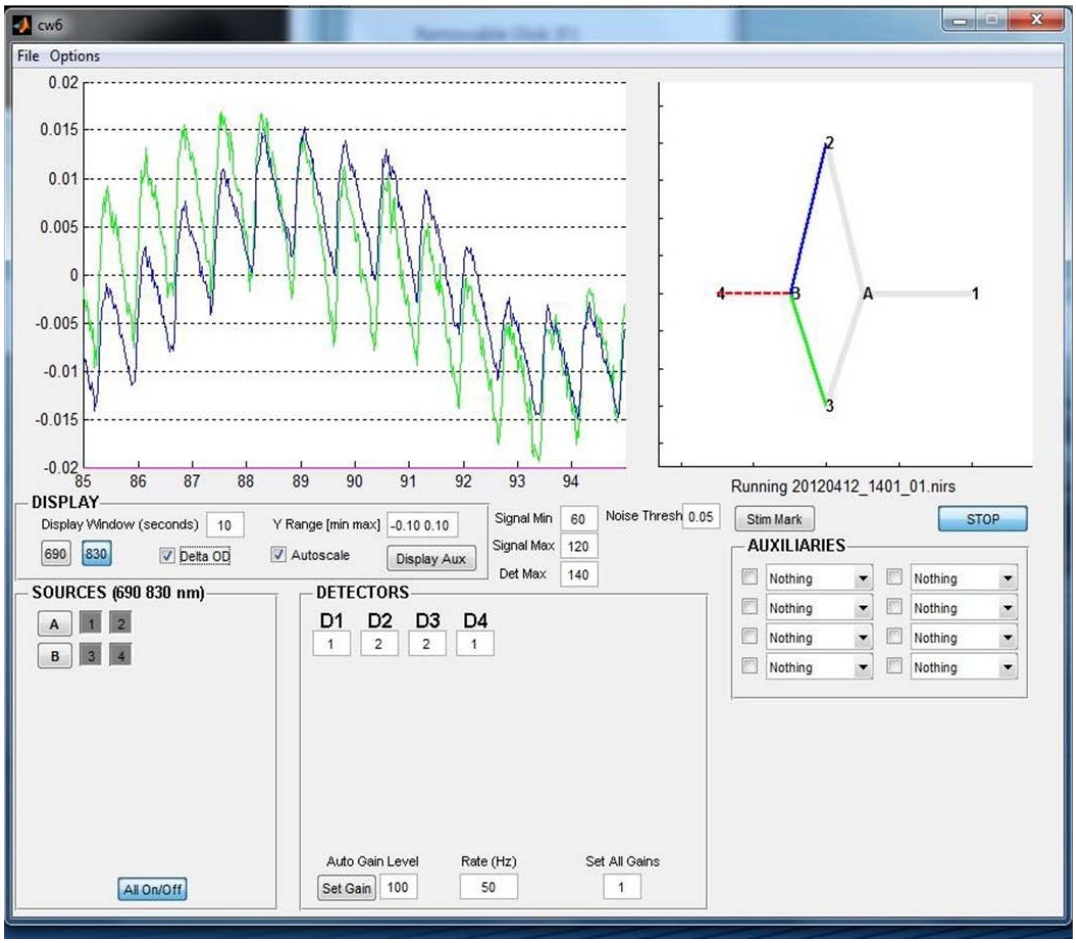

Figure 2.3. Real time display of data collection. Channels shown are from source B to detector 3 (green), and source B to detector 2 (blue).

Galileo™ Tactile Stimulus System: For the passive somatosensory stimulus conditions, a Galileo™ somatosensory stimulator was used to deliver punctate, pneumotactile stimulation to the structures under investigation. Three plastic pressurized TAC-Cells (O.D. = 15 mm, I.D. = 6mm, H = 6mm) driven by channels 1-3 from the Galileo™ via silicone tubing were placed on the fingertips of the thumb, index finger, and middle finger of the right hand, and channels 4-6 were programmed to synchronously

stimulate three areas of the lower face at the oral angle using double adhesive collars (shown in Figure 2.4). The Galileo™ generated a biphasic pulse train (-80 to 140 cmH_2O, 50-ms pulse width, and a 10 ms rise/fall time). TTL output was sent to the CW6 NIRS device to synchronize pulses from the Galileo™.

Figure 2.4. Galileo™ housing and position of TAC cells on the face and hand.

Grip force and lip compression force strain gages: To control for consistent hand and lip force, and to standardize motor tasks across all subjects, a grip force strain gage isometric dynamometer (ADInstruments) and a custom lip compression force strain gage was used (Figure 2.5). The grip force transducer is a pre-conditioned strain sensor with a linear response from DC-50 Hz in the 0-800 N range. The lip compression strain gage transducer is also DC-coupled and conditioned by a BioCom 501 bridge amplifier,

Butterworth low-pass filtered at 50 Hz, with a linear response through the passband. An ADInstruments PowerLab DAQ module with accompanying LabChart Pro (v. 8.0) software was used for data acquisition and recording (low-pass filtered at 50 Hz, sampling rate of 1 kHz, 16 bits ADC). To ensure the motor tasks occurred at the target rate, a 2 Hz pulse was synthesized with the ADI box while the participants' force signals were digitized in real time and displayed as a separate channel on a 42" digital HD monitor positioned approximately 1.25 meters directly in the participants' line of vision (after Moon et al., 2015). The pulses were used to assist participants in visuomotor tracking at the 2 Hz rate during hand and lip force motor tasks (Figure 2.6).

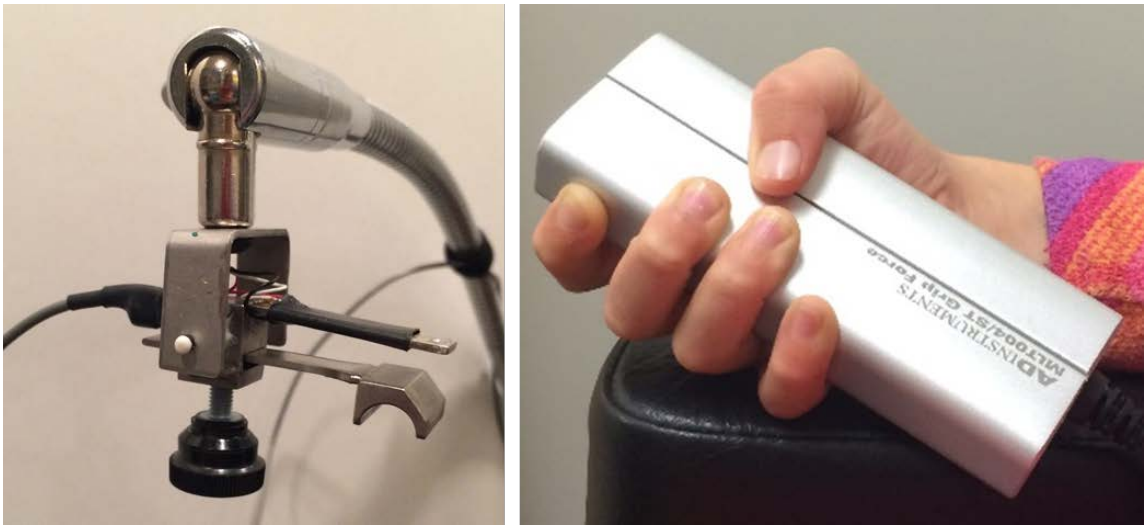

Figure 2.5. The custom lip force strain gage and ADInstrument grip force strain gage.

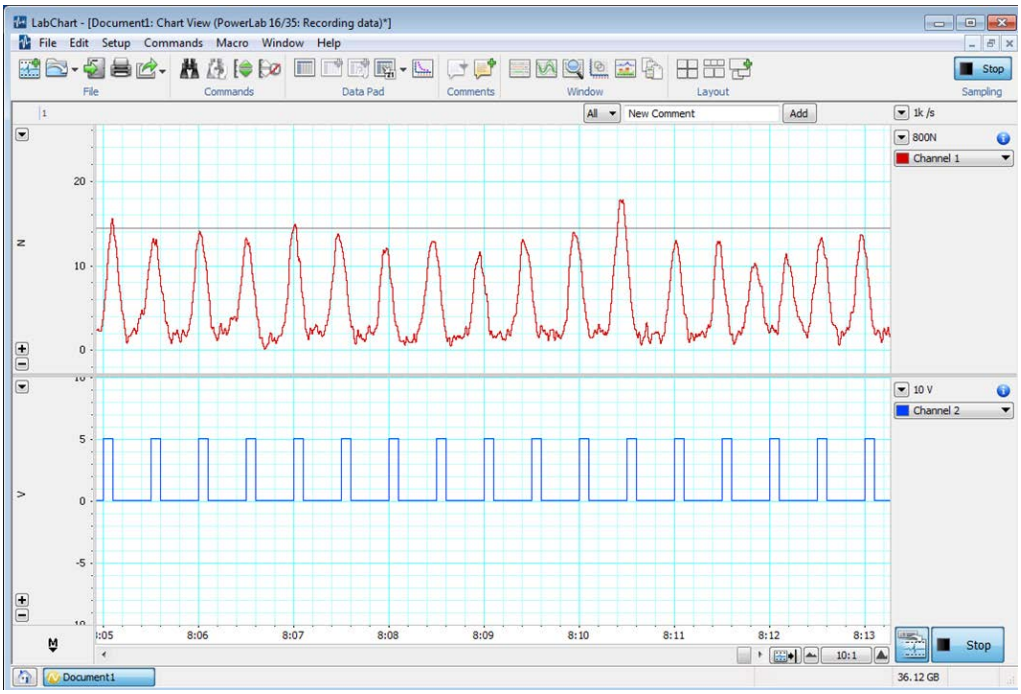

Figure 2.6. A subject performing the 2 Hz grip task with grip force transducer in LabChart.

For both the hand gripping and lip compression activities, maximum voluntary contractions (MVCs) were performed by each subject prior to fNIRS testing, and 10% MVC was used as each individual's target force for the hand grip and bilabial compressions. Each individual's target force was labeled in the LabChart display with a guide line (see line in top channel in Figure 2.6). To avoid any additional pressure placed on the transducer by the lips, a custom-built gooseneck arm was used in order to hold the strain gage transducer at a comfortable position for the participant. An adjustable spindle mount was added to the arm to allow for appropriate adjustments based on individual participant height and head position (Figure 2.7).

Figure 2.7. Flexible gooseneck arm with strain gage attached for bilabial compressions.

NIRS Probe Design

The NIRS probe array consisted of a 5x3 optode layout (4 sources, 12 detectors), featuring an interoptode distance of 3-3.35 cm, with 2 short separation channels at a distance of 1 cm to remove biological interference (e.g. heartbeat, respiration) (Figure 2.8; channels 12 and 13 at top and bottom of probe). It is now widely accepted that systemic interference occurring in the superficial layers of the scalp and underlying skull bone is problematic in NIRS research. Therefore, adding short separation optodes (at a maximum of 1.5 cm) to record signals at shallow depths, then regressing the signal out of the longer separation optode data, improves the contrast-to-noise ratio of the standard

NIRS signals (Gagnon et al., 2012). The probe was made of .032" thick medical grade silicone sheeting, with holes punched out at the above mentioned distances. Nylon shoulder washers with 2/64" thick rims on the flange were snapped into the holes to securely hold the bayoneted NIRS optodes flat against the scalp. This probe was specifically designed to cover somatosensory and motor areas in cerebral cortex. It was placed over left central-parietal cortex, according to each individual's cortical anatomy (as seen on the structural MR images) so as to lie directly above pre- and postcentral gyri.

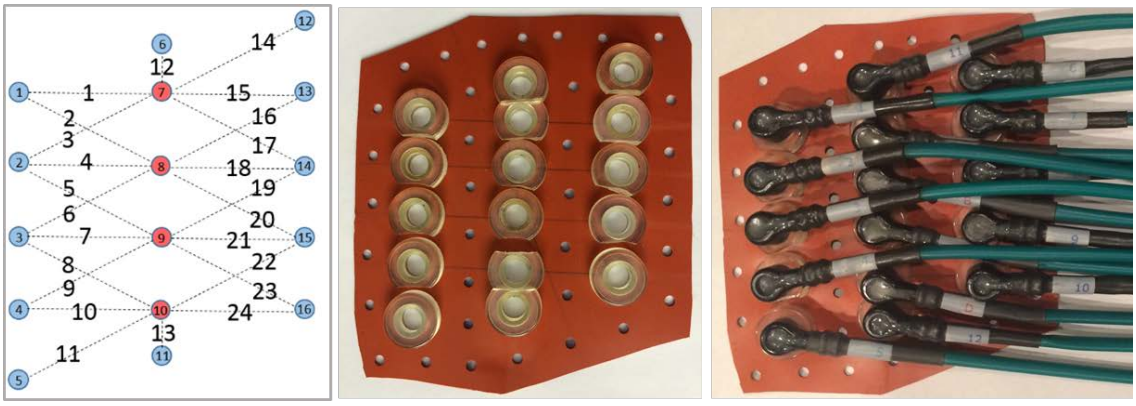

Figure 2.8. Optode probe array without and with optodes attached.

Participant Preparation

Testing took place in a single session at the CB3 at the University of Nebraska-Lincoln (UNL). First, a structural MRI scan was performed. Prior to scanning, participants filled out the MRI Safety Screening Form (Appendix A). The MRI technician reviewed the form prior to performing the scan to determine participant eligibility. If needed, subjects were provided with scrubs to ensure no metal entered the magnetic scanning environment. The MRI technician scanned each subject for metallic

items, provided them with foam insert earplugs, and helped position the subject in the scanner. The scanning sequence took 3 minutes 49 seconds. If, after reviewing the anatomical scan, the placement of the vitamin-E capsules was not accurately aligned with the central sulcus, capsules were repositioned and the 3:49 minute scan was repeated. Following the anatomical MRI scan, participants were escorted to the fNIRS laboratory suite at CB3. Prior to the fNIRS recording session, each participant's anatomical MRI scan was reviewed, and probe array position on the scalp was determined by each individual's pre- and postcentral gyri location relative to the fiducial landmarks mentioned above. The optode locations (based on the locations of washers on the probe) were then marked on the scalp, and the hair was neatly parted, braided (if necessary for longer hair), and securely pinned/hair sprayed to expose the scalp and keep hair from interfering with the light path. The scalp was cleaned and the probe was secured to the scalp using hair pins. For males with shorter hair, a cotton mesh fabric was placed over the head to secure the probe (see Figure 2.9). Once the probe was in place, the corresponding optodes were snapped into the washers, and signals were checked for appropriate baseline intensity levels (optimum level should be between 90 dB and 120 dB with subject at rest). Once the desired signal levels were reached, TAC-Cells were placed on the hand and face, and the subject was instructed on experimental tasks.

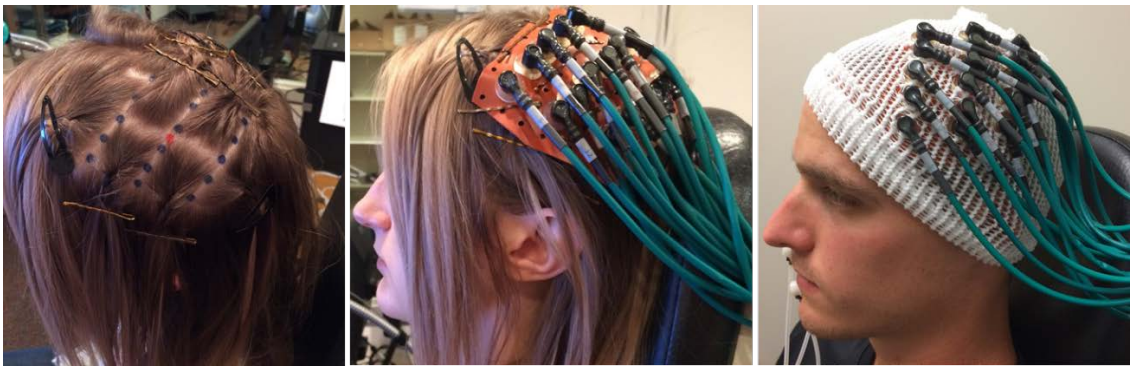

Figure 2.9. Subject scalp preparation and probe array attachment. Red dot indicates position of C3, blue dots indicate position of optodes.

Stimulus Paradigm

The two motor tasks consisted of a repetitive hand grip on a grip force strain gage at 10% MVC, and a repetitive bilabial compression task on a lip compression force strain gage at 10% MVC, each at 2 Hz (20 sec ON/20 sec OFF, repeat 10x). As previously mentioned, a monitor was placed in the participant's line of vision (approximately 1.25 meters away) that displayed the synthesized 2 Hz pulses, with the participant's digitized force signals displayed in a separate channel. The participants were instructed to maintain the 2 Hz rate with their grip force transducer squeezes and lip strain gage compressions, and to use the resultant digitized signals as a feedback mechanism (see Figure 2.10 for setup). Because the feedback on the monitor was purely visual, it is highly unlikely that it interfered with activity in somatosensory and motor cortices; however, 20 seconds of rest while the monitor was on occurred while NIRS signals were recorded prior to starting any of the somatosensory or motor tasks, in an effort to rule out the visual stimulation as a confounding variable. Subjects were allowed a practice

session prior to beginning the study. The passive somatosensory conditions consisted of Galileo™ pneumatic stimulation applied through TAC-Cells also at a pulse rate of 2 Hz (20 sec ON/20 sec OFF, repeat 10x). The program to run this specialized sequence on the Galileo™ is coded as an *.xml file and is available in Appendix B. The order of the 4 conditions (face somatosensory, hand somatosensory, face motor, hand motor) were counterbalanced among participants, each lasting 7 minutes.

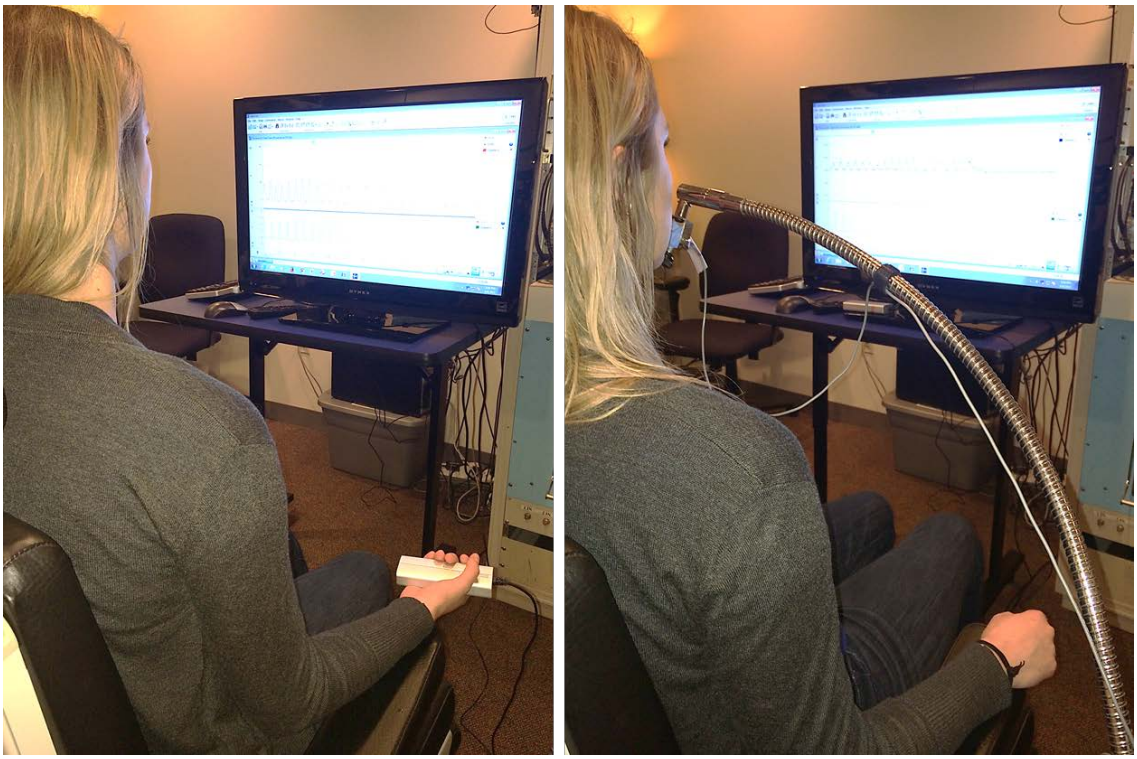

Figure 2.10. Experimental setup for grip force transducer and lip compression strain gage. 2 Hz pulses and digitized force signals displayed on screen.

Data Processing

The fNIRS data was preprocessed using freeware called Homer2, a set of MATLAB scripts used to process and analyze fNIRS data (http://www.nmr.mgh.harvard.edu/PMI/resources/ homer2/home.htm). A custom processing stream was used to perform the following functions (see Figure 2.11): raw data was bandpass filtered (0 - 0.3 Hz) to remove low frequency drift and cardiac and respiratory oscillations. PCA-based filtering was not used. Motion artifacts were rejected using an automated detection algorithm based on standard deviation. Block averages spanning the period of -10 to +30 seconds relative to stimulus onset were performed (somatosensory stimulus or motor task lasted from 0 to 20 seconds), and changes in optical density for each source-detector pair were converted to changes in hemoglobin concentration (HbO, HbR, and total hemoglobin [HbT]—a reflection of cerebral blood volume) using the modified Beer-Lambert Law (Delpy et al., 1988). Finally, short separation measurements were defined as any channel that does not meet a threshold length of 15 mm, and data from those channels were regressed out of data from the other channels, providing a more localized response.

For each subject, visualization and localization of vitamin-E capsules, brain extraction, and 3D surface rendering was performed in the non-commercial software Mango (http://ric.uthscsa.edu/mango/). See Appendix C for a detailed description of this process.

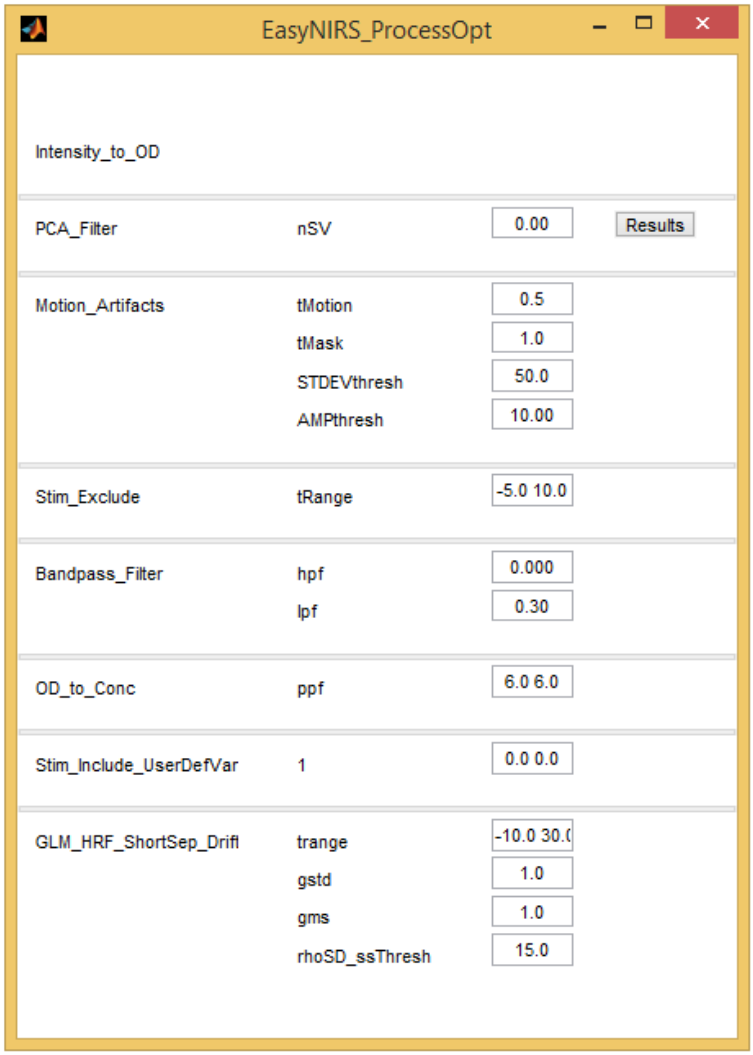

Figure 2.11. Customized processing stream built in Homer2.

Outcome Measures

Block averages (-10 to +30 seconds relative to stimulus onset) of HbO, HbR, and HbT were calculated across all channels for each condition (providing the hemodynamic response function [HRF]), and were pooled and averaged across all 10 repetitions of each task. This 40-second analysis time window displayed data from 10 seconds pre-stimulus (t = -10 to 0 s), 20 seconds post-stimulus onset (t = 0 to 20 s), and 10 seconds following

stimulus offset (t = 20 to 30 s). A feature in Homer2 called "Plot Probe" allowed for viewing the HRF in probe space after the data had been processed, showing which channels exhibited the greatest amount of activity. Measurements of oxygenation levels were examined in both the putative hand and face cortical areas (in M1 and S1) across both motor and somatosensory conditions.

A partial sums integral was calculated over the 20 second stimulus window for HbO across each condition to estimate the area under the hemodynamic curves for all channels (after Estep et al., 2007; Custead et al., 2015). An integral (here, a definite integral, not indefinite) is used to approximate the area of a curvilinear region in a xy-plane that is bounded by two points on the x-axis (here, the time of the stimulus is the boundary: x=0 and x=20). The area above the x-axis adds to the total integral value and that below the x-axis subtracts from the total integral value. For each condition, the four adjacent channels that yielded the greatest mean HbO integral (as HbO is typically used as a measurement of cortical activation) were chosen as channels of interest and were used as the dependent measures in statistical analyses.

Behavioral data was digitized using LabChart Pro (v. 8.0), and power spectra were calculated for all adults' and children's hand and face motor tasks. Power spectra use the Fast Fourier Transform (FFT) to indicate which frequencies contain the majority of the signal's power (energy per unit time). Both hand and face motor traces were filtered with a digital band-pass filter (0.5-10 Hz), and spectra were calculated with an FFT size of 128K, and a Hamming window with a 50% window overlap. Because participants were prompted to perform motor tasks at 2 Hz, it was expected that a majority of the power for each task would be relatively close to 2 Hz (see examples of

hand and face spectra from an adult participant in Figure 2.12a and b, respectively). Also, a peak-finding MATLAB code (http://www.mathworks.com/matlabcentral/fileexchange/25500-peakfinder/content/peakfinder.m) customized for this study (Appendix D) was used to identify peak forces in all participants' traces across both motor tasks, and average peak forces were expected to lie near each individual's 10% MVC force.

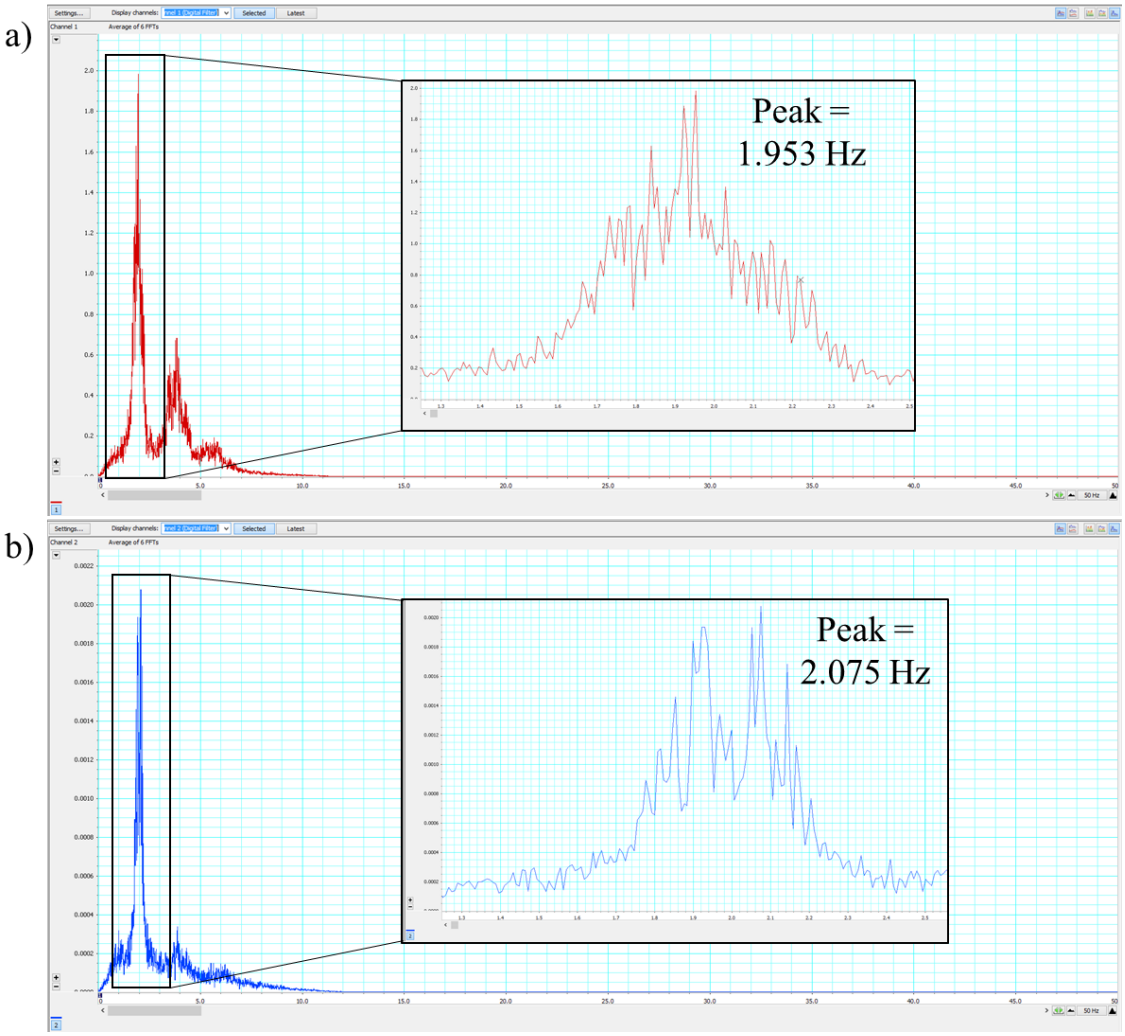

Figure 2.12. Hand (a) and face (b) power spectra from a single adult subject.

Power Analysis

The total sample size (N=33) selected for this study was based on previous measurements of the response variables (HbO/HbR means, standard deviations), and yielded statistical power greater than .95, medium-large effect size, and $p<.05$.

Statistical Analyses

Analysis of variance (ANOVA) was performed to compare mean partial sums integral values across motor and somatosensory cortical areas during the same condition (face motor M1 vs. face motor S1, etc.), across the same stimulus but different site (face motor M1 vs. hand motor M1, etc.), across type of stimulus within the same site (face motor M1 vs. face sensory S1, etc.), and across stimulus time (pre vs. during, etc.). A priori contrasts were performed when appropriate. A priori comparisons were used rather than post hoc tests, as planned comparisons are statistically more powerful, and the more post hoc test performed the greater the familywise Type I error rate.

Polynomial regression analyses were performed to examine adaptation trends of the HRF in all groups across all stimulus conditions. The response variable was mean HbO concentration values (microMolars) during the 20-second stimulus periods, and the predictor variable was time of stimulus. This model was used to assess the trends of HbO levels in cortex following sensorimotor stimulation.

To ensure subjects were matching the 2 Hz frequency during motor tasks, a power spectrum was performed to quantify each subject's dominant tracking frequency (as previously described). To ensure subjects were matching their individualized 10% MVC

amplitude, peak force (mean and standard deviation) was quantified and averaged across all 10 trials of each motor task. T-tests were used to determine if difference existed between behavioral targets and achieved rates and forces. Neurobehavioral correlations were performed between the HbO partial sums integral values in respective cortical regions and the measured behavioral variables (after Kurz et al., 2014). All statistical analyses were performed in either SPSS (v. 22) or Minitab (v. 17.2.1).

Hypotheses & Interpretations

H_0 Aim #1: It is hypothesized that somatosensory stimulation delivered via the Galileo™ somatosensory stimulator will produce HRFs in respective contralateral somatosensory cortex areas (hand vs. face), and that the amplitude of HRFs will vary between the different stimulation sites. It is hypothesized that due to the extremely high innervation density of mechanoreceptors at the finger tips, the amplitude of neural response will be greater than on the perioral skin, therefore the HRF will also be greater.

H_A Aim #1: The alternative hypothesis suggests that though this form of somatosensory stimulation may activate corresponding brain areas, the amount of HbO will not be significantly elevated (as measured with fNIRS), which would be in accordance with other studies that did not find an elevated BOLD response following visual (Marcar et al., 2004) and auditory stimulation (Moses et al., 2014a) using fMRI (note: these studies were conducted in children), but contrary to countless other studies demonstrating an elevated BOLD response following sensory stimulation.

H_0 Aim #2: It is hypothesized that HRFs will be significantly elevated during motor tasks, beyond that of the pure somatosensory conditions, and that HRFs will be

apparent in both motor and somatosensory cortices, due to the fact that both motor and somatosensory mechanisms are utilized during motor activity. It is also hypothesized that the HRFs will differ across hand and face areas during respective motor activities, due to differences in regional arterial/venous anatomy, cortical vascular beds, extent and orientation of somatotopy, task dynamics, and mechanoreceptor typing in hand and face.

H_A Aim #2: The alternative hypothesis suggests that though motor activation may be occurring in cortex, the amount of HbO will not be significantly elevated (as measured with fNIRS), which would be in accordance with another study that did not find an elevated BOLD response following motor activity (Moses et al., 2014b) using fMRI (note: this study was conducted in children), but contrary to countless other studies demonstrating an elevated BOLD response following motor stimulation (participant-driven or elicited by TMS).

H_0 Aim #3: It is hypothesized that age-related differences in HRFs will be observed, and that as children develop, neural responses and HRFs become more adult-like. Because there is much debate on the precise timing of when adult-like changes in neurovascular coupling occur in developing children, this aim will be exploratory in nature, and may provide new data on when somatosensory and motor cortices exhibit HRFs comparable to adults, or new HRF trends that may occur throughout late childhood/early adolescence.

H_A Aim #3: The alternative hypothesis is that no age-related differences in HRFs will be observed, which may suggest that somatosensory and motor cortices are already exhibiting adult-like HRFs by 6 years old.

Summary

The precise delivery of natural, pneumatic stimulation as well as functionally relevant and measurable motor tasks, allows for a novel examination of hemodynamic changes in somatosensory and motor cortices using fNIRS technology. These data are expected to present a longitudinal picture of normal physiologic connectivity and function across a wide range of age (6-13; 19-30 years), which will provide a broader view of how the healthy cerebral cortex operates (in terms of neuronal responses to specific types of stimuli, neurovascular coupling, and cerebral oxygenation).

CHAPTER THREE: RESULTS

After exporting the raw data from the TechEn CW6 device, data points from the 20-second stimulus window across all subjects in each stimulus condition were selected for partial sums integral calculation (performed in Minitab v. 17.2.1). Partial sums integrals have previously been used in studies from our laboratory to estimate the area under the curve of specific time windows in integrated electromyography (IEMG) (Estep & Barlow, 2007) and EEG data (Custead et al., 2015). The partial sums method was used here in an effort to avoid taking block-averaged hemoglobin values during the task periods, as such average sample-based analyses do not provide information regarding the shape of the HRF following stimuli (Tak & Ye, 2014). To calculate the partial sums integral of each channel, all hemoglobin data points between time 0 and 20 seconds were summed and divided by 20, to account for the 50 Hz sampling rate (data sampled in 20 ms increments).

Processed fNIRS data from each participant were first examined for direction of the hemodynamic response in respective cortical gyri (pre-central gyrus for motor conditions, post-central gyrus for somatosensory conditions). If HbO trended positively in putative hand/face regions, it was included in a positive (POS) HRF group, if HbO trended negatively, it was included in a negative (NEG) HRF group (see Figure 3.1 for examples). Partial sums integrals were also examined in putative hand/face channels, and were used to determine group placement. A negative HRF may be indicative of cortical steal, as it is possible that the NIRS probe may not have been placed directly over face/hand pre- and post-central gyri, therefore it may have been capturing hemodynamic

changes from areas adjacent to the active area. Nevertheless, analyses were conducted on both POS and NEG groups.

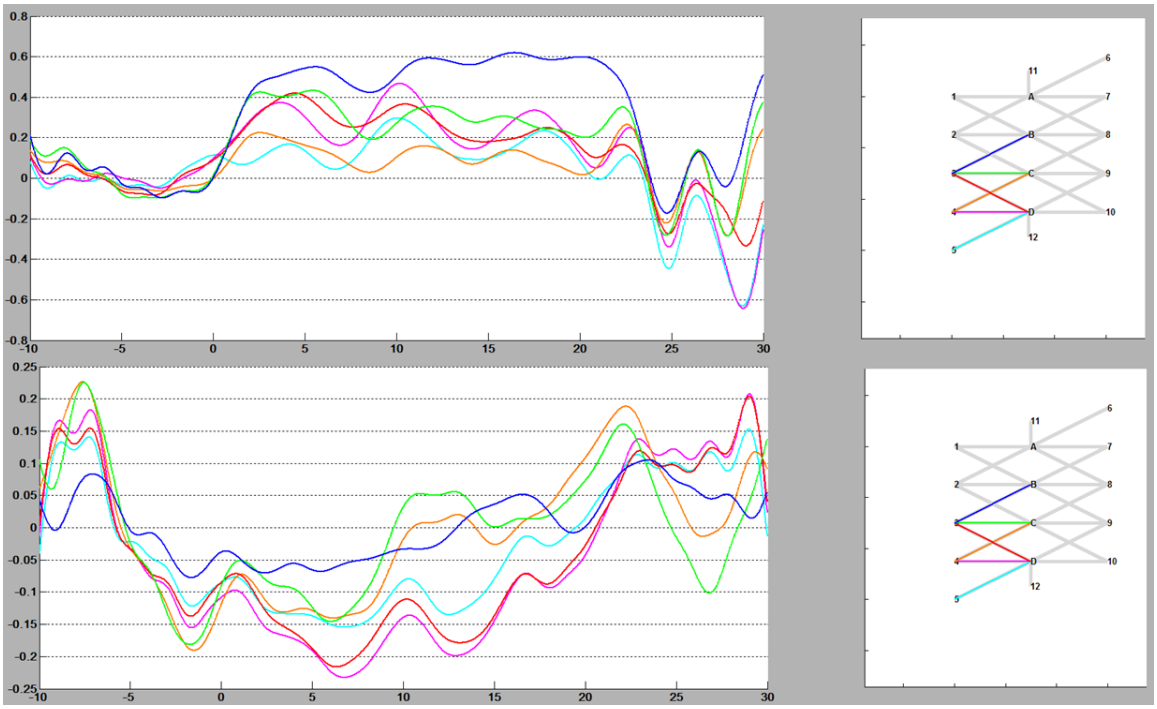

Figure 3.1. Examples of POS and NEG hemodynamic responses during the face motor task, processed in Homer2 (adult subjects N16 and N02, respectively).

Adult Channels of Interest

Only the POS group was used to identify channels of interest, as previous studies have shown that HbO (as opposed to HbR or HbT) is the most sensitive indicator of rCBF in fNIRS (Hoshi, 2007) and has better spatiotemporal correlations with BOLD fMRI (Strangman et al., 2002b), and only those participants who exhibited a positive trending HbO response could provide information regarding channels of activation (and therefore, regions of activation). HbO partial sums integral values were calculated across

all channels in POS participants, and the four adjacent channels that yielded the greatest mean HbO integral were chosen as channels of interest (Figure 3.2), and were included in statistical analyses. In the figure, the channels corresponding to pre-central gyrus (1 through 11) are shown in the left graph, and the channels corresponding to post-central gyrus (14-24) are shown in the right graph, both represented on the respective y-axes. The x-axes are the partial sums (PARSUM) integral values, whose units are in microMolars of HbO per millisecond.

For the hand motor task, NIRS optode channels 4-7 were chosen. For the face motor task, channels 6-9 were chosen. For the hand sensory task, channels 16-19 were chosen. For the face sensory task, channels 18-21 were chosen.

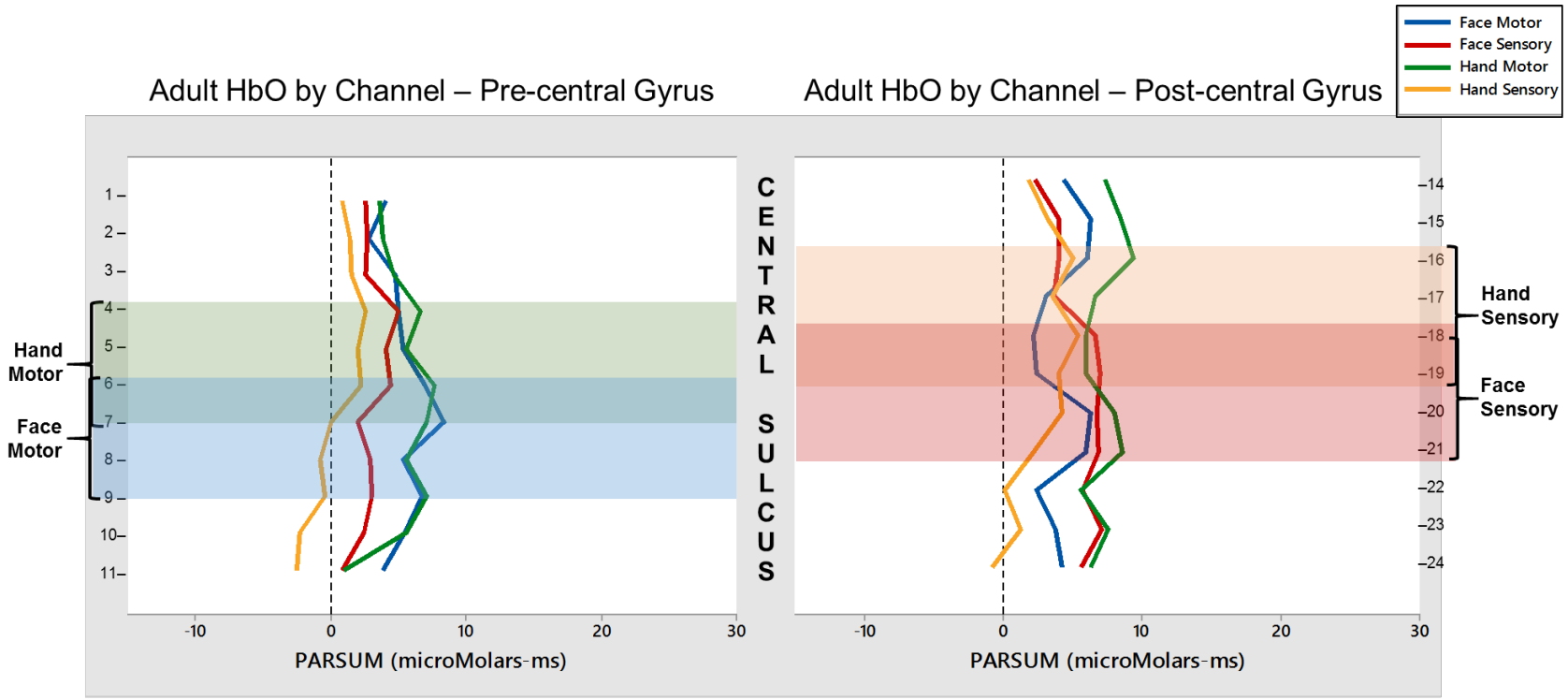

Figure 3.2. Adult channels of interest. The four adjacent channels with the greatest partial sums integral were chosen, and are highlighted in respective colors (hand motor = green, face motor = blue, hand sensory = orange, face sensory = red).

Child Channels of Interest

Just as in the adult data, only child data in the POS group were used to identify channels of interest. HbO partial sums integral values were calculated across all channels in POS participants, and the four adjacent channels that yielded the greatest mean HbO integral were chosen as channels of interest (Figure 3.3), and were included in statistical analyses.

For the hand motor task, channels 5-8 were chosen. For the face motor task, channels 6-9 were chosen. For the hand sensory task, channels 14-17 were chosen. For the face sensory task, channels 21-24 were chosen.

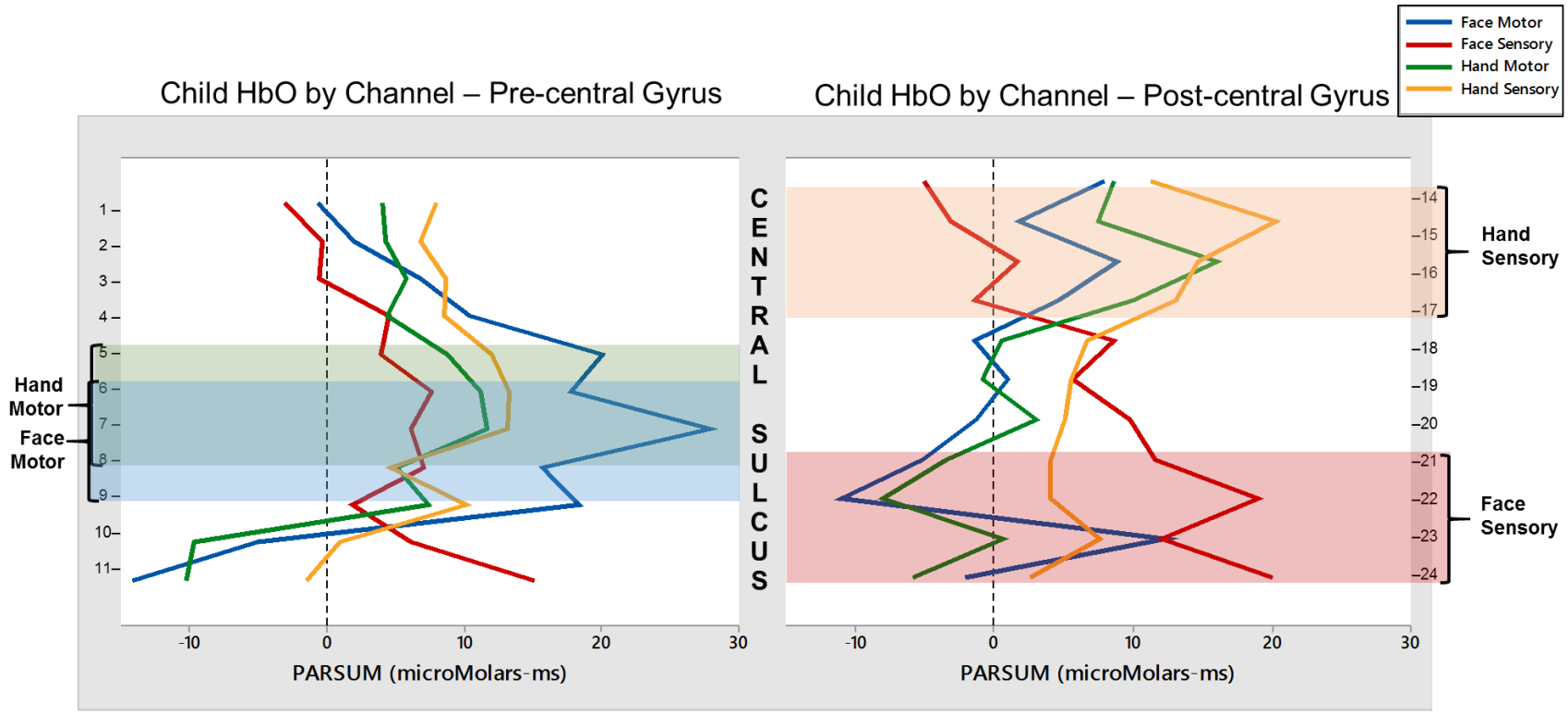

Figure 3.3. Child channels of interest. The four adjacent channels with the greatest partial sums integral were chosen, and are highlighted in respective colors (hand motor = green, face motor = blue, hand sensory = orange, face sensory = red).

POS Group Hemodynamic Response Curves

For visual inspection of the group HRFs, the Plot Probe feature in Homer2 was used. This view provides group averaged HbO and HbR (red and blue, respectively) data across the -10 to +30 time window in all 22 channels (processed fNIRS data, not partial sums integrals). Green lines represent the short separation channels whose signals were regressed out of the processed data, removing systemic interference of superficial origin (i.e. heartbeat). Figures 3.4, 3.5, 3.6, and 3.7 correspond to adult face, adult hand, child face, and child hand conditions, respectively. The sample sizes listed indicate the number of participants allotted to the POS group.

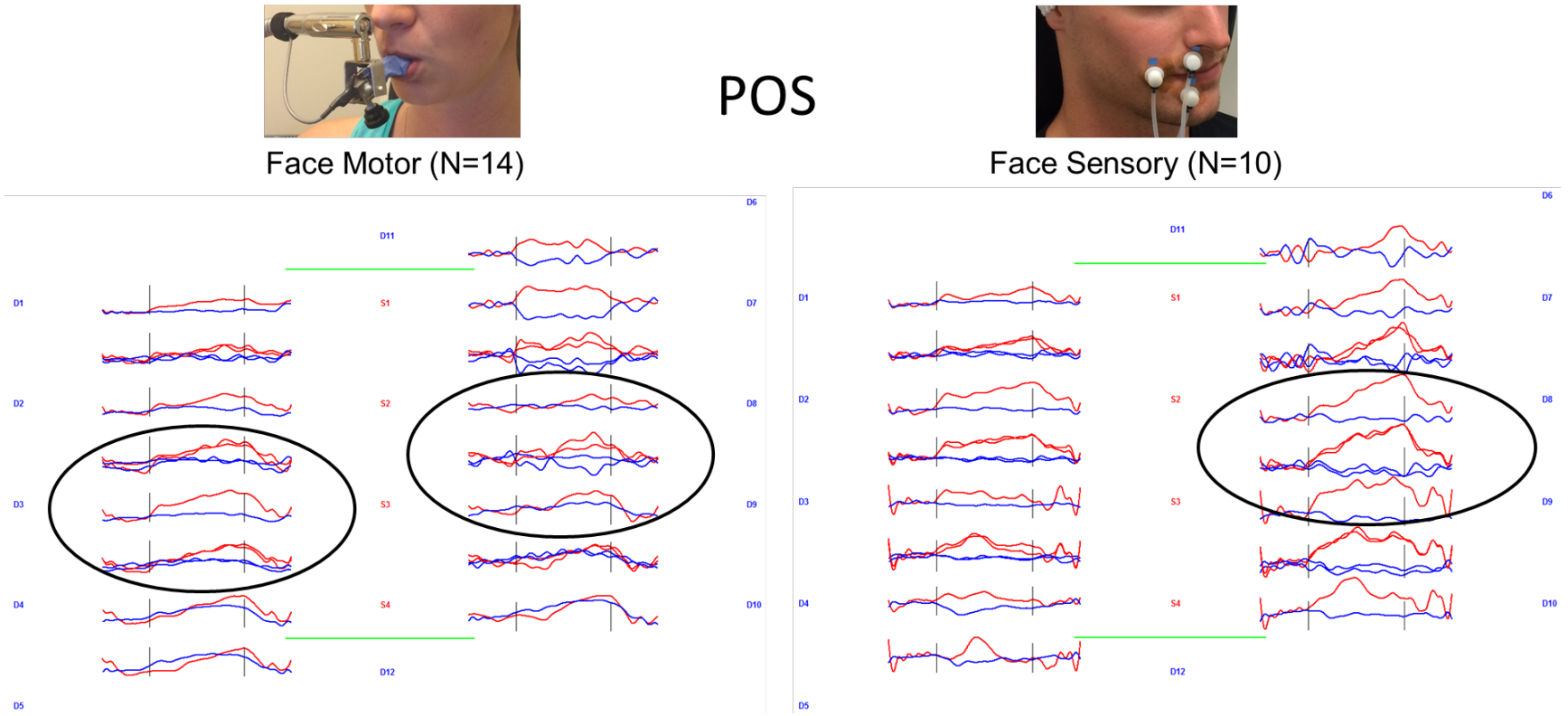

Figure 3.4. POS adult face conditions. Channels circled indicate those chosen using the partial sums integral method. Red lines = oxyhemoglobin, blue lines = deoxyhemoglobin.

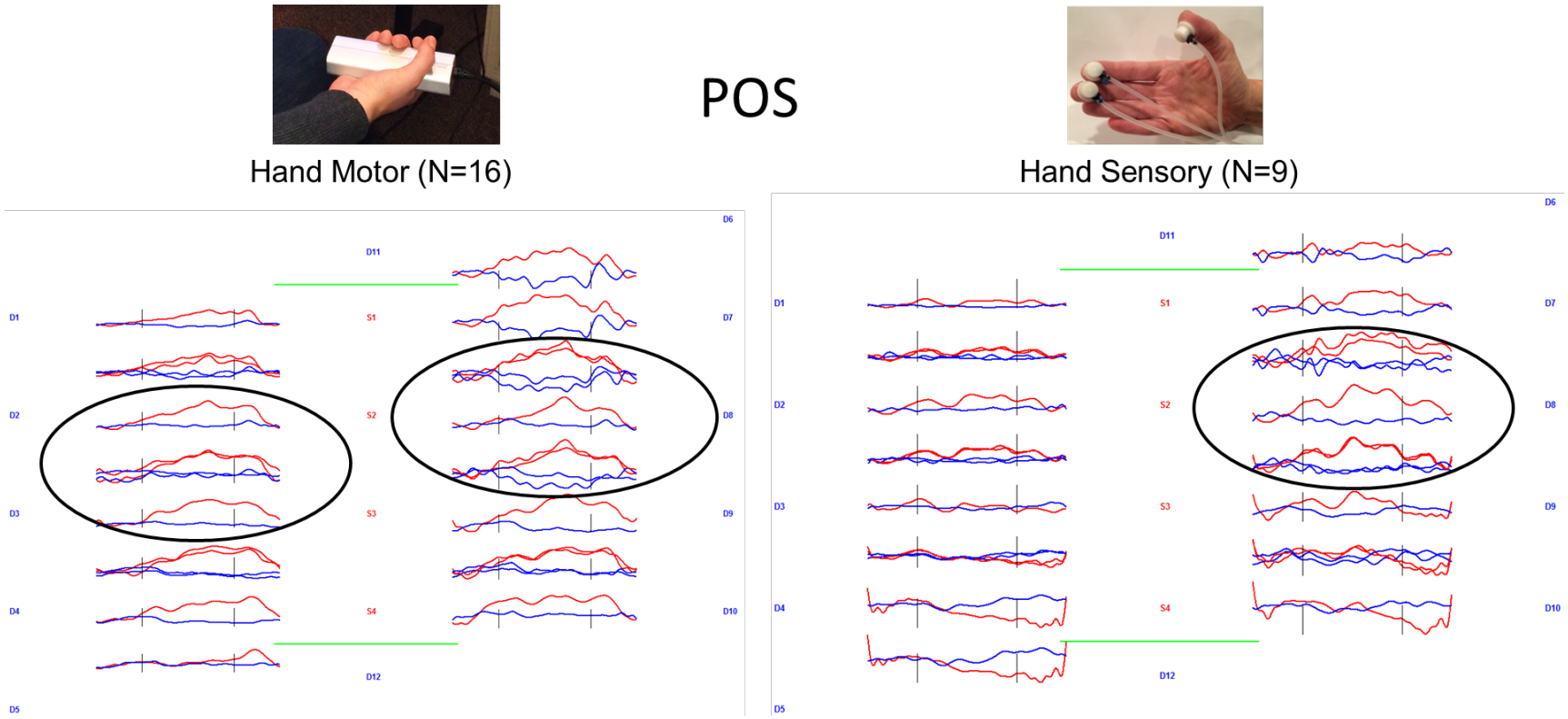

Figure 3.5. POS adult hand conditions. Channels circled indicate those chosen using the partial sums integral method. Red lines = oxyhemoglobin, blue lines = deoxyhemoglobin.

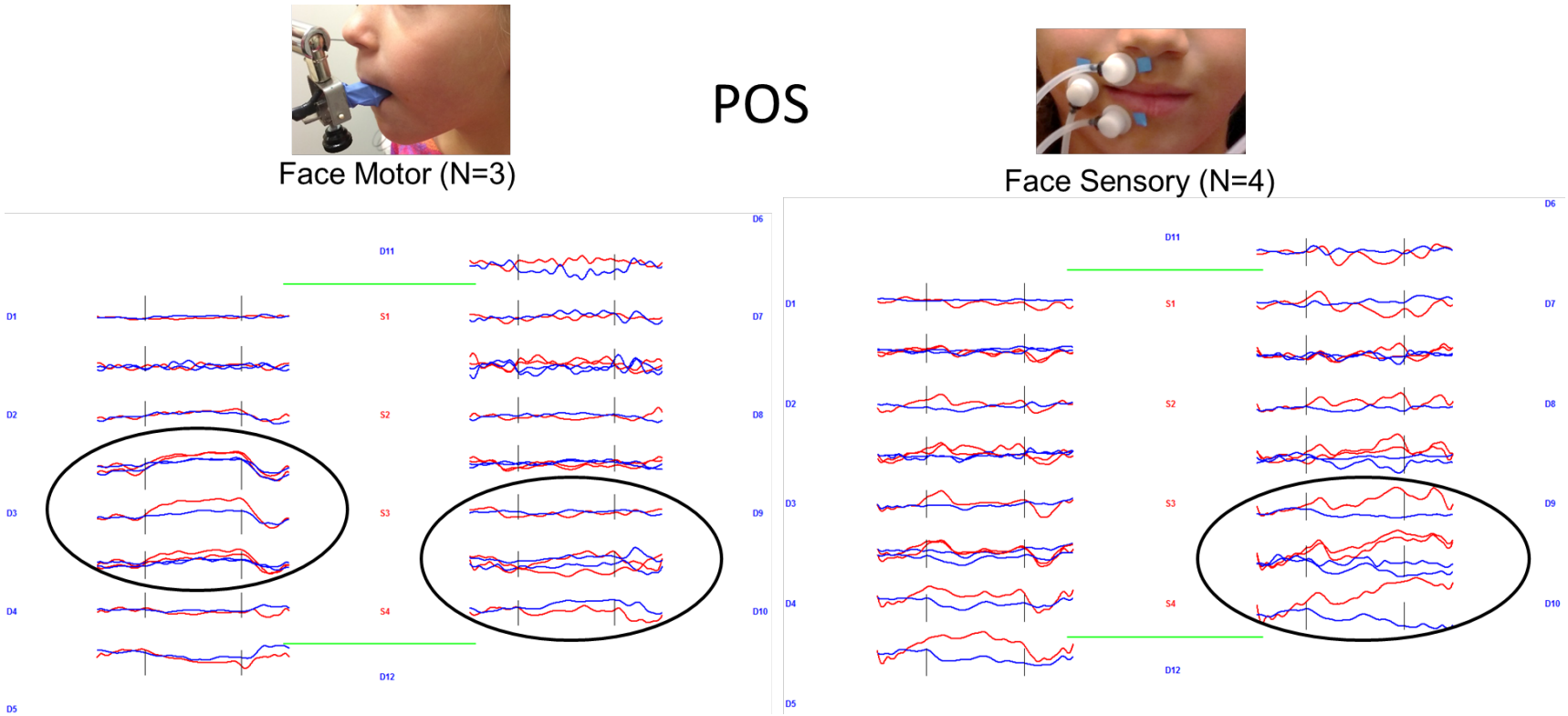

Figure 3.6. POS child face conditions. Channels circled indicate those chosen using the partial sums integral method. Red lines = oxyhemoglobin, blue lines = deoxyhemoglobin.

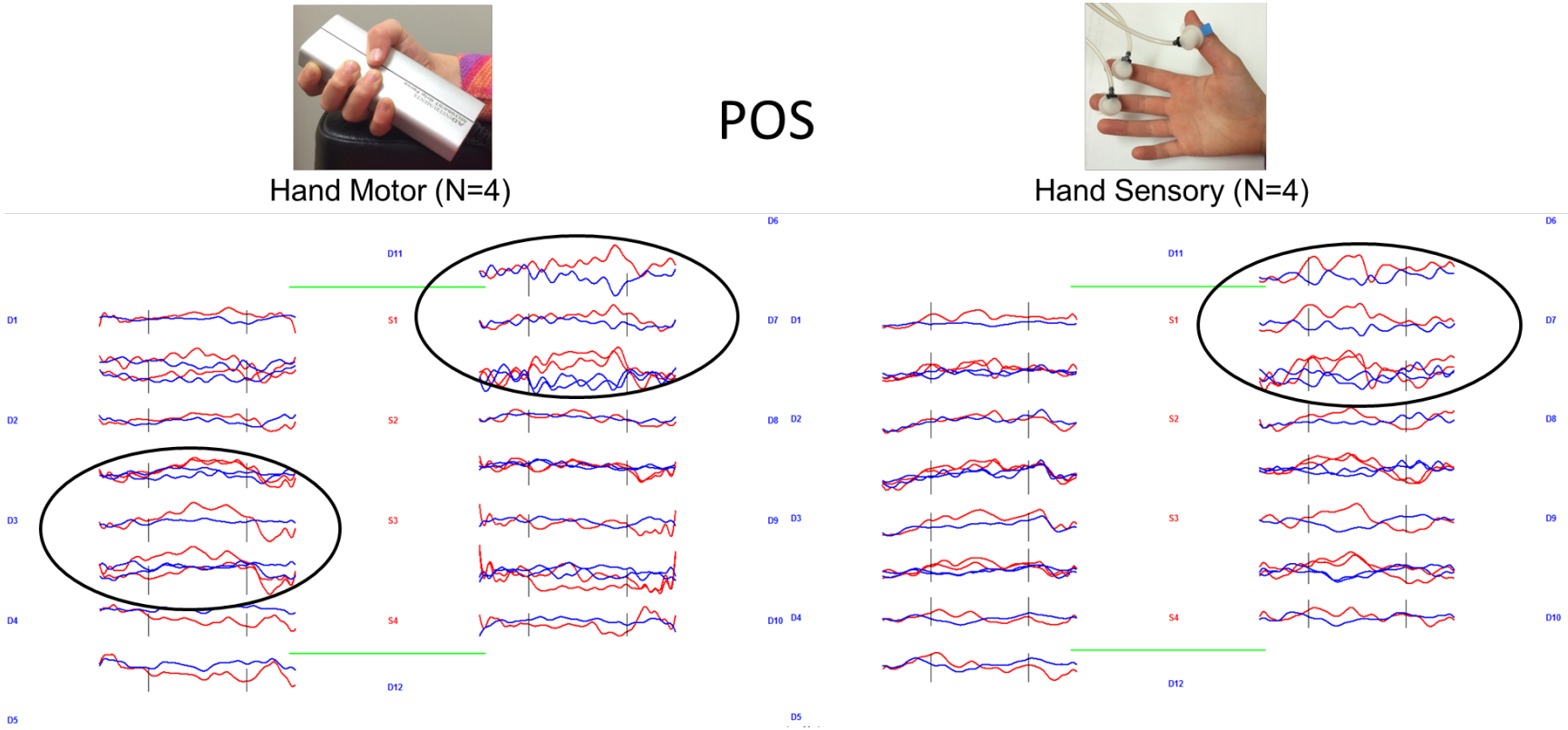

Figure 3.7. POS child hand conditions. Channels circled indicate those chosen using the partial sums integral method. Red lines = oxyhemoglobin, blue lines = deoxyhemoglobin.

NEG Group Hemodynamic Response Curves

The same Plot Probe feature in Homer2 that was used for visual inspection of the POS group HRFs was used to view the NEG group HRFs. Figures 3.8, 3.9, 3.10, and 3.11 correspond to adult face, adult hand, child face, and child hand conditions, respectively. The sample sizes listed indicate the number of participants allotted to the NEG group. The channels circled are those channels of interest that were chosen in the POS group, and they are circled in the NEG group for comparison. Though the HRF in some channels may appear to trend positively, the mean HbO integral of the channels of interest was typically either negative, or very close to zero.

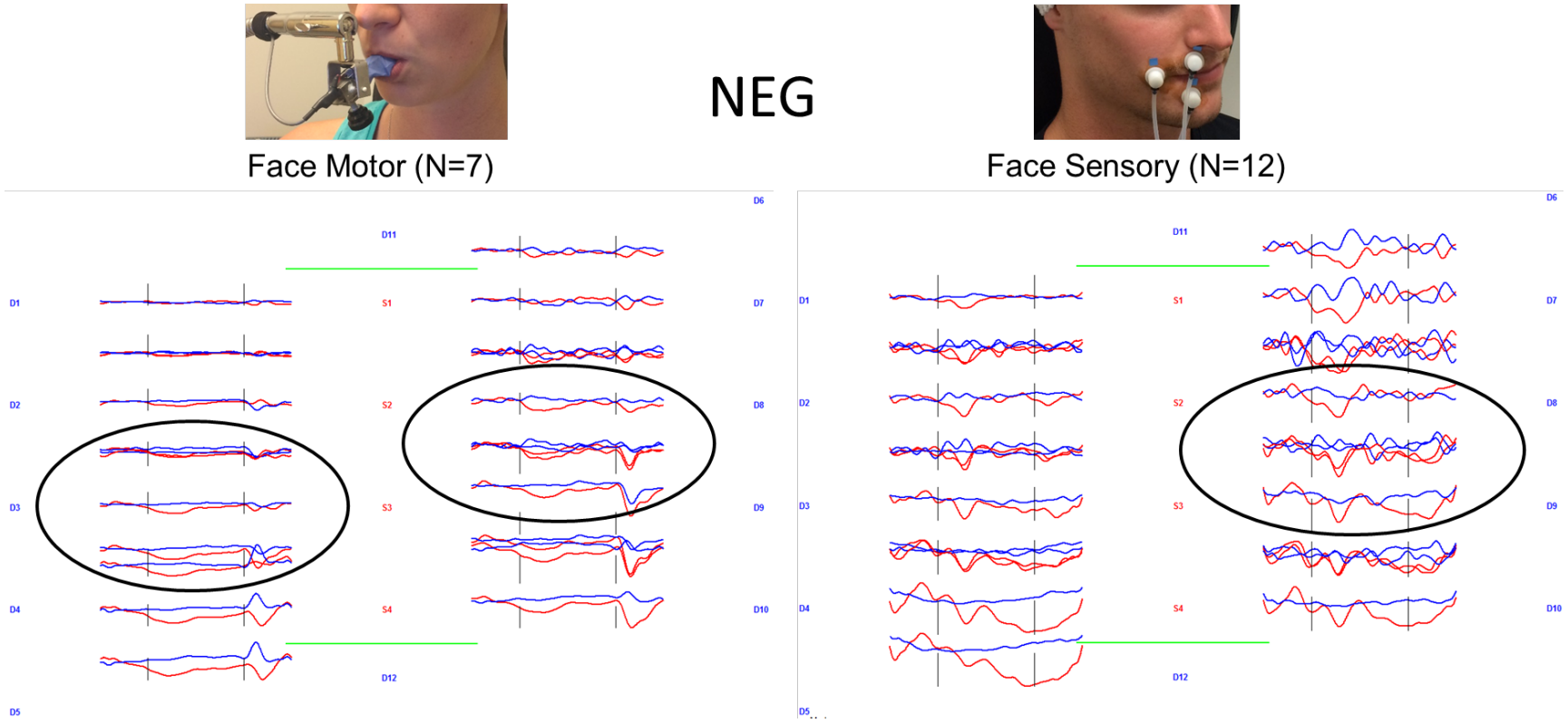

Figure 3.8. NEG adult face conditions. Channels circled indicate those chosen using the partial sums integral method. Red lines = oxyhemoglobin, blue lines = deoxyhemoglobin.

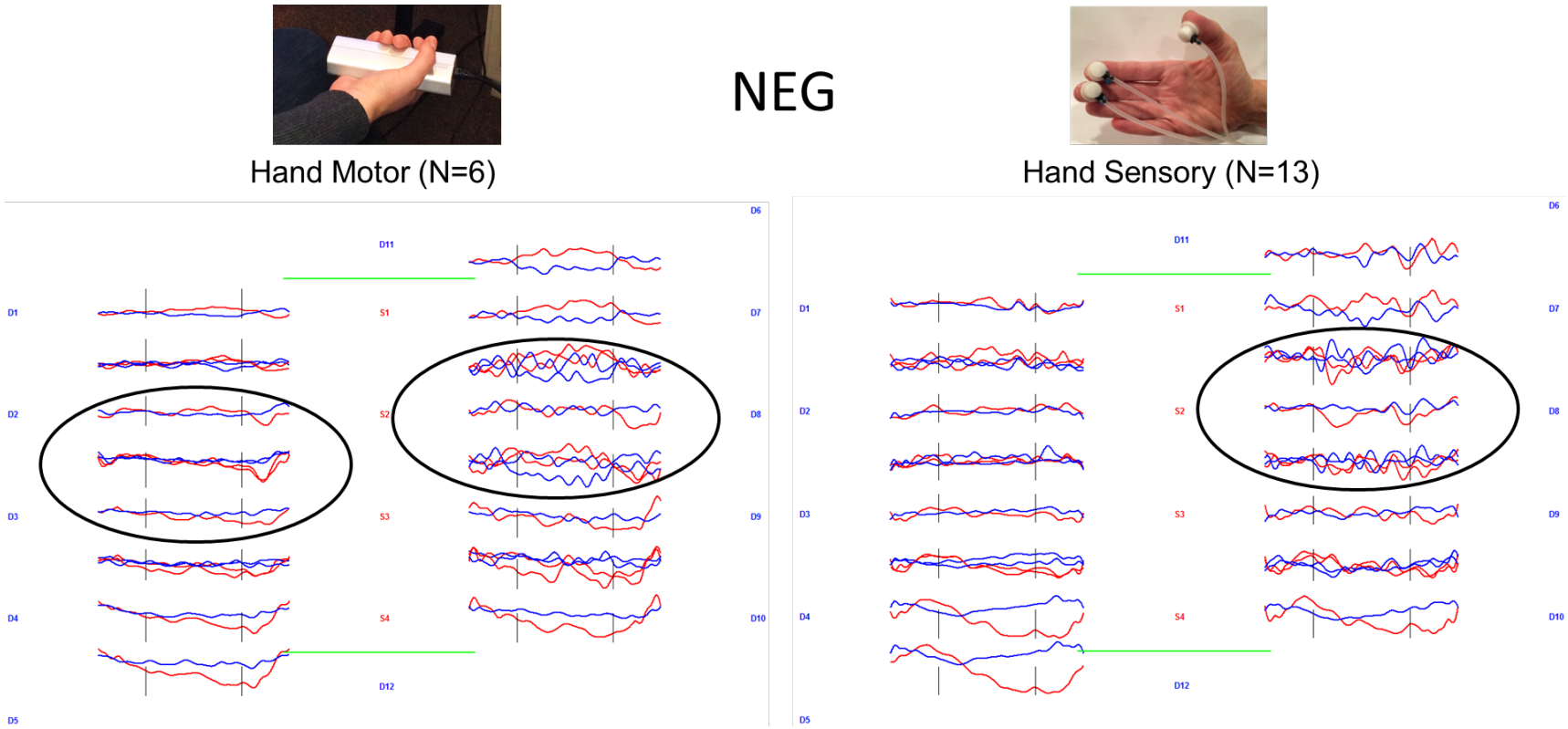

Figure 3.9. NEG adult hand conditions. Channels circled indicate those chosen using the partial sums integral method. Red lines = oxyhemoglobin, blue lines = deoxyhemoglobin.

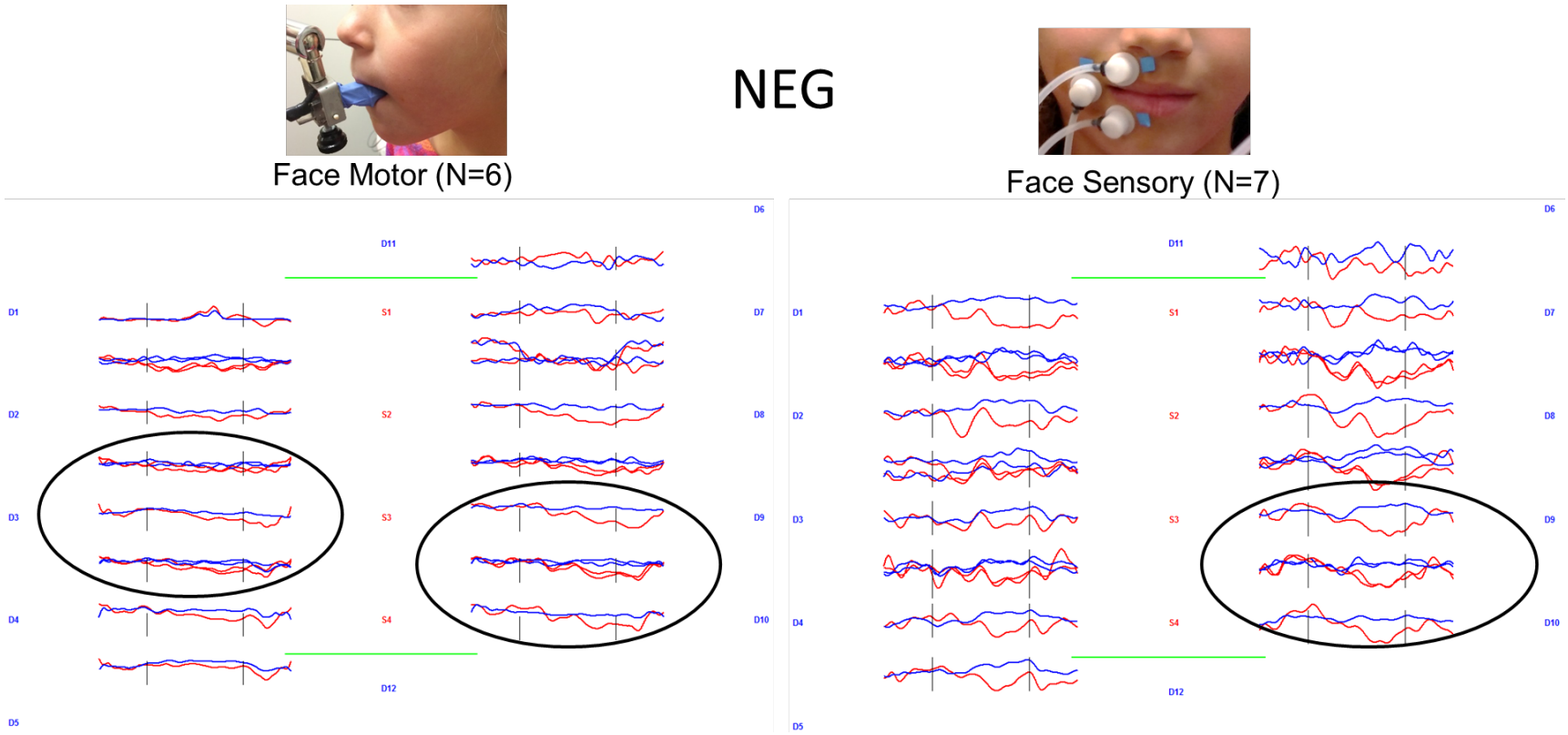

Figure 3.10. NEG child face conditions. Channels circled indicate those chosen using the partial sums integral method. Red lines = oxyhemoglobin, blue lines = deoxyhemoglobin.

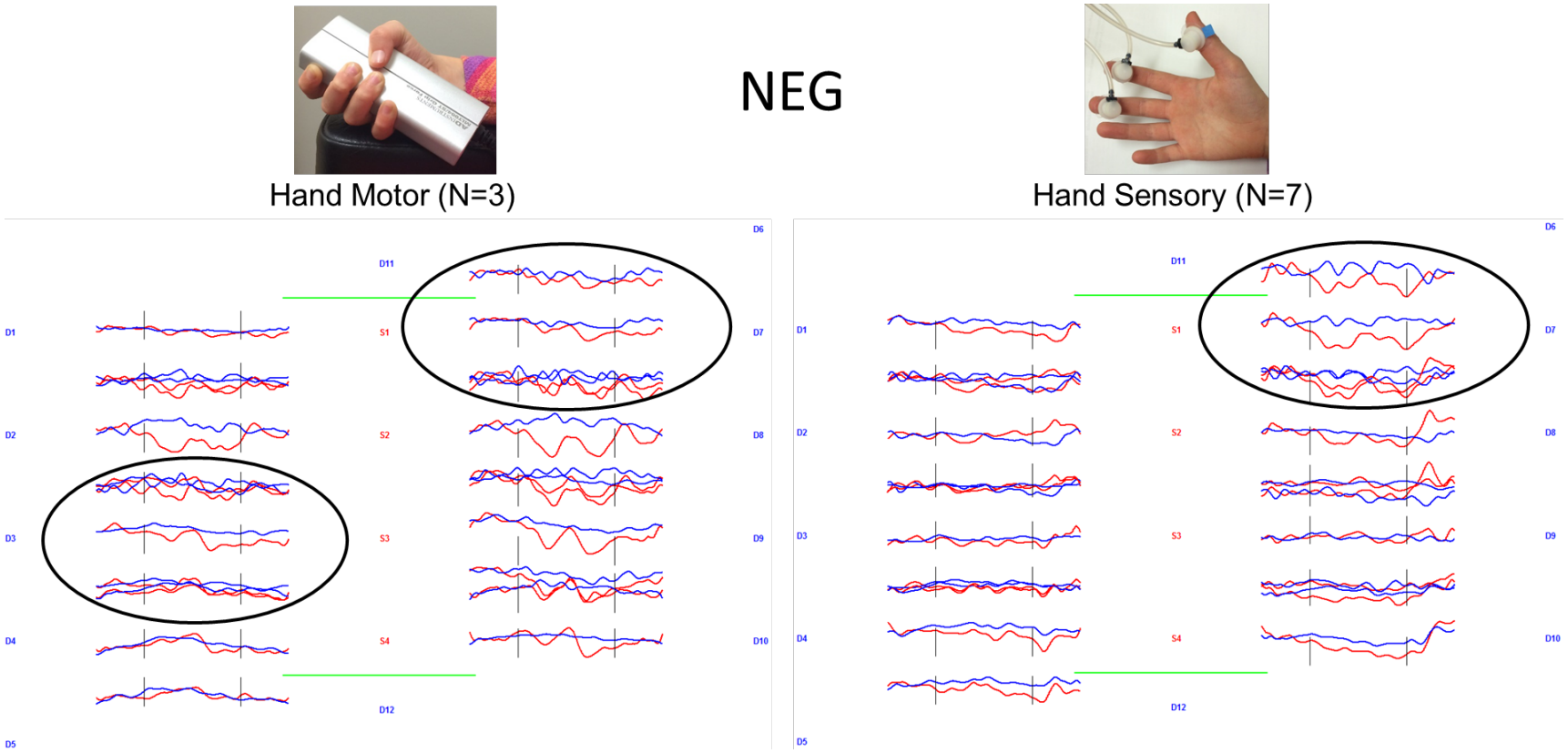

Figure 3.11. NEG child hand conditions. Channels circled indicate those chosen using the partial sums integral method. Red lines = oxyhemoglobin, blue lines = deoxyhemoglobin.

HbO Outcomes by Cortical Region (M1 vs. S1)

The HbO partial sums integrals were calculated across all four channels of interest for statistical analyses. To examine the effect that a single stimulus modality had on the HbO levels in different cortical regions, the motor and somatosensory channels of interest were compared using ANOVA. Since the assumption of homogeneity of variance was not met for all of the data, and because of the unequal sample sizes across the conditions, the Welch's adjusted F-ratio was used. For the POS group, significant differences were found between mean M1 and S1 HbO levels during the face and hand somatosensory stimulus conditions for the adults, and during the face motor and face somatosensory stimulus conditions for children (Table 3.1). The face motor task elicited significantly greater HbO levels in M1 in children only. Face and hand somatosensory stimulation elicited significantly greater HbO levels in S1 in adults, while HbO levels were only significantly greater in S1 for children during the face somatosensory condition. Mean HbO was greater in S1 than M1 during hand somatosensory stimulation in children, though it was not significant.

For the NEG group, ANOVA revealed a significant difference during the hand sensory condition for both adults and children (Table 3.2). In this particular condition, HbO levels were significantly lesser in S1 than in M1. No other conditions elicited significantly different HbO concentration levels in the different cortical regions for the NEG group.

Table 3.1. Oxyhemoglobin outcomes by cortical region of interest for the POS group.

Task	Primary Cortical Region	Mean (HbO PARSUM)	Standard Error (HbO PARSUM)	Welch's F	p-value	Effect size
ADULT						
Face Motor	**M1**	6.8702	0.7421	3.79	.054	0.37
	S1	4.2420	1.1271			
Face Sensory	**M1**	3.1330	0.7786	4.64	.035	0.48
	S1	6.8189	1.5230			
Hand Motor	**M1**	6.7600	1.0031	0.02	.889	0.03
	S1	6.9710	1.1340			
Hand Sensory	**M1**	1.7061	0.3599	32.62	<.001	1.35
	S1	4.4864	0.3278			
CHILD						
Face Motor	**M1**	19.9173	6.8879	6.55	.019	1.05
	S1	-1.4720	4.7376			
Face Sensory	**M1**	5.2600	1.1803	20.83	<.001	1.61
	S1	15.7006	1.9598			
Hand Motor	**M1**	9.1642	1.8499	0.19	.665	0.15
	S1	10.5544	2.5779			
Hand Sensory	**M1**	10.7401	3.0509	0.72	.404	0.30
	S1	14.8154	3.7156			

Table 3.2. Oxyhemoglobin outcomes by cortical region of interest for the NEG group.

Task	Primary Cortical Region	Mean (HbO PARSUM)	Standard Error (HbO PARSUM)	Welch's F	p-value	Effect size
ADULT						
Face Motor	**M1**	-4.3857	1.1345	0.11	.743	0.09
	S1	-4.9735	1.3729			
Face Sensory	**M1**	-1.9878	0.4771	0.09	.765	0.06
	S1	-2.1885	0.4684			
Hand Motor	**M1**	-1.5743	0.6802	3.02	.093	0.50
	S1	2.3887	2.1751			
Hand Sensory	**M1**	0.3644	0.5979	6.69	.011	0.51
	S1	-1.7512	0.5582			
CHILD						
Face Motor	**M1**	-5.6454	2.0312	0.25	.620	0.14
	S1	-7.1442	2.2121			
Face Sensory	**M1**	-2.9547	2.9211	0.53	.472	0.19
	S1	-5.4360	1.7822			
Hand Motor	**M1**	-3.2077	2.3796	1.67	.214	0.53
	S1	-6.6445	1.1878			
Hand Sensory	**M1**	-0.6934	1.5204	10.56	.002	0.87
	S1	-11.7127	3.0316			

HbO Outcomes by Stimulus Site (Face vs. Hand)

To examine the effect that the same type of stimulus had on different stimulus sites, a one-way ANOVA was performed on HbO levels in both cortical regions across all groups (POS adults, POS children, NEG adults, NEG children), and a priori contrasts determined if HbO differences existed in respective cortical regions during the same type of activity in different body sites (e.g. face motor vs. hand motor, face sensory vs. hand sensory.). Again, because the assumption of homogeneity of variance was not met for all data, and because of the unequal sample sizes across the conditions, the Welch's adjusted F-ratio was used. For the POS adult group, a significant difference was found between HbO levels in M1 during the conditions [Welch's $F(3,100.9) = 17.8$, $p < .001$], but not in S1. For the POS child group, a significant difference was found between HbO levels in S1 during the conditions [Welch's $F(3,28.24) = 3.92$; $p = .019$], but not in M1. However, a priori contrasts revealed that there were no significant HbO differences between hand and face stimulation of either type in respective cortical regions for adults or children (Table 3.3). For the NEG adult group, significant differences were found between HbO levels in M1 [Welch's $F(3,66.16) = 5.62$, $p = .002$] and S1 [Welch's $F(3,58.07) = 2.95$, $p = .04$] during the conditions, while no significant differences were seen in the NEG child group. A priori contrasts revealed a significant HbO difference between hand and face motor stimulation for NEG adults, with lesser HbO values in M1 during the face motor task, while no difference was seen during the somatosensory stimulation conditions. (Table 3.4).

Table 3.3. Oxyhemoglobin outcomes by stimulus site for the POS group.

Task	Primary Cortical Region	Mean (HbO PARSUM)	Standard Error (HbO PARSUM)	p-value	Effect size
ADULT					
Motor	**Face M1**	6.8702	0.7421	.930	0.02
	Hand M1	6.7600	1.0031		
Sensory	**Face S1**	6.8189	1.5230	.142	0.33
	Hand S1	4.4864	0.3278		
CHILD					
Motor	**Face M1**	19.9173	6.8879	.156	0.65
	Hand M1	9.1642	1.8499		
Sensory	**Face S1**	15.7006	1.9598	.835	0.07
	Hand S1	14.8154	3.7156		

Table 3.4. Oxyhemoglobin outcomes by stimulus site for the NEG group.

Task	Primary Cortical Region	Mean (HbO PARSUM)	Standard Error (HbO PARSUM)	p-value	Effect size
ADULT					
Motor	**Face M1**	-4.3857	1.1345	.039	0.57
	Hand M1	-1.5743	0.6802		
Sensory	**Face S1**	-2.1885	0.4684	.550	0.12
	Hand S1	-1.7512	0.5582		
CHILD					
Motor	**Face M1**	-5.6454	2.0312	.443	0.26
	Hand M1	-3.2078	2.3796		
Sensory	**Face S1**	-5.4360	1.7822	.081	0.48
	Hand S1	-11.7127	3.0316		

HbO Outcomes by Type of Stimulus (Active vs. Passive)

To examine the effect that different types of stimuli had on the same stimulus site, a one-way ANOVA was performed on HbO levels in respective cortical regions (M1 for

motor conditions, S1 for somatosensory conditions) during the different types of stimuli (active motor vs. passive somatosensory) in the same site (hand or face). For the POS adult group, a significant difference was found between HbO integral values in the adult hand stimuli conditions [Welch's $F(1,75.62) = 4.64$, $p = .034$], with the active motor task eliciting greater HbO concentration levels in M1 than the passive somatosensory stimulation in S1 (Table 3.5). There were no significant findings in the face stimulus conditions for the POS adults. The POS child group exhibited no differences in HbO values for either type of stimulus in either stimulus site. For the NEG group, a significant difference was found only in the child hand stimulus conditions [Welch's $F(1,36.51) = 4.87$, $p = .034$], with the passive somatosensory stimulation eliciting more negative HbO concentration levels than the active motor task (Table 3.6).

Table 3.5. Oxyhemoglobin outcomes by type of stimulus for the POS group.

Site	Task & Primary Cortical Region	Mean (HbO PARSUM)	Standard Error (HbO PARSUM)	p-value	Effect size
ADULT					
Face	**Motor M1**	6.8702	0.7421	.976	0.01
	Sensory S1	6.8189	1.5230		
Hand	**Motor M1**	6.7600	1.0031	.034	0.35
	Sensory S1	4.4864	0.3278		
CHILD					
Face	**Motor M1**	19.9173	6.8879	.566	0.25
	Sensory S1	15.7006	1.9598		
Hand	**Motor M1**	9.1642	1.8499	.187	0.48
	Sensory S1	14.8154	3.7156		

Table 3.6. Oxyhemoglobin outcomes by type of stimulus for the NEG group.

Site	Task & Primary Cortical Region	Mean (HbO PARSUM)	Standard Error (HbO PARSUM)	p-value	Effect size
ADULT					
Face	**Motor M1**	-4.3857	1.1345	.082	0.46
	Sensory S1	-2.1885	0.4684		
Hand	**Motor M1**	-1.5743	0.6802	.841	0.05
	Sensory S1	-1.7512	0.5582		
CHILD					
Face	**Motor M1**	-5.6454	2.0312	.939	0.02
	Sensory S1	-5.4360	1.7822		
Hand	**Motor M1**	-3.2078	2.3796	.034	0.60
	Sensory S1	-11.7127	3.0316		

HbO Outcomes by Stimulus Time (Pre vs. During, During vs. Post)

To examine the overall effect of stimulation on HbO across the duration of the analysis time window, ANOVA was performed to determine whether significant differences existed between the partial sums integral values in the channels of interest at the following times relative to stimulus onset across all conditions: -10 to 0 (pre-stimulus), 0 to 20 (during stimulus), and 20 to 30 (post-stimulus). Figures 3.12 through 3.15 show the omnibus Welch's F statistics (used due to the violation of the assumption of homogeneity of variances), as well as the *p*-values for the a priori contrasts. These contrasts tested for differences between integral values at pre-stimulus and during stimulus times, and between during stimulus and post-stimulus times across adult and child participants (both POS and NEG groups). Across all groups and all stimulus conditions, the pre-stimulus mean integral value was very near to zero at baseline. In general, the post-stimulus mean integral trended back toward baseline (more negative in

the POS group, more positive in the NEG group) following the offset of the stimulus, though very rarely did it cross zero.

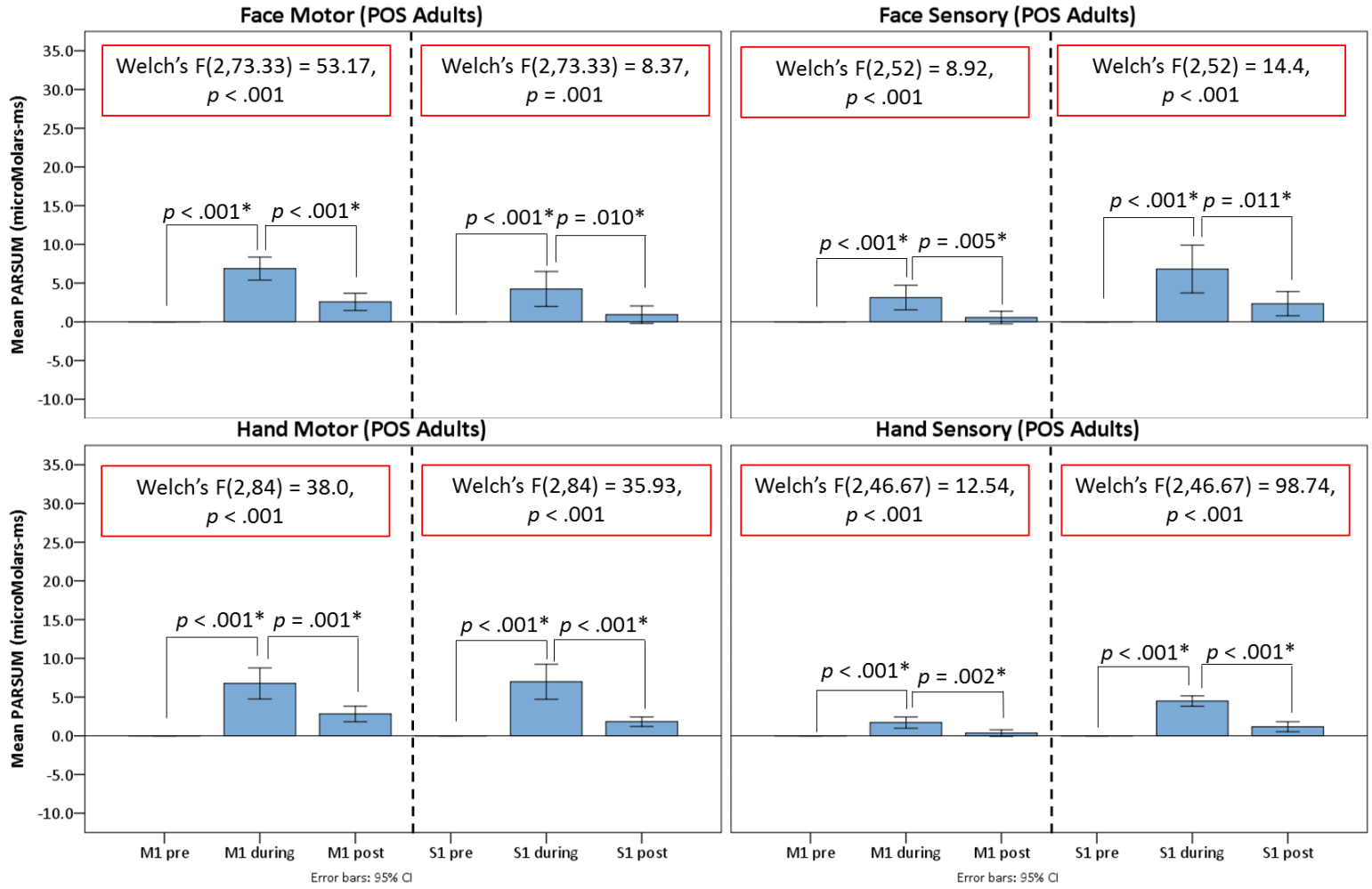

Figure 3.12. Oxyhemoglobin outcomes by stimulus time for the adult POS group. The dotted line divides the motor and somatosensory channels in each stimulus condition.

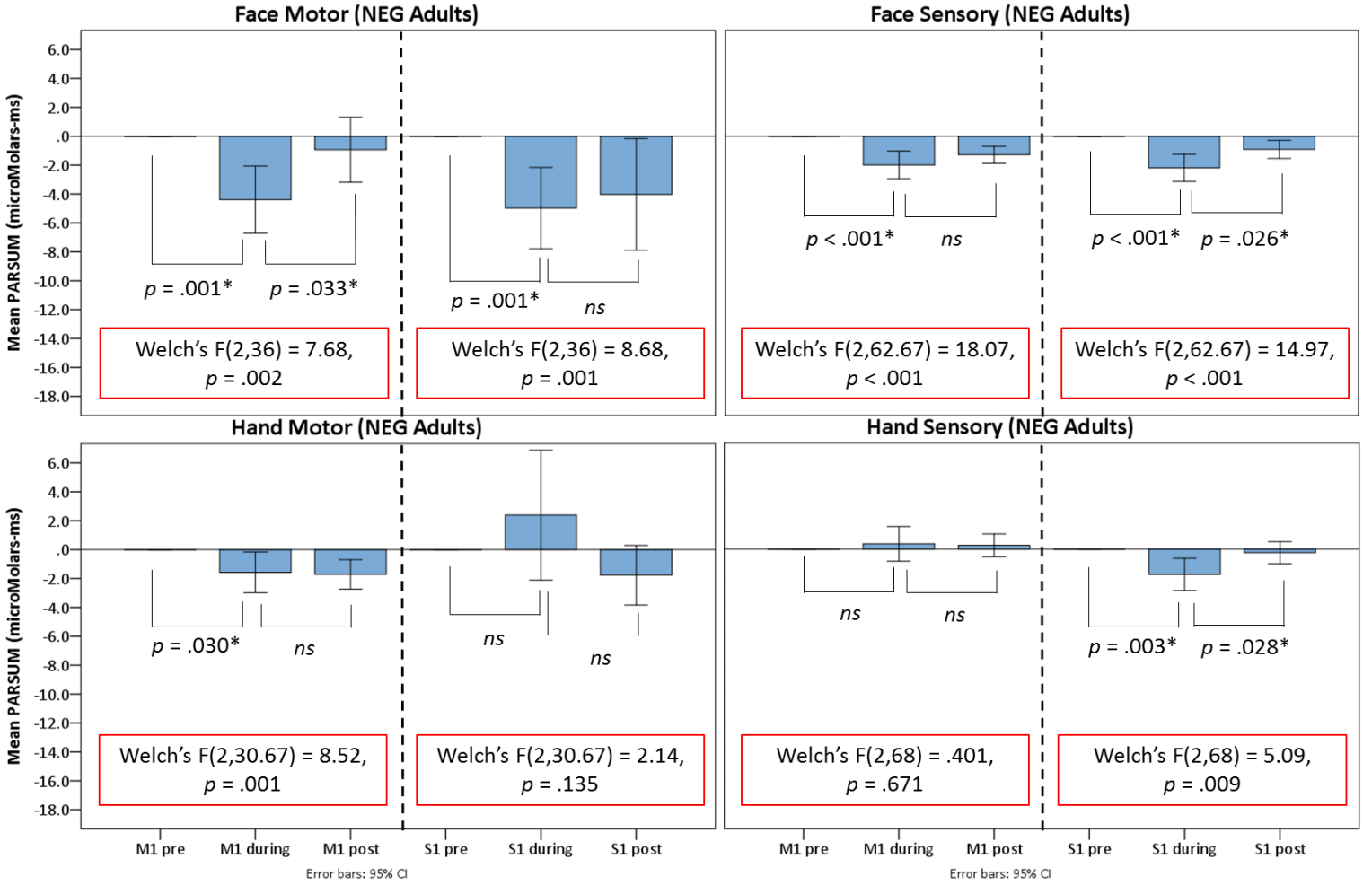

Figure 3.13. Oxyhemoglobin outcomes by stimulus time for the adult NEG group. The dotted line divides the motor and somatosensory channels in each stimulus condition.

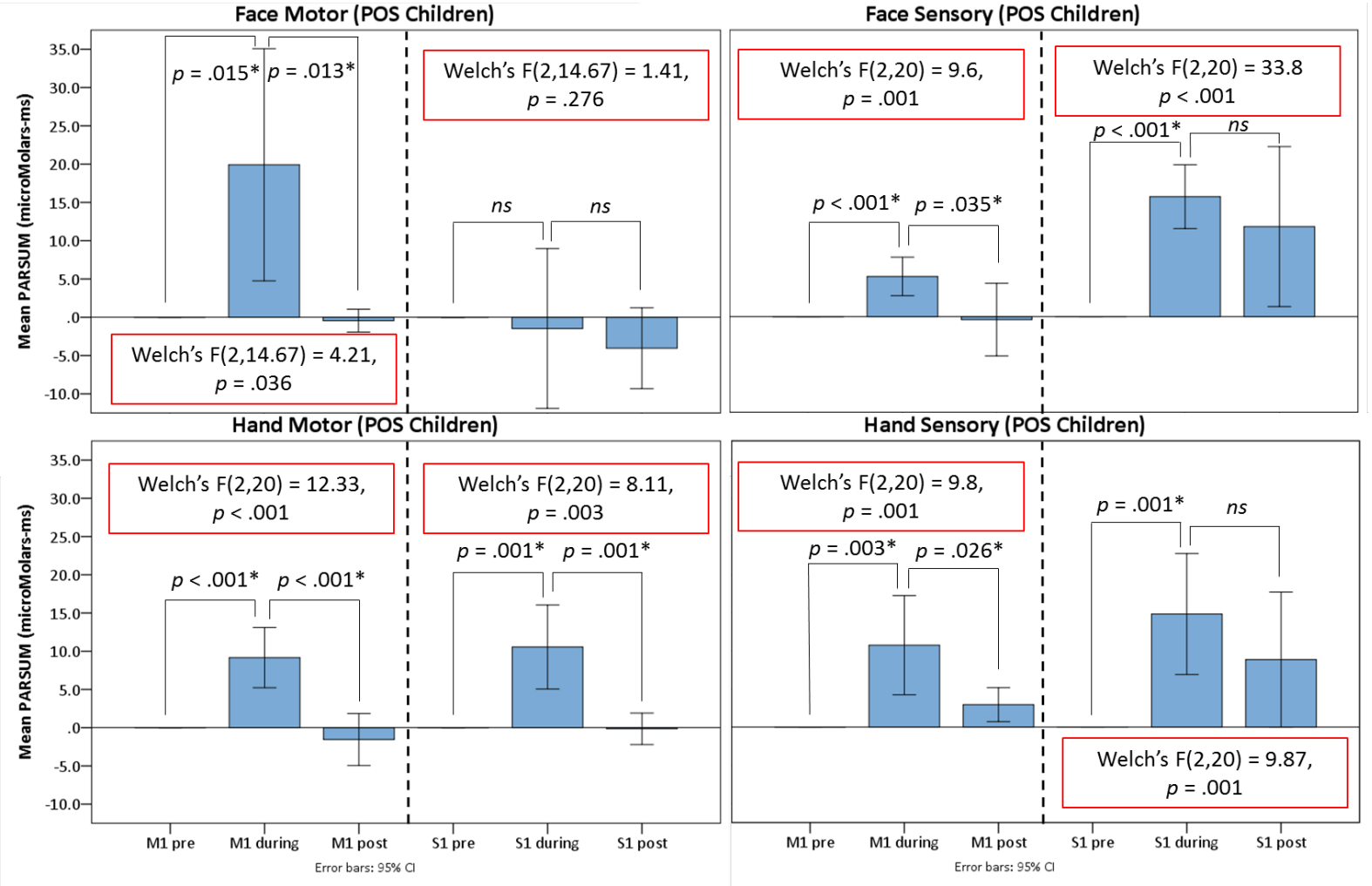

Figure 3.14. Oxyhemoglobin outcomes by stimulus time for the child POS group. The dotted line divides the motor and somatosensory channels in each stimulus condition.

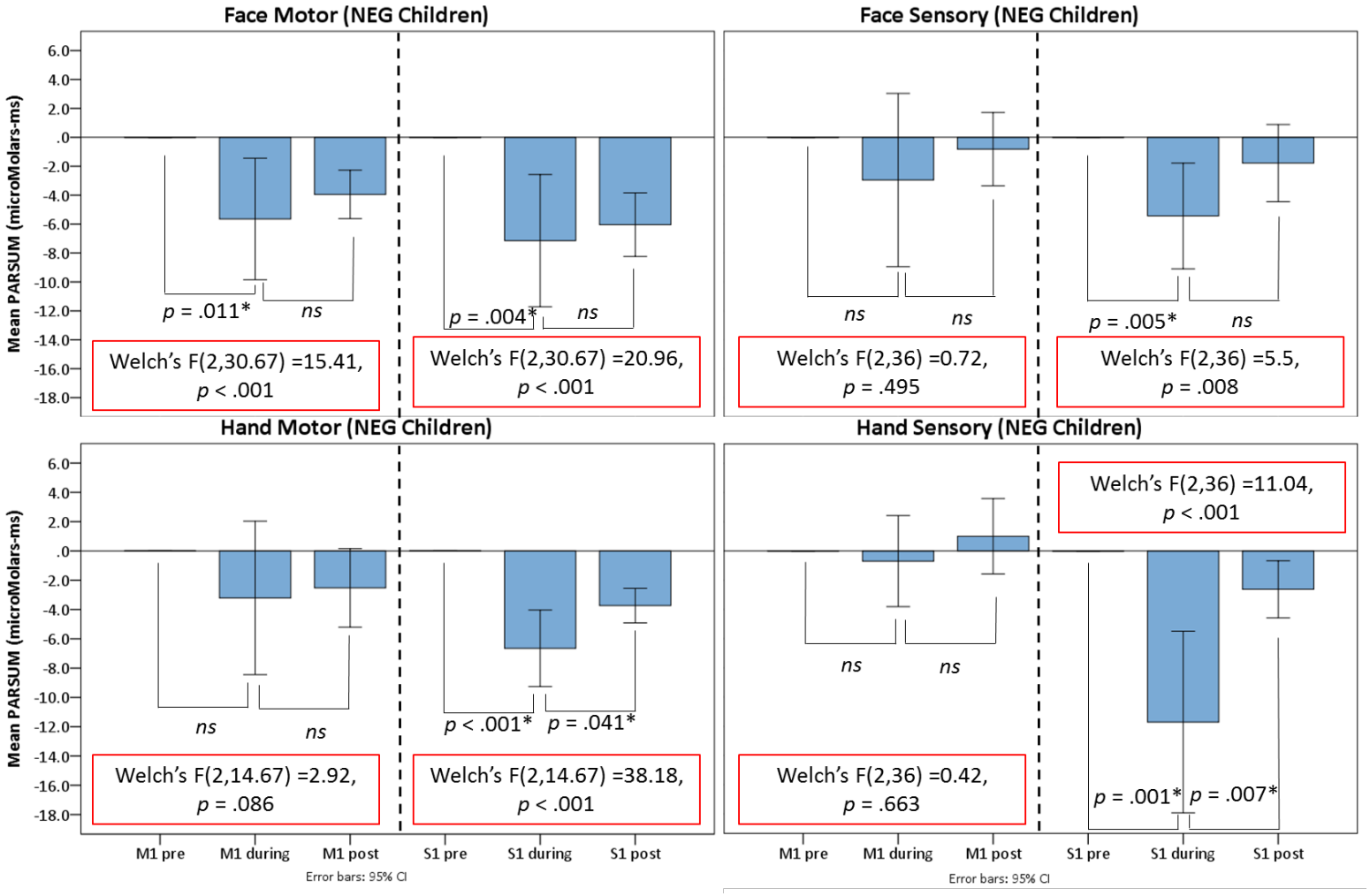

Figure 3.15. Oxyhemoglobin outcomes by stimulus time for the child POS group. The dotted line divides the motor and somatosensory channels in each stimulus condition.

Adaptation Patterns

To examine adaptation patterns among participant groups, raw fNIRS data was processed in Homer2, and group HRFs from the channels of interest were averaged to yield mean HbO concentration levels in M1 and S1 over the entire 20 second stimulus period for all conditions. Partial sums integral values could not be used for this analysis, as that calculation provides a single point estimate for the area under the curve. Because adaptation occurs over time, the average HbO levels for the 4 motor and 4 somatosensory channels of interest were calculated over the 20 second stimulus block of each condition, and a polynomial regression analysis was performed to examine quadratic trends in fNIRS data.

It is well established that hemodynamic activity occurs on a much longer time scale than neuronal activity (seconds as opposed to milliseconds), therefore it was of particular interest to examine the "early" (first 10 seconds) and "late" (last 10 seconds) components of the hemodynamic responses during the stimulus blocks. By breaking down the HRFs into early and late components, HbO trends can be examined more thoroughly for adaptation patterns. Tables 3.7 and 3.8 (adults and children, respectively) list the quadratic regression equations, coefficients of determination (R^2), F-statistics, and significance values (*p*-values) across all stimulus conditions for both POS and NEG groups in each respective cortical area. Figures 3.16-3.19 correspond to the adult HRF data, and Figures 3.20-3.23 correspond to the child HRF data. Processed HRFs in channels of interest from Homer2 are shown on the left side of the figures, and average HbO concentration levels over the stimulus blocks are shown on the right side. Quadratic

trend lines for early and late components are represented by dotted lines. All regressions were significant.

Table 3.7. Polynomial regression results for adult groups.

Task	Group	Cortical Region	Model (early)	R^2 (%)	F (2,498)	*p*-value	Model (late)	R^2 (%)	F (2,498)	*p*-value
Face Motor	**POS**	**M1**	$y= 0.03528 + 0.01247 x - 0.000253 x^2$	87.9	1809.70	< .001	$y= -0.1015 + 0.03342 x - 0.000897 x^2$	80.8	1050.11	< .001
		S1	$y= 0.02903 - 0.006196 x + 0.001018 x^2$	46.9	219.50	< .001	$y= -0.2896 + 0.05457 x - 0.001736 x^2$	63.2	428.53	< .001
	NEG	**M1**	$y= - 0.05942 - 0.03416 x + 0.003229 x^2$	98.4	15440.19	< .001	$y= - 0.03433 - 0.008112 x + 0.000442 x^2$	96.6	7049.50	< .001
		S1	$y= - 0.04589 - 0.05246 x + 0.005015 x^2$	96.6	6977.90	< .001	$y= - 0.3019 + 0.03018 x - 0.000894 x^2$	41.2	174.39	< .001
Face Sensory	**POS**	**M1**	$y=0.03351 + 0.009411 x - 0.000382 x^2$	90.9	2492.47	< .001	$y= 0.1990 - 0.01735 x + 0.000508 x^2$	69.7	572.65	< .001
		S1	$y=0.03394 + 0.01132 x + 0.000063 x^2$	93.3	3450.79	< .001	$y= 0.2153 - 0.01159 x + 0.000594 x^2$	89.9	2210.55	< .001
	NEG	**M1**	$y= 0.01312 - 0.02790 x + 0.002669 x^2$	55.4	309.04	< .001	$y= 0.06315 - 0.01154 x + 0.000280 x^2$	78.6	914.35	< .001
		S1	$y= - 0.008950 - 0.03177 x + 0.003328 x^2$	58.6	352.94	< .001	$y= 0.1112 - 0.01496 x + 0.000354 x^2$	70.4	591.80	< .001
Hand Motor	**POS**	**M1**	$y=0.04362 + 0.01311 x - 0.000295 x^2$	90.4	2333.25	< .001	$y= - 0.1823 + 0.05122 x - 0.001765 x^2$	72.9	669.02	< .001
		S1	$y=0.06270 + 0.004237 x + 0.000620 x^2$	97.9	11877.82	< .001	$y= - 0.4343 + 0.09175 x - 0.003265 x^2$	84.4	1349.84	< .001
	NEG	**M1**	$y= 0.02175 - 0.01865 x + 0.001410 x^2$	90.4	2345.25	< .001	$y= - 0.1645 + 0.02251 x - 0.000918 x^2$	74.8	739.11	< .001
		S1	$y= 0.08018 - 0.01814 x + 0.002080 x^2$	81.0	1026.31	< .001	$y= 0.2213 - 0.01469 x + 0.000369 x^2$	27.3	93.66	< .001
Hand Sensory	**POS**	**M1**	$y= 0.06210 - 0.01939 x + 0.001811 x^2$	70.9	605.74	< .001	$y= - 0.02092 + 0.01018 x - 0.000382 x^2$	41.7	177.82	< .001
		S1	$y= 0.07935 - 0.01508 x + 0.001949 x^2$	66.6	495.44	< .001	$y= 0.1196 + 0.002476 x - 0.000192 x^2$	65.6	475.17	< .001
	NEG	**M1**	$y= 0.02507 - 0.009343 x + 0.000848 x^2$	84.3	1336.09	< .001	$y= 0.03927 - 0.003439 x + 0.000087 x^2$	28.0	96.84	< .001
		S1	$y= 0.03778 - 0.04254 x + 0.003999 x^2$	91.9	2823.42	< .001	$y= - 0.2271 + 0.03477 x - 0.001363 x^2$	66.6	496.58	< .001

Table 3.8. Polynomial regression results for child groups.

Task	Group	Cortical Region	Model (early)	R^2 (%)	F (2,498)	*p*-value	Model (late)	R^2 (%)	F (2,498)	*p*-value
Face Motor	**POS**	**M1**	$y = 0.1110 + 0.08677\,x - 0.005358\,x^2$	98.7	19596.80	< .001	$y = -0.00463 + 0.06199\,x - 0.001706\,x^2$	73.3	683.77	< .001
		S1	$y = -0.1480 + 0.002848\,x + 0.000488\,x^2$	38.0	152.71	< .001	$y = -1.237 + 0.1668\,x - 0.005466\,x^2$	40.9	172.13	< .001
	NEG	**M1**	$y = -0.01575 - 0.005615\,x - 0.000512\,x^2$	91.9	2807.79	< .001	$y = 0.1798 - 0.04332\,x + 0.001347\,x^2$	75.4	761.84	< .001
		S1	$y = 0.04486 - 0.01425\,x - 0.001006\,x^2$	67.3	512.80	< .001	$y = 1.162 - 0.1666\,x + 0.004763\,x^2$	86.1	1538.37	< .001
Face Sensory	**POS**	**M1**	$y = 0.2447 - 0.01305\,x - 0.000889\,x^2$	65.5	473.17	< .001	$y = 0.5255 - 0.06784\,x + 0.002530\,x^2$	86.1	1227.11	< .001
		S1	$y = 0.3225 - 0.03052\,x + 0.001328\,x^2$	34.9	133.27	< .001	$y = -0.6727 + 0.1051\,x - 0.002103\,x^2$	97.8	11155.69	< .001
	NEG	**M1**	$y = -0.05044 - 0.01307\,x + 0.001841\,x^2$	29.1	102.07	< .001	$y = 1.159 - 0.1671\,x + 0.005505\,x^2$	76.6	817.33	< .001
		S1	$y = 0.1167 - 0.04504\,x + 0.002348\,x^2$	94.3	4108.13	< .001	$y = 1.055 - 0.1702\,x + 0.005524\,x^2$	93.4	3505.27	< .001
Hand Motor	**POS**	**M1**	$y = 0.01549 + 0.01956\,x + 0.000816\,x^2$	95.2	4902.27	< .001	$y = -0.1521 + 0.05763\,x - 0.002085\,x^2$	49.4	243.41	< .001
		S1	$y = 0.1488 + 0.004356\,x + 0.000339\,x^2$	23.8	77.94	< .001	$y = -0.00060 + 0.02926\,x - 0.000687\,x^2$	15.2	44.59	< .001
	NEG	**M1**	$y = 0.05432 - 0.04779\,x + 0.004773\,x^2$	69.0	553.32	< .001	$y = 1.379 - 0.1896\,x + 0.005841\,x^2$	87.2	1699.69	< .001
		S1	$y = 0.06261 - 0.06355\,x + 0.004894\,x^2$	79.2	946.29	< .001	$y = 1.607 - 0.2330\,x + 0.007346\,x^2$	90.3	2310.66	< .001
Hand Sensory	**POS**	**M1**	$y = 0.1952 - 0.01627\,x + 0.002852\,x^2$	87.7	1775.45	< .001	$y = 0.9540 - 0.09473\,x + 0.002945\,x^2$	63.2	428.43	< .001
		S1	$y = 0.3836 - 0.07046\,x + 0.007865\,x^2$	63.2	427.52	< .001	$y = 1.451 - 0.1614\,x + 0.004728\,x^2$	44.0	195.38	< .001
	NEG	**M1**	$y = 0.05690 - 0.03528\,x + 0.003017\,x^2$	65.0	463.25	< .001	$y = -0.1236 + 0.01303\,x - 0.000346\,x^2$	14.0	40.64	< .001
		S1	$y = -0.06815 - 0.08713\,x + 0.007144\,x^2$	82.4	1162.21	< .001	$y = -0.4021 + 0.05154\,x - 0.002542\,x^2$	88.6	1928.73	< .001

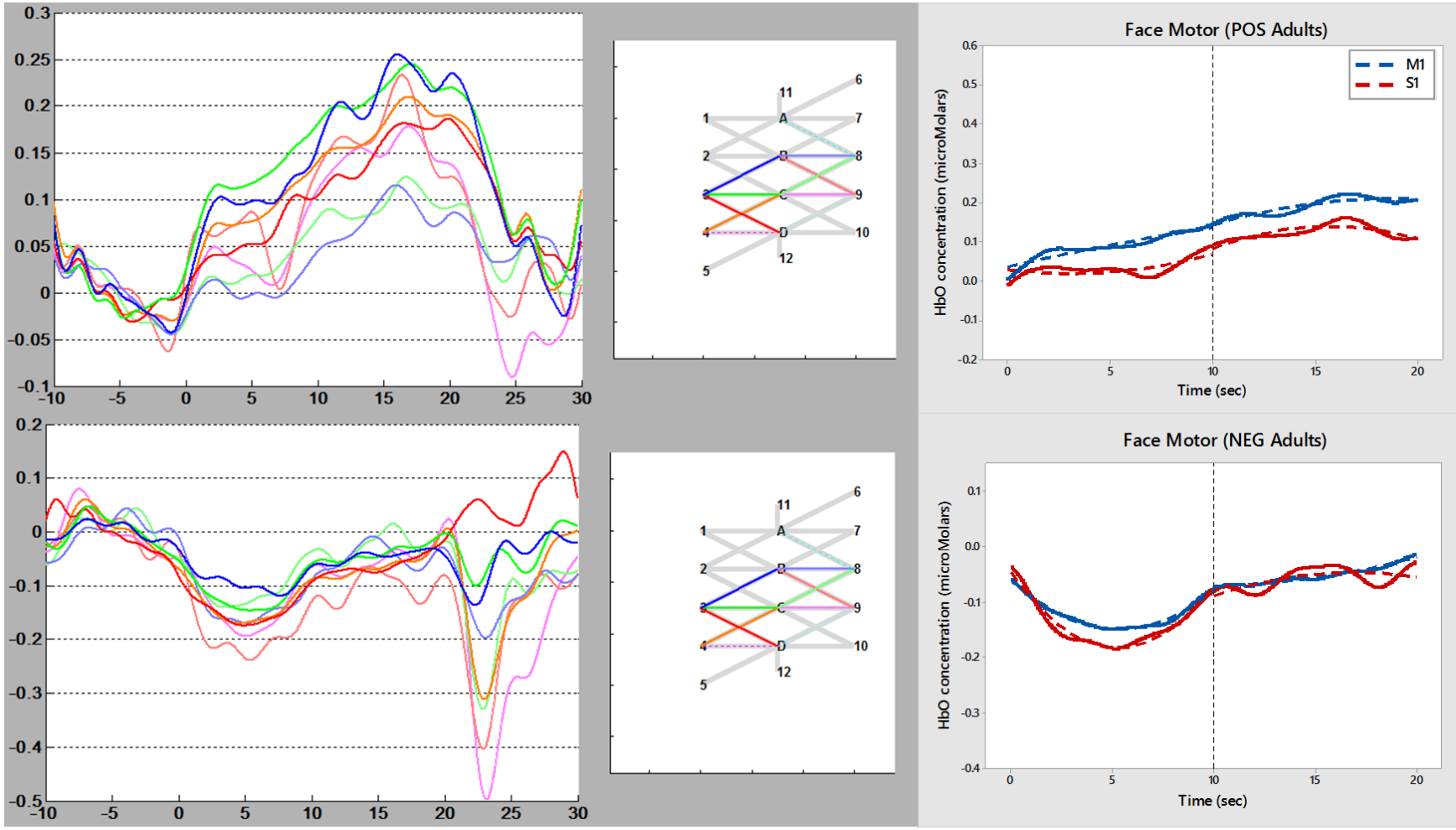

Figure 3.16. HRF trends during face motor tasks in adults (individual channels of interest shown on left, average of channels of interest shown on right; POS group in top panels, NEG group in bottom panels).

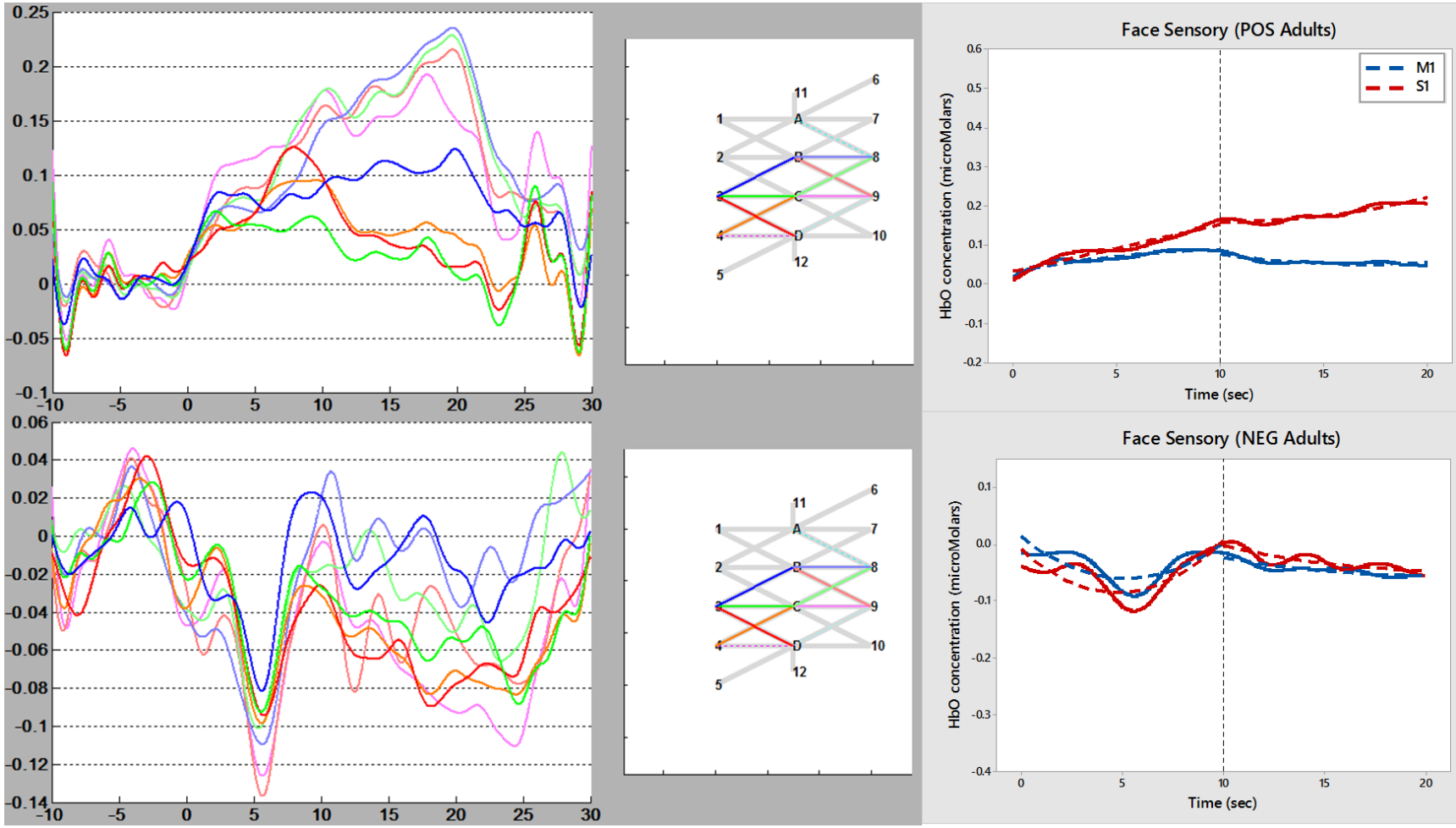

Figure 3.17. HRF trends during face somatosensory stimulation in adults (individual channels of interest shown on left, average of channels of interest shown on right; POS group in top panels, NEG group in bottom panels).

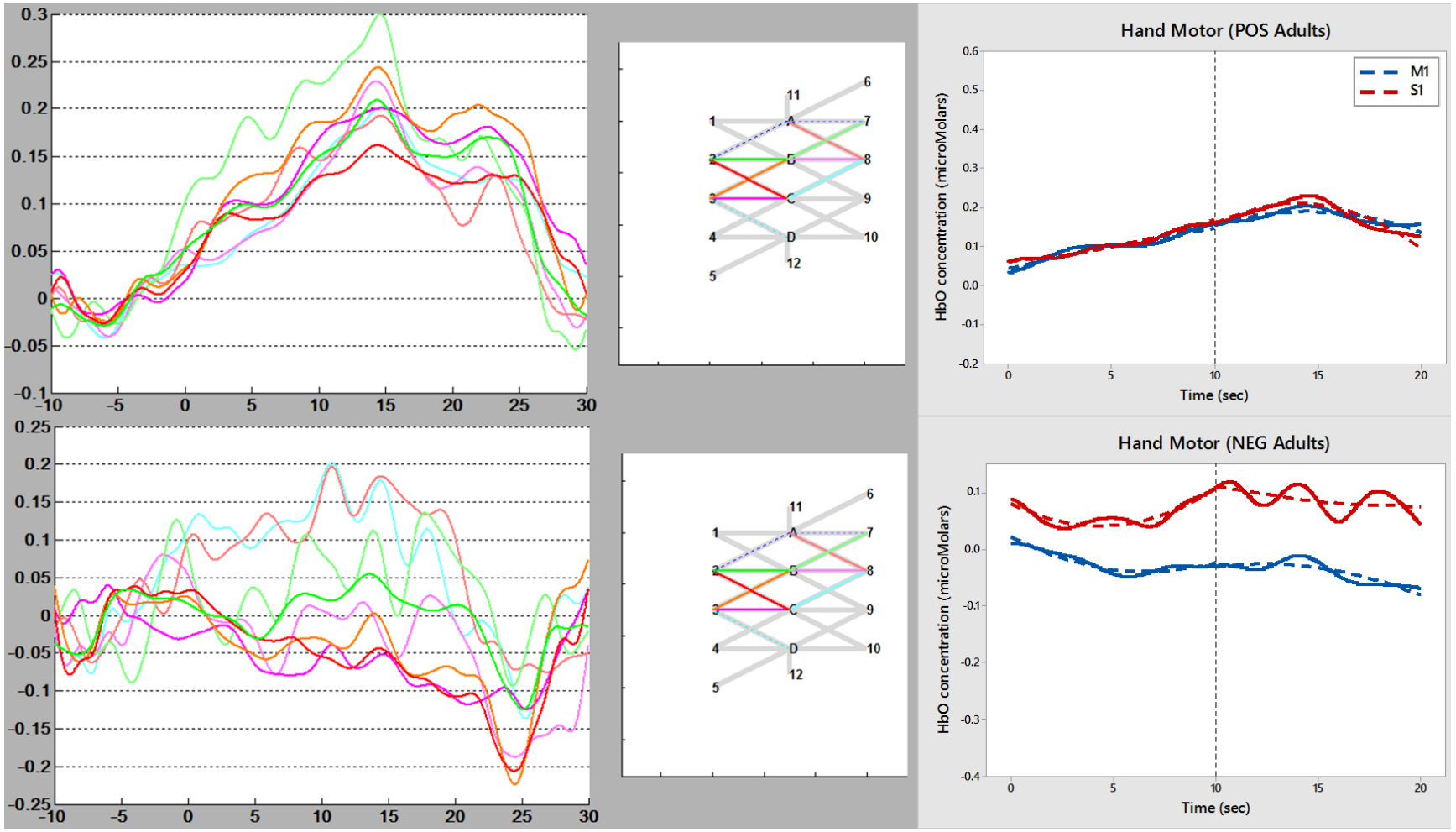

Figure 3.18. HRF trends during hand motor tasks in adults (individual channels of interest shown on left, average of channels of interest shown on right; POS group in top panels, NEG group in bottom panels).

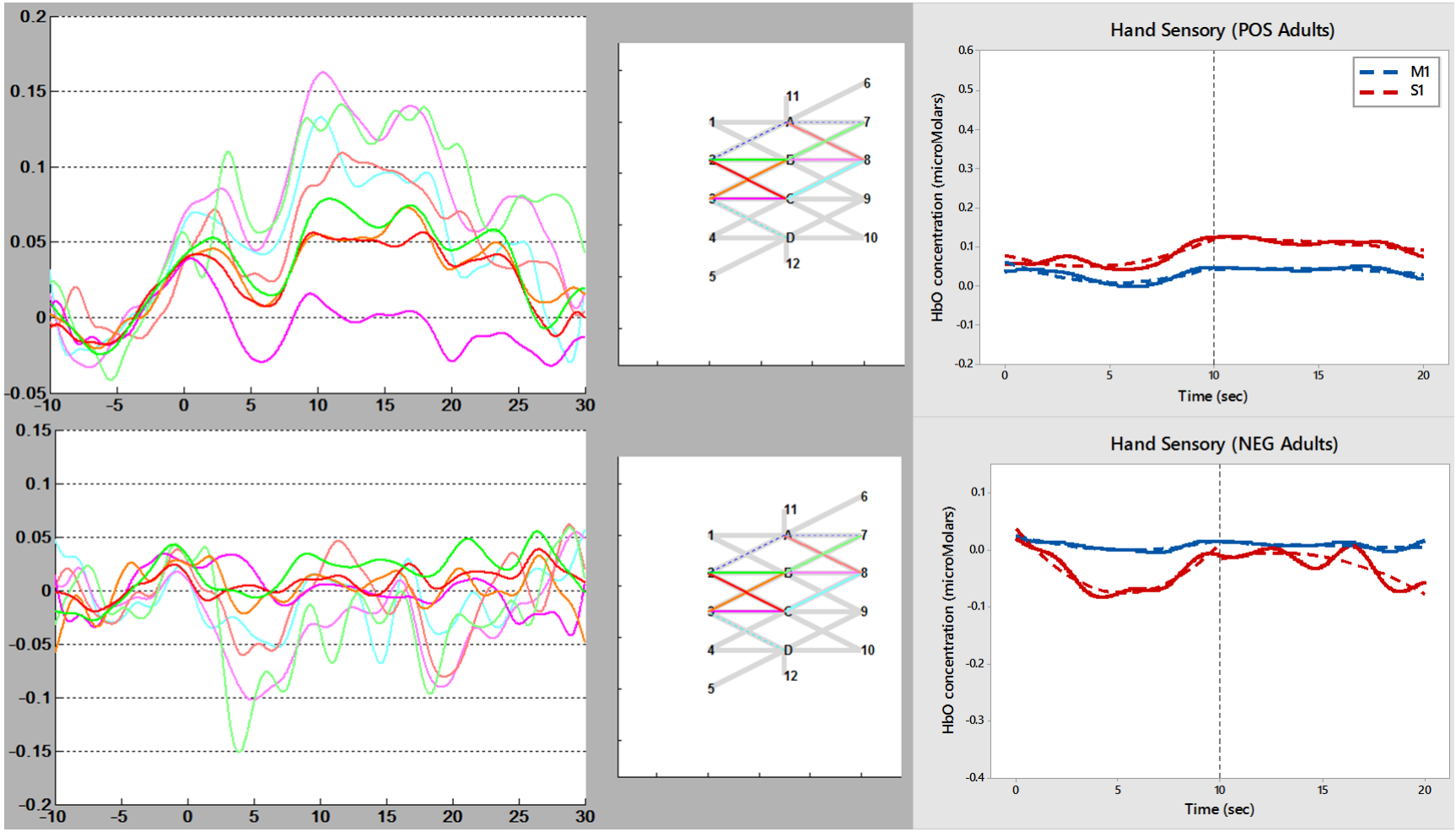

Figure 3.19. HRF trends during hand somatosensory stimulation in adults (individual channels of interest shown on left, average of channels of interest shown on right; POS group in top panels, NEG group in bottom panels).

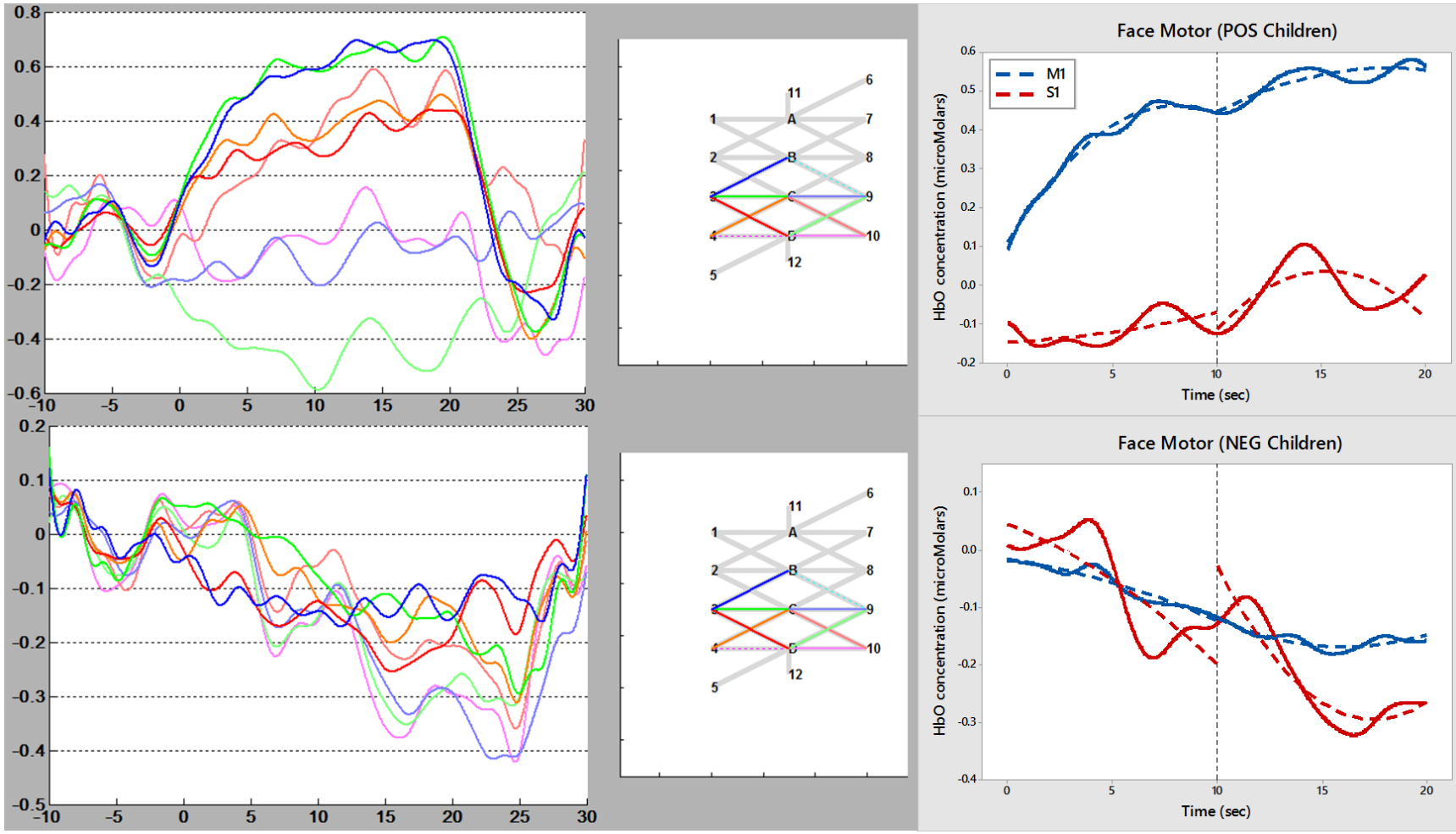

Figure 3.20. HRF trends during face motor tasks in children (individual channels of interest shown on left, average of channels of interest shown on right; POS group in top panels, NEG group in bottom panels).

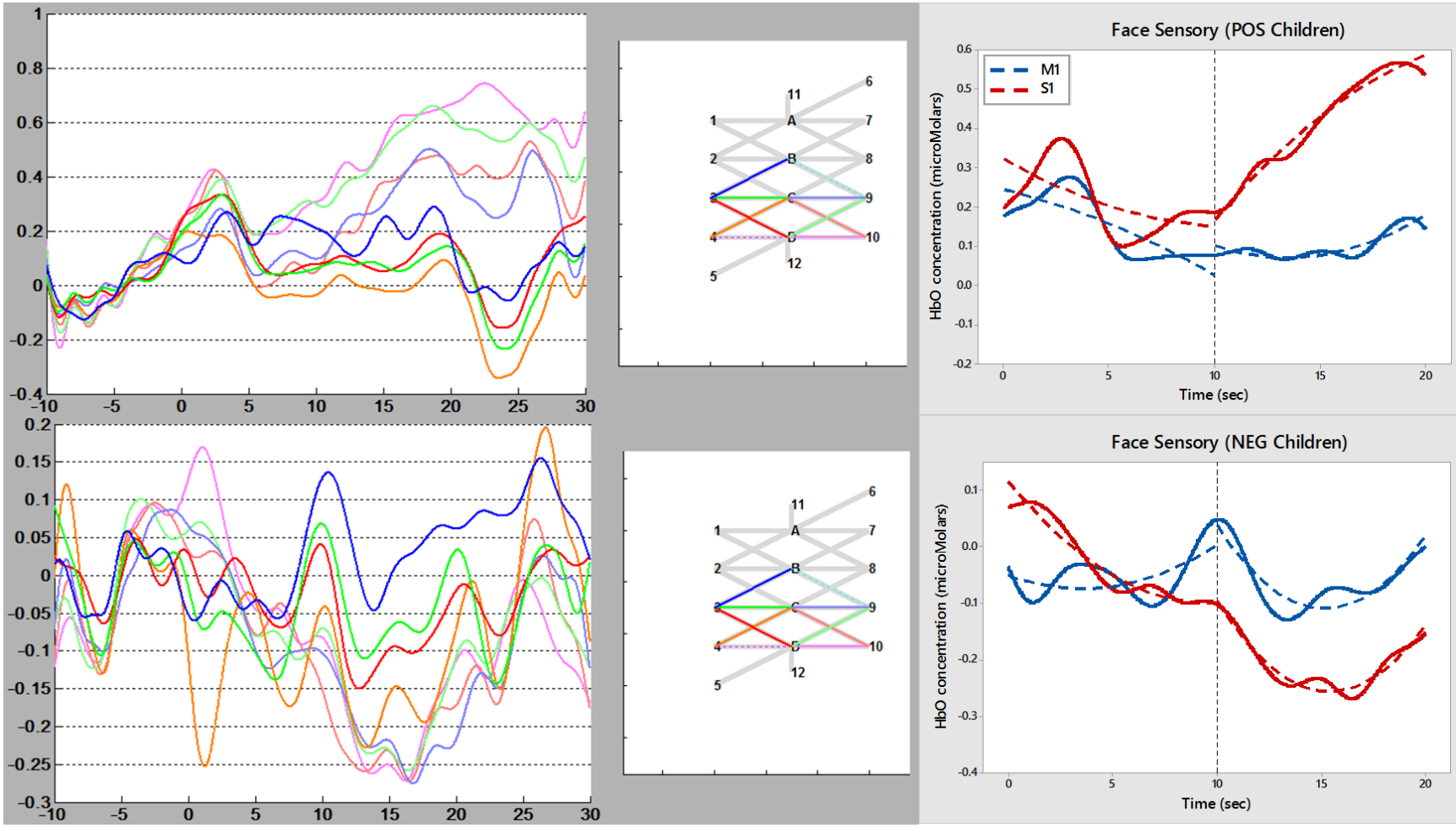

Figure 3.21. HRF trends during face somatosensory stimulation in children (individual channels of interest shown on left, average of channels of interest shown on right; POS group in top panels, NEG group in bottom panels).

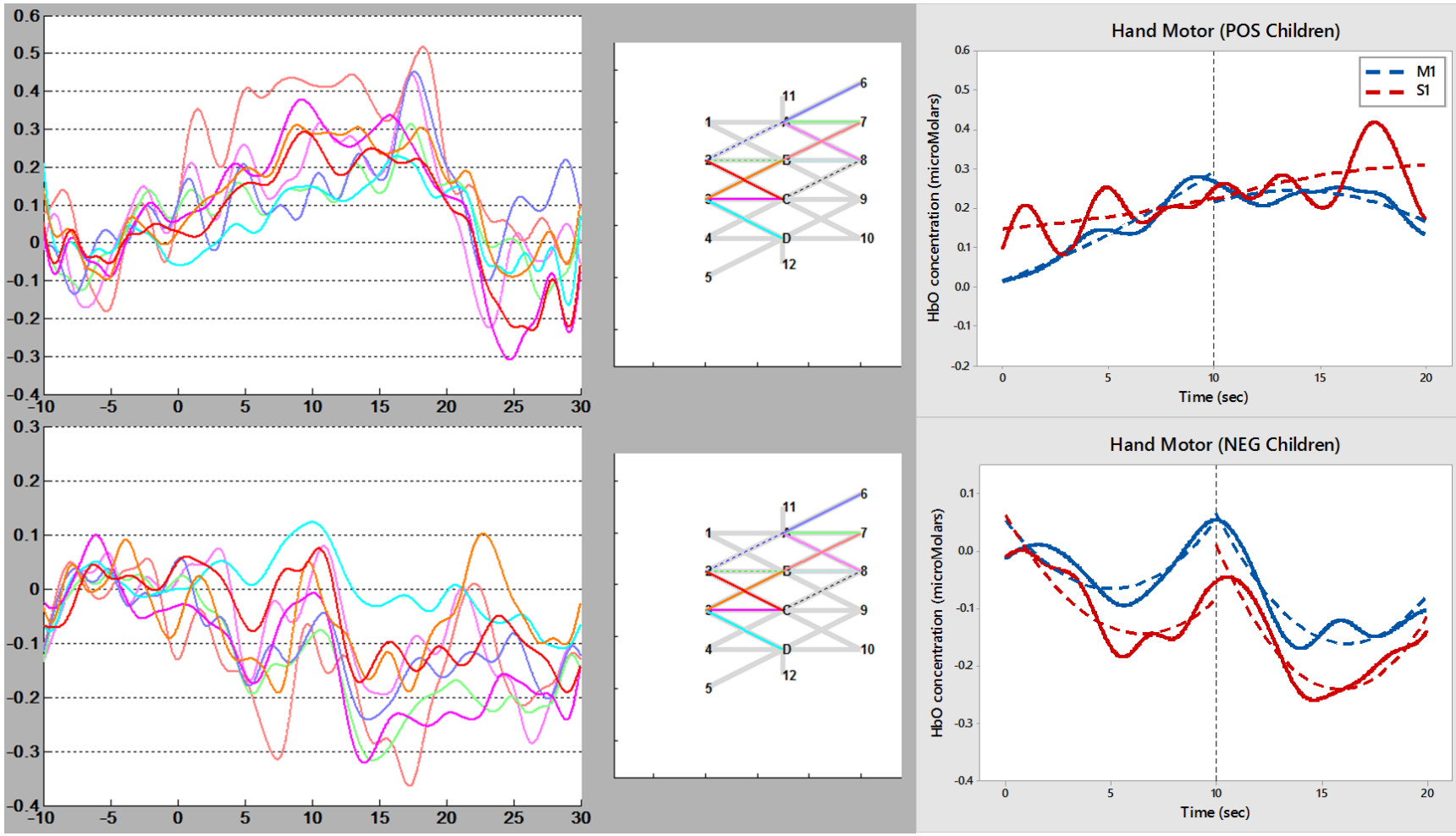

Figure 3.22. HRF trends during hand motor tasks in children (individual channels of interest shown on left, average of channels of interest shown on right; POS group in top panels, NEG group in bottom panels).

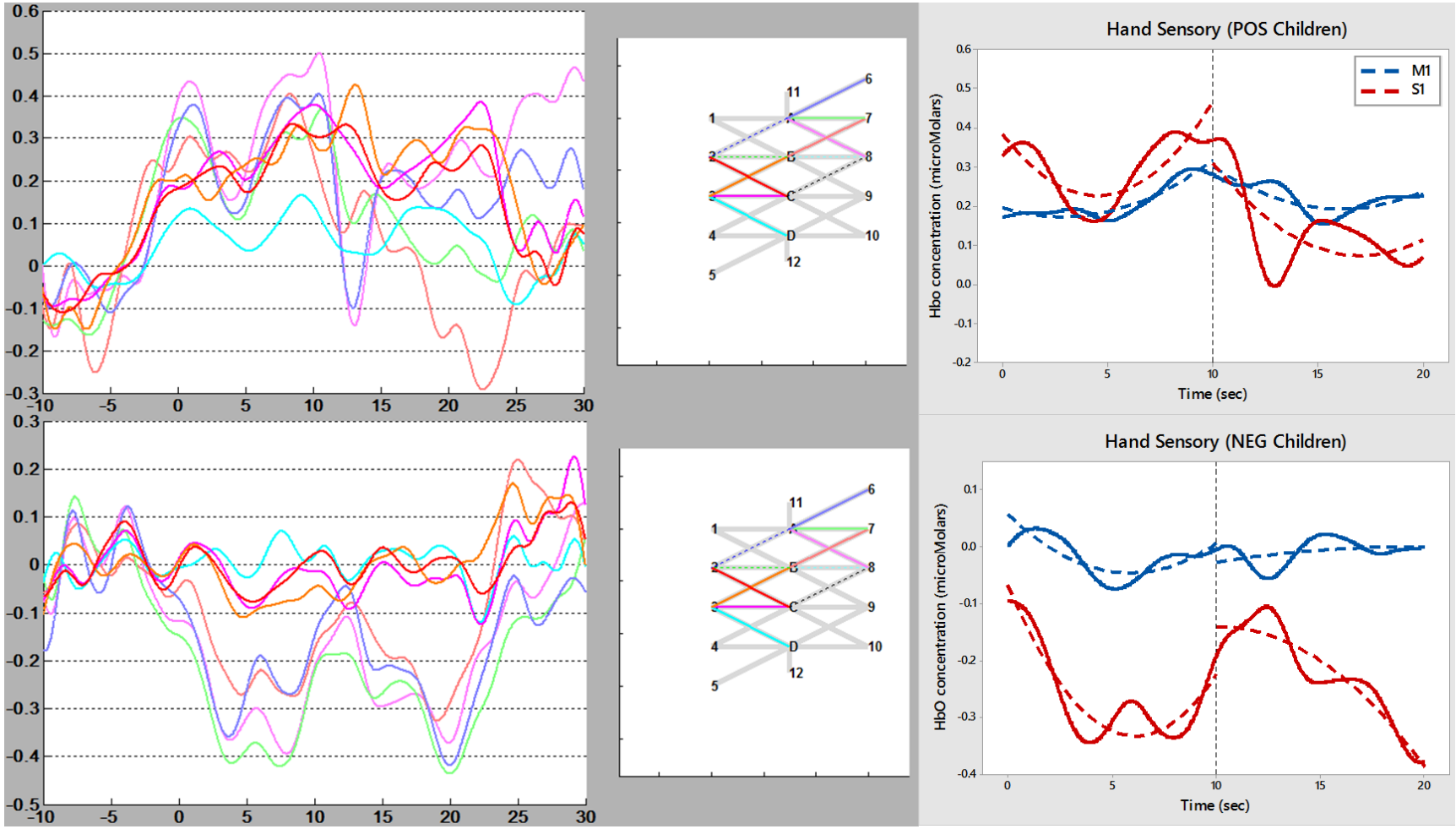

Figure 3.23. HRF trends during hand somatosensory stimulation in children (individual channels of interest shown on left, average of channels of interest shown on right; POS group in top panels, NEG group in bottom panels).

Behavioral Outcomes

Behavioral data was acquired from all participants to ensure a standard rate and force of motor tasks across all subjects. Table 3.9 provides the mean frequency at which the visuomotor force tasks were performed. A series of one sample t-tests with a Bonferroni correction ($\alpha = .05/4$ [number of t-tests] = .0125) determined that the mean frequency at which adults and children performed the motor tasks was not significantly different from the target rate (2 Hz).

Table 3.9. Frequency at which groups performed motor tasks (in Hz).

Group & Site	Mean Frequency (Hz)	SD	t-value	*p*-value	Effect size
Adult Hand	1.8776	0.3503	-1.639	.116	0.35
Adult Face	1.8553	0.3067	-2.213	.038	0.47
Child Hand	1.7129	0.6322	-1.506	.163	0.45
Child Face	1.7380	0.7672	-1.133	.284	0.34

A peak finding algorithm coded in MATLAB was used to determine the amplitude of the peaks of each hand grip and bilabial compression force. Table 3.10 provides the mean target force (which was defined as 10% MVC), actual achieved force, margin of error, and percent of variance around the mean for each of the motor conditions, as well as the results of pairwise comparisons between the target and achieved forces, and the effect sizes. Again, using a Bonferroni correction ($\alpha = .0125$), significant differences were found between target and achieved forces for face motor conditions in adults and children, though an extremely high level of correlation (> .90) existed between

the achieved and target forces across all groups and motor conditions ($p < .0001$ for each). In all cases, the mean achieved force was greater than the mean 10% MVC target force. These data suggest that perhaps the face motor task was more difficult to perform than that of the hand motor task, in terms of achieving a pre-determined amount of force.

Table 3.10. Force with which groups performed motor tasks (in N of force).

Group & Site	Target Force in N (mean (SD))	Achieved Force in N (mean (SD))	Margin of Error of Achieved Force (95% CI)	% Variance around Mean	t-value	*p*-value	Effect size
Adult Hand	27.6773 (10.3521)	28.8187 (11.4864)	± 0.5903	± 2.05%	2.112	.047	0.10
Adult Face	0.5638 (0.2014)	0.6730 (0.2334)	± 0.0220	± 3.20%	5.778	< .0001*	0.50
Child Hand	15.3418 (6.4152)	17.1479 (8.2329)	± 0.6166	± 3.60%	1.693	.121	0.25
Child Face	0.6818 (0.5471)	0.8889 (0.5165)	± 0.0570	± 6.43%	3.709	.004*	0.39

To determine whether or not there was a relationship between HbO levels and motor behaviors, Pearson product moment correlations between the mean partial sums integral values in the motor and somatosensory channels of interest and the measured motor behavior variables were performed. Table 3.11 provides the correlation coefficients and significance values between the HbO integral values (in both M1 and S1) and the achieved rate and force across the motor tasks in all adults and children. None of the correlations were significant.

Table 3.11. Pearson correlations between the HbO partial sums integral values in respective channels of interest and the motor task behavioral variables.

Group & Site	Cortical Region	HbO/Rate Correlation (r)	*p*-value	HbO/Force Correlation (r)	*p*-value
Adult Hand	**M1**	-.071	.752	-.212	.343
	S1	-.179	.424	-.071	.755
Adult Face	**M1**	.330	.144	.098	.673
	S1	.182	.430	-.092	.691
Child Hand	**M1**	.503	.250	.017	.971
	S1	.145	.756	.523	.229
Child Face	**M1**	.284	.459	.639	.064
	S1	.271	.480	.180	.643

CHAPTER FOUR: DISCUSSION

Specific Aims Discussion

Specific Aim #1: To examine the hemodynamic differences between hand and face cortical representations during passive somatosensory conditions, as measured with fNIRS.

The hemodynamic differences between hand and face cortical representations during passive pneumotactile stimulation were ubiquitous among adult and child participants, as evidenced by the extent of significant findings in Tables 3.1 and 3.2, which revealed that passive somatosensory stimulation yielded greater mean HbO integral values in S1 (as opposed to M1) in the POS group [adult face somatosensory: Welch's $F(1,58.08) = 4.64$, $p = .035$; adult hand somatosensory: Welch's $F(1,69.4) = 32.62$, $p < .001$; child face somatosensory: Welch's $F(1,24.62) = 20.83$, $p < .001$] and lesser mean HbO integral values in S1 in the NEG groups [adult hand somatosensory: Welch's $F(1,101.52) = 6.69$, $p = .011$; child hand somatosensory: Welch's $F(1,39.77) = 10.56$, $p = .002$]. HbO mean integral values were greater in S1 than M1 during hand stimulation in the POS child group, and lesser in S1 than M1 during face stimulation in the NEG adult and child groups, revealing a similar trend in somatosensory HRFs across stimulus sites, though these differences were not significant. However, no significant differences were found between mean HbO levels in S1 when comparing face and hand somatosensory stimulation (see Tables 3.3 and 3.4), suggesting that the passive, pneumatic somatosensory stimulus used in the current study to stimulate either site on the body elicited equally strong HRFs in respective cortical areas. When comparing across the two types of stimuli (motor vs. somatosensory) on the same body site, only one

example of a stronger HRF during somatosensory stimulation was found (Table 3.6). In the NEG child group, the passive somatosensory stimulus applied to the hand elicited more negative HbO levels that that of the hand motor task [Welch's $F(1,36.51) = 4.87$, $p = .034$], though this finding was not corroborated in adult participants or in the POS group.

Specific Aim #2: To examine the hemodynamic differences between hand and face cortical representations during motor tasks, as measured with fNIRS.

Hemodynamic differences between hand and face cortical representations during active, voluntary motor tasks were also seen in the adult and child participants, as evidenced by the significant findings in Table 3.1, which revealed that active motor tasks elicited greater mean HbO integral values in M1 in the POS child group during face motor tasks [Welch's $F(1,19.51) = 6.55$, $p = .019$]. Significant differences were not found between M1 and S1 HRFs during the hand or the face motor task in the POS adult group or either adult or child NEG groups (Table 3.2), though this finding is not surprising given the fact that all motor tasks have sensory consequences. However, when comparisons were made between HbO levels in M1 during hand and face motor tasks, no significant differences were found in the POS group (Table 3.3), though the NEG adult group revealed significantly lower HbO levels during the face motor task (Table 3.4). Despite this finding, these data suggest that the performance of these specific, repetitive motor tasks with either structure elicited equally strong HRFs in respective cortical areas. When comparing across the two types of stimuli (motor vs. somatosensory) on the same body site, only one example of a stronger HRF during active motor tasks was found

(Table 3.5). In the POS adult group, the hand motor task elicited greater HbO concentration levels than that of passive somatosensory stimulation [Welch's $F(1,75.62) = 4.64$, $p = .034$], though this finding was not corroborated in child participants or in the NEG group.

Specific Aim #3: To examine developmental changes in patterns of cortical adaptation and hemodynamic responses to somatosensory stimulation and voluntary motor activity in pediatric (age 6-13 years) and adult participants (age 19-30 years), in an effort to provide a preliminary cross-sectional picture of normal physiologic connectivity and function in children and adults.

Many differences were found between the HRFs of adults and children, most notably the overall increased mean HbO concentration values in children, as well as the greater amount of variability in HRFs across the child participants in all stimulus conditions. Below is a list of differences in hemodynamic trends seen between POS and NEG groups across all stimulus conditions:

<u>Face Motor</u> (Figures 3.16 and 3.20)

POS groups:

Both adults and children showed a significant increase in HbO in M1, beyond that of HbO in S1, in the early and late components, though the mean child HbO levels in M1 exhibited a nearly 3-fold increase above that in adults. S1 HbO levels showed very slight increases over the 20 second stimulus period, with children exhibiting more variability in the S1 HRF.

NEG groups:

Both adults and children showed a decrease in both M1 and S1 HbO levels in the early component of the HRF, but adult HbO levels began returning to baseline in the late component while child HbO levels decrease even further, particularly in S1, though none of the differences were significant.

Face Somatosensory (Figures 3.17 and 3.21)

POS groups:

Adults exhibited a slight increase in S1 HbO early in the response, which was significantly elevated even more in the late component. M1 HbO was relatively unremarkable, and remained near baseline. Child HbO levels in M1 and S1 exhibited similar patterns in the early component, with an immediate increase in HbO peaking around 4 seconds, then M1 HbO leveled off near baseline while S1 HbO levels dramatically and significantly increased in the late component.

NEG groups:

Adults exhibited a prominent decrease in both M1 and S1 HbO in the early component, peaking at 6 seconds (S1 levels slightly more negative than M1 levels, though their mean difference was not significant), then returning to baseline and slightly decreasing over the late component. Children exhibited a sharp decrease in S1 HbO that continued until approximately 16 seconds, then began to increase slightly at the end of the late component. M1 HbO levels were variable with a positive-going peak at 10 seconds, followed by a decrease in HbO in the late component, though due to the overall variability in the HRF the differences were not significant.

Hand Motor (Figures 3.18 and 3.22)

POS groups:

Adult M1 and S1 HRFs were highly similar in concentration level, shape, and trend, with peaks at approximately 15 seconds followed by a gradual return to baseline (no discernable difference between M1 and S1). Child M1 HbO levels showed a slight peak around 8-9 seconds, with a gradual trend toward baseline in the late component, while child S1 HbO levels slightly increased over the entire 20 second stimulus period, though the differences between M1 and S1 were not significant.

NEG groups:

Adults in this group exhibited a small but steady decrease in M1 HbO, while S1 HbO levels were positive, though the differences were not significant. Child HRFs in M1 and S1 followed a similar pattern (though S1 HbO levels were more negative than M1 HbO levels), with a negative peak around 6 seconds, return to near baseline around 10 seconds, and another negative peak at approximately 14 seconds followed by another trend toward baseline. The mean difference between M1 and S1 HbO levels was not significant.

Hand Somatosensory (Figures 3.19 and 3.23)

POS groups:

Both adults and children demonstrated peaks in S1 and M1 HbO levels between 8-10 seconds (S1 peaks greater than M1 in both groups, though children yielded mean HbO levels much greater than adults), and while adults showed a somewhat steady return to baseline, children showed a sharp decrease in S1 HbO in the late component, beyond that

of M1 HbO levels. The difference between S1 and M1 HbO values was significant in adults, but due to variability, it was not significant in the child group.

NEG groups:

Both adults and children exhibited an average negative peak in the early component in S1 HbO around 5 seconds. Adults also showed a relatively steady return to baseline, while children showed another sharp decrease in S1 HbO in the late component. In both groups the M1 HbO levels were relatively unremarkable, though the difference between M1 and S1 HbO values in children was significant.

The increased mean and variability in child HRFs may be due to the sizeable age range and number of participants in the child group, as these participants may have been at different neurodevelopmental stages with different head and brain sizes, and varying levels of synaptogenesis and synaptic pruning in M1 and S1 (Figure 4.1, after Thompson & Nelson, 2001; Casey et al., 2005).

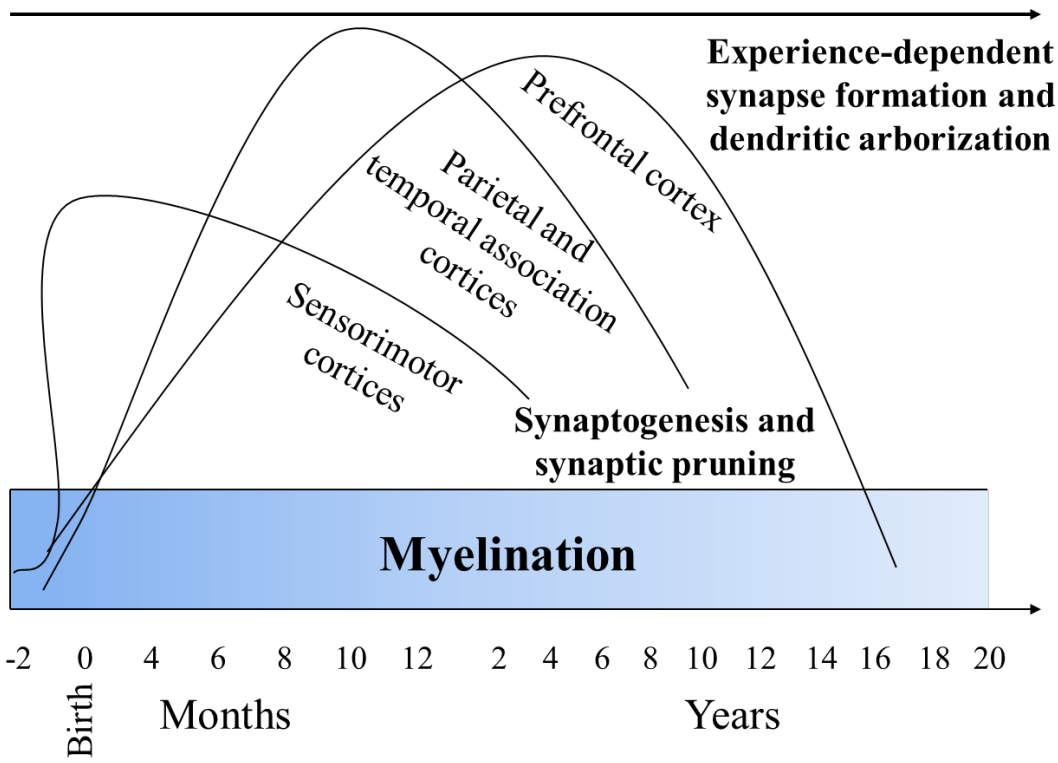

Figure 4.1. Course of human brain development (adapted from Thompson & Nelson, 2001; Casey et al., 2005).

It is not particularly surprising that HRF differences were seen across child and adult participants given that gray matter maturation in the sensorimotor cortex is completed around ages 5 or 6 (Gogtay et al., 2004) and synaptic pruning continues throughout adolescence (Bourgeois et al., 1994; Huttenlocher, 1994; Rakic, 1996). This is prominent in cortical areas underlying higher-order multisensory integration and motor coordination (Gogtay et al., 2004; Pangelinan et al., 2011; Sowell, Thompson & Toga, 2004).

Many neuroimaging studies have demonstrated significant age-related differences in cortical activation, even across pediatric age ranges. An EEG study by Pangelinan and

colleagues (2011) determined that younger children (6-7 year olds) exhibited greater task-related activation of frontal areas and less task-related activation of parietal areas than adults during multi-joint, goal-directed movements, and that older children (9-11 year olds) exhibited transitional activation patterns, meaning patterns between those of younger children and adults. Another study using fMRI (Thomason et al., 2005) demonstrated that children exhibited greater percent BOLD signal changes and greater noise in the BOLD response than adults during a breath holding task, which causes a global systemic state change in brain oxygenation. Breath holding has been shown to be a good surrogate for task activation (particularly those using sensorimotor paradigms), as it uses the same basic vasodilation mechanism for up-regulation of local CBF (Bandettini & Wong, 1997; Davis et al., 1998; Riecker et al., 2003; Thomason et al., 2004), though breath holding causes more global BOLD signal changes, while task activation causes more localized responses. Other fMRI studies in young children have shown the BOLD signal to be more variable (Rumsey & Ernst, 2009) and diffuse (Durston et al., 2006) than those in older children and adults. These findings provide some support for the differences found between adult and child HRFs in the current study.

Contrary to these findings, other researchers (Schapiro et al., 2004) have shown that the percent signal change associated with the BOLD effect increases with age in children ages 5-19 during sensorimotor and language tasks. Taken together with the results presented here, it is clear that neuroimaging findings vary considerably across different age ranges, particularly in pediatric populations, which may be due to age-related changes in the cerebrovascular system, different stages of synaptogenesis, synaptic pruning, and myelination, as well as general issues and difficulties with data

collection in children (i.e., noise, motion artifact, compliance, etc.; more on this in the section on study limitations).

Additional Findings

Behavioral Data

In general, adults and children performed similarly on the hand and lip visuomotor tasks. After performing an FFT power spectrum on each participants' motor traces in LabChart, and using one sample t-tests with a Bonferroni correction ($\alpha = .05/4$ [number of t-tests] = .0125), it was determined that the rate at which the motor tasks were performed was not significantly different from the target rate of 2 Hz (Table 3.9). Using the peakfinder MATLAB code it was determined that on average the achieved forces were significantly greater than the 10% MVC target forces during the face tasks for adults and children, though children exhibited more variance in their behavioral data than adults. It is well established that children show greater movement variability than adults during a variety of hand motor tasks (Jansen-Osmann et al., 2002; Kuhtz-Buschbeck et al., 1998; Takahashi et al., 2003; Yan et al., 2000) and articulatory movements (i.e. upper lip, lower lip, and jaw) (Goffman & Smith, 1999; Green et al., 2000; 2002; Sharkey & Folkins, 1985; Smith et al., 1998; 2004; Walsh & Smith, 2002; Walsh et al., 2006), thus providing support for some of the motor findings in the current study.

It was not surprising to discover no significant correlations between the HbO partial sums integral values and the behavioral data, as the motor tasks were tightly controlled with very little behavioral variance across participants (see Tables 3.9 and 3.10). Therefore, observed differences and variations in the HRF were most likely neural

in nature and reflect real neurophysiological differences in these particular cortical regions, and are not due to variations in motor behavior.

Limitations

Sample Size/Characteristics

This study had a sample size of 22 adults and 11 children, which is an adequate number of participants to yield acceptable statistical power, however the smaller sample of children produces more uncertainty in central tendency and the interpretation of the data. Also, the age range of children used in the study was fairly broad (6-13 years), and as previously discussed, the children in this study were undoubtedly at different neurodevelopmental stages, which may have contributed to the variability in the data. The sample size for this study was not large enough to further subdivide the children into younger and older groups, though a larger sample size might reveal that as children age, their fNIRS signals become more stable and adult-like.

Children as Participants

There are numerous conceptual and methodological concerns when working with school-aged children as research participants that require consideration, such as ensuring participant compliance, choosing adequate comparison tasks (without making behavioral goals too easy for adults or too difficult for children), assessing and accounting for performance, and making direct statistical comparisons (which were not done between adults and children in this study) (Fair et al., 2006). Also, children tended to get bored or tire more easily than adults, therefore task vigilance may have suffered. Along these

same lines, motion artifact was greater in child participants, as children were more active during the tasks, despite the instructions to stay as still as possible. Though less susceptible to artifact than other imaging methods, head movement during NIRS recording can cause uncoupling between the optical fiber and the skin, creating sharp spikes and increased magnitude of fNIRS signals (Tak & Ye, 2014). Motion correction analyses were performed in Homer2 (Figure 2.11) in an effort to reduce noise and remove erroneous motion data from the raw fNIRS signals. Future studies using motor tasks in orofacial and hand regions of children (and even adults) may consider using gentle restraints to minimize head and arm motion artifact, and could potentially use a shorter protocol (perhaps 10 or 15 seconds of STIM/10 seconds REST, rather than the 20 seconds STIM/20 seconds REST used here).

fNIRS Probe Design

In the current study, the same probe array was used on all participants, regardless of age or gender. Because NIRS as a functional neuroimaging technique is relatively new, there is still much uncertainty as to optimal source-detector distances to provide adequate depth of NIR light penetration to yield the most accurate signals. The optimal source-detector distance for measuring cortical surface hemoglobin changes has been estimated to be 3 cm in adults (Obata et al., 2003; Okada & Delpy, 2003; Sato et al., 2006; Watanabe et al., 1996), and 2 cm in infants (Taga et al., 2007), though studies on children between infancy and adulthood have used many different distances (ranging from 2 to 4 cm), and a 3 cm distance is commonly used in school-aged children (Kurz et al., 2014; Zhu et al., 2014). Customizing probes for each participant based on individual

anatomy would be ideal, however the feasibility of such a task may not be practical for research with large sample sizes.

fNIRS Data

Though the merits of NIRS technology are numerous, many concerns still exist regarding the accuracy and reliability of data, as well as how to analyze and interpret data. While fNIRS has high temporal resolution of the hemodynamic response (millisecond range), it lacks spatial resolution (≤ 1 cm) (Ferrari & Quaresima, 2012), and has limited penetration depth (< 5.5-6 cm) (Parks, 2013) making it possible to only measure from superficial regions of the cortex. Also, because fNIRS lacks anatomical information, source localization can be extremely difficult (Ferrari et al., 2004; Kleinschmidt et al., 1996; Lloyd-Fox et al., 2010; Villringer et al., 1993), which is why structural MRI was used for pre-planning in this study. The fNIRS signal can also be corrupted by motion artifact, measurement noise, and physiological noise (i.e. cardiac pulsation, respiration, blood pressure Mayer waves) (Boas et al., 2004), therefore short separation channels should be used to remove noise arising from superficial layers (Gagnon et al., 2012), and careful processing must be done to ensure signals are truly related to the HRF. Analytical approaches to fNIRS data vary widely, and depend upon the questions and goals of the research.

Cortical Variation in Humans

Humans are inherently unique, and likewise their brains are uniquely and continually shaped and organized by genetics and their own experiences with the world.

These plastic changes occur throughout the lifespan (Buonomano & Merzenich, 1998; Hebb 1947; 1949). In terms of primary motor and somatosensory cortices, there is wide variation in the configuration of these gyri and the central sulcus (Rademacher et al., 1993; White et al., 1997), as well as in functional somatotopic arrangement (Ianetti et al., 2003; Kurth et al., 1998; Meier et al., 2008; Sato et al., 2005). It is possible that, despite the MRI scan prior to NIRS data collection to help localize the probe to M1 and S1, the probe may not have been centered over each individual's hand and face cortical areas. This could explain the negative going HRFs in some participants (those allotted to the NEG group), as cortical steal may have been occurring in the areas directly in the NIR light paths.

Negative hemodynamic responses seen in NIRS data are not unique to the current study. Kennerley and colleagues (2012) used optical imaging spectroscopy in rodents to study somatosensory hemodynamic responses during electrical whisker stimulation, and found negative responses in a 'surround region' adjacent to the whisker barrel somatosensory cortex (suggestive of cortical steal). In human fNIRS research, Lloyd-Fox and colleagues (2015) found that during natural interactions, infants produced "the opposite pattern or responses" in certain channels, characterized by HbO decrease and/or HbR increase. These authors called these "deactivations", which may also be indicative of cortical steal, though "not all decreases are deactivations" (Gusnard & Raichle, 2001). Kotilahti et al. (2010) also found negative hemodynamic responses in the infant auditory cortex during speech and music sounds, suggesting that the results may be due to "the so-called blood stealing effect", and that the negative responses "may be a result of activity deeper in the brain or in areas that were close to but not inside the area measured with

NIRS". In adult NIRS studies, cortical steal (often termed "hypo-oxygenation") has been observed in areas of prefrontal cortex during reading tasks (Liu et al., 2008), and during different taste conditions (sweet, sour) (Hu, Kato & Luo, 2014). Specific to the healthy adult sensorimotor cortex, Seiyama and colleagues (2005) found that median nerve stimulation produced decreases in HbO in supramarginal gyrus (which corresponded to a negative BOLD signal), and Sato and colleagues (2005) found both positive and negative hemodynamic responses in sensorimotor cortex during a finger tapping task, which the authors suggest is due to large intersubject anatomical variability. Therefore, it is highly likely that the POS and NEG hemodynamic responses seen in the current study reflects the variable nature of each individual's cortical anatomy, as well as the variance in the NIRS probe placement relative to individual anatomy.

Future Studies

A number of subsequent studies could be conducted based on the findings presented here. Increasing the sample size, especially in the child group, and perhaps stratifying the children into younger and older age groups may provide some clarity on the age-related variability in the signals. Also, more advanced co-registration techniques could be used to project fNIRS findings onto individual anatomical images for better source localization of the hemodynamic signals. Probe designs could also be altered to examine larger or smaller cortical areas, and the use of bilateral probes could prove valuable, given different research questions.

It would also be advantageous to pair fNIRS with other imaging modalities, such as EEG, to examine the link between electrocortical and hemodynamic activity. Studies

using EEG and fNIRS would provide excellent temporal resolution regarding the time course of neural activity and subsequent CBF. Conducting the same study using fMRI would potentially corroborate the findings, though much of the paradigm would need to be modified for use in a magnetic and motion-restricted environment. Previous studies have shown that fMRI and fNIRS agree quite well on measurements of cortical oxygenation changes (Kleinschmidt et al., 1996; Mehagnoul-Shipper et al., 2002; Sassaroli et al., 2005; Toronov et al., 2001), and a study of this nature would further validate the effectiveness of the stimulus paradigm used here in activating hand and face specific areas of sensorimotor cortex.

Comparison of HRFs and adaptation patterns between normal healthy adults and children and different clinical populations (such as adults with cerebrovascular stroke or traumatic brain injury, or children with autism spectrum disorders, sensory processing or motor deficits) may shed light on changes in neuronal processing of somatosensory and motor information due to disorder or disease. Also, the experimental paradigm used in the current study could be used to examine the neural mechanisms of functional recovery in sensorimotor cortex following a cortical insult, and to assess the effectiveness of rehabilitative or neuroprotective interventions in a variety of patient populations (Mihara et al., 2010).

Conclusions

The results of this study revealed that fNIRS is sensitive to localized HbO changes in the sensorimotor cortex, that the novel stimulus paradigm used was successful in activating somatotopically distinct areas in M1 and S1, and that children and adults

exhibit different patterns of hemodynamic activity in these cortical areas. These data present a picture of normal physiologic connectivity and function across a wide range of ages, which provides a broader view of how the neurotypical cerebral cortex operates in terms of neuronal responses to specific types of stimuli, neurovascular coupling, and cerebral oxygenation. The current findings have increased our understanding of changes in cortical hemodynamics across a developmental timeline, though further research with larger sample sizes, and potentially other imaging modalities, is warranted to more fully understand the variation in the sign and spatial organization of hemodynamic responses throughout human development.

References

Abbott LF, Varela JA, Sen K, Nelson SB. (1997). Synaptic depression and cortical gain control. *Science,* 275:220-224.

Abraira VE, Ginty DD. (2013). The sensory neurons of touch. *Neuron*, 79(4):618-839.

Adkins DL, Boychuk J, Remple MS, Kleim JA. (2006). Motor training induces experience-specific patterns of plasticity across motor cortex and spinal cord. *Journal of Applied Physiology*, 101:1776-1782.

Ahissar E, Sosnik R, Haidarliu S. (2000). Transformation from temporal to rate coding in a somatosensory thalamocortical pathway. *Nature,* 406:302-306.

Andreatta RD, Barlow SM. (2003). Movement-related modulation of vibrotactile detection thresholds in the human orofacial system. *Experimental Brain Research*, 149:75-82.

Ances BM, Buerk DG, Greenberg JH, Detre JA. (2001). Temporal dynamics of the partial pressure of brain tissue oxygen during functional forepaw stimulation in rats. *Neuroscience Letters*, 306:106-110.

Arezzo JC, Vaughan HG, Jr., Legatt AD. (1981). Topography and intracranial sources of somatosensory evoked potentials in the monkey. II. Cortical components. *Electroencephalography and Clinical Neurophysiology*, 51:1-18.

Asanuma H, Pavlides C. (1997). Neurobiological basis of motor learning in mammals. *Neuroreport*, 8:i-vi.

Bandettini PA, Wong EC. (1997). A hypercapnia-based normalization method for improved spatial localization of human brain activation with fMRI. *NMR in Biomedicine*, 10:197-203.

Bardouille T, Ross B. (2008). MEG imaging of sensorimotor areas using inter-trial coherence in vibrotactile steady-state responses. *NeuroImage*, 42**:**323-31.

Barker D. (1974). "The morphology of muscle receptors" in Hunt CC (ed) *Handbook of Sensory Physiology III/2 Muscle Receptors*. Springer-Verlag: Berlin.

Barlow SM. (1987). Mechanical frequency detection thresholds in the human face. *Experimental Neurology*, 96:253-261.

Barlow SM. (1998). Real time modulation of speech-orofacial motor performance by means of motion sense. *Journal of Communication Disorders*, 31:511-534.

Barlow SM, Estep M. (2006). Central pattern generation and the motor infrastructure for suck, respiration, and speech. *Journal of Communication Disorders*, 39:366-380.

Barlow SM, Finan D, Bradford PT, Andreatta R. (1993). Transitional properties of the mechanically evoked perioral reflex from infancy through adulthood. *Brain Research,* 623:181-188.

Barlow SM, Lund JP, Estep M., Kolta A. (2010). "Central pattern generators for speech and orofacial activity" in Brudzynski SM (ed), *Handbook of Mammalian Vocalization*. Elsevier: Oxford, pp. 351-370.

Bigland-Ritchie B, Fuglevand AJ, Thomas CK. (1998). Contractile properties of human motor units: is man a cat? *Neuroscientist*, 4:240-249.

Boas DA, Dale AM, Franceschini MA. (2004). Diffuse optical imaging of brain activation: approaches to optimizing image sensitivity, resolution, and accuracy. *NeuroImage*, 23:S278-S288.

Boorman L, Kennerley AJ, Johnston D, Jones M, Zheng Y, Redgrave P, Berwick J. (2010). Negative blood oxygen level dependence in the rat: A model for investigating the role of suppression in neurovascular coupling. *The Journal of Neuroscience,* 30:4285-4294.

Bourgeois JP, Goldman-Rakic PS, Rakic P. (1994). Synaptogenesis in the prefrontal cortex of rhesus monkeys. *Cerebral Cortex*, 4:78-96.

Brenner N, Bialek W, de Ruyter van Steveninck R. (2000). Adaptive rescaling maximizes information transmission. *Neuron*, 26:695-702.

Brooks VB. (1986).*The Neural Basis of Motor Control*. Oxford University Press: New York.

Buonomano DV, Merzenich MM. (1998). Cortical plasticity: from synapses to maps. *Annual Reviews of Neuroscience*, 21:149-186.

Burke RE, Levine DN, Tsairis P, Zajac FE. (1973). Physiological types and histochemical profiles in motor units of the cat gastrocnemius. *Journal of Neurophysiology*, 234:723-748.

Burke RE, Levine DN, Zajac FE, Tsairs P, Engel K. (1971). Mammalian motor units: physiological- histochemical correlation in three types in cat gastrocnemius. *Science* 174:709-712.

Burke RE, Tsairis P. (1974). Trophic functions of the neuron. II. Denervation and regulation of muscle. The correlation of physiological properties with histochemical characteristics in single muscle units. *Annals of the New York Academy of Science*, 228:145-159.

Burton H, Fabri M, Alloway K. (1995). Cortical areas within the lateral sulcus connected to cutaneous representations in areas 3b and 1: a revised interpretation of the second somatosensory area in macaque monkeys. *Journal of Comparative Neurology*, 355:539-562.

Carandini M, Ferster D. (1997). A tonic hyperpolarization underlying contrast adaptation in cat visual cortex. *Science*, 276:949-952.

Casey BJ, Tottenham N, Liston C, Durston S. (2005). Imaging the developing brain: what I have learned about cognitive development. *TRENDS in Cognitive Sciences*, 9:104-110.

Catalano SM, Shatz CJ. (1998). Activity-dependent cortical target selection by thalamic axons. *Science*, 281:559-562.

Chakravarthy VS, Joseph D, Bapi RS. (2010). What do the basal ganglia do? A modeling perspective. *Biological Cybernetics*, 103:237-253.

Chen TL, Babiloni C, Ferretti A, Perrucci MG, Romani GL … Del Gratta C. (2008). Human secondary somatosensory cortex is involved in the processing of somatosensory rare stimuli: an fMRI study. *NeuroImage*, 40:1765-1771.

Chudler EH. (2014). Conduction Velocity. Retrieved March 10, 2015, from https://faculty.washington.edu/chudler/cv.html.

Chung S, Li X, Nelson SB. (2002). Short-term depression at thalamocortical synapses contributes to rapid adaptation of cortical sensory responses in vivo. *Neuron*, 24:437-446.

Constantinidis C, Bucci DJ, Rugg MD. (2013). Cognitive functions of the posterior parietal cortex. *Frontiers in Integrative Neuroscience*, 7, article 35.

Contreras-Vidal JL, Stelmach GE. (1996). Effects of Parkinsonism on motor control. *Life Sciences*, 58:165-176.

Cortes JM, Marinazzo D, Series P, Oram MW, Sejnowski TJ, van Rossum MCW. (2012). The effect of neural adaptation on population coding accuracy. *Journal of Computational Neuroscience*, 32:387-402.

Classen J, Liepert J, Wise SP, Hallet M, Cohen LG. (1998). Rapid plasticity of human cortical movement representation induced by practice. *Journal of Neurophysiology*, 79:1117-1123.

Custead R, Oh H, Rosner AO, Barlow SM. (2015). Adaptation of the cortical somatosensory evoked potential following pulsed pneumatic stimulation of the lower face in adults. *Brain Research*, 1622:81-90.

Davis TL, Kwong KK, Weisskoff RM, Rosen BR. (1998). Calibrated functional MRI: mapping the dynamics of oxidative metabolism. *Proceedings of the National Academy of Sciences USA*, 95:1834-1839.

DeBakey ME, Burch G, Ray T, Ochsner A. (1947). The "borrowing-lending" hemodynamic phenomenon (hemometakinesia) and its therapeutic application in peripheral vascular disturbances. *Annals of Surgery*, 126:850-865.

Delpy D, Cope M, van der Zee P, Arridge S, Wray S, Wyatt J. (1988). Estimation of optical path length through tissue from direct time of flight measurements. *Physics in Medicine and Biology*, 33:1433-1442.

Devor A, Dunn AK, Andermann ML, Ulbert I, Boas DA, Dale AM. (2003). Coupling of total hemoglobin concentration, oxygenation, and neural activity in rat somatosensory cortex. *Neuron*, 39:353-359.

Dijkerman HC, de Haan EH. (2007). Somatosensory processing subserving perception and action. *Behavioral Brain Science*, 30:198-201.

Disbrow E, Roberts T, Krubitzer L. (2000). Somatotopic organization of cortical fields in the lateral sulcus of Homo sapiens: evidence for SII and PV. *Journal of Comparative Neurology*, 418:1-21.

Dragoi V, Sharma J, Miller EK, Sur M. (2002). Dynamics of neuronal sensitivity in the visual cortex and local feature discrimination. *Nature Neuroscience*, 5:883-891.

Duchateau J, Enoka RM. (2011). Human motor unit recordings: origins and insight into the integrated motor system. *Brain Research*, 1409:42-61.

Durston S, Davidson MC, Tottenham N, Galvan A, Spicer J, Fossella JA, Casey BJ. (2006). A shift from diffuse to focal cortical activity with development. *Developmental Science*, 9:1-20.

Edin BB, Trulsson M. (1992). Neural network analysis of the information content in population responses from human periodontal receptors. *Proceedings of SPIE*, 1710:257-266.

Enager P, Piilgaard H, Offenhauser N, Kocharyan A, Fernandes P, Hamel E, Lauritzen M. (2009). Pathway-specific variations in neurovascular and neurometabolic coupling in rat primary somatosensory cortex. *Journal of Cerebral Blood Flow & Metabolism*, 29:976-986.

Estep E, Barlow SM. (2007). Modulation of the trigeminofacial pathway during syllabic speech. *Brain Research*, 1171:67-74.

Eyre JA, Miller S, Ramesh V. (1991). Constancy of central conduction delays during development in man: investigation of motor and somatosensory pathways. *Journal of Physiology*, 434:441-452.

Eyzaguirre C, Fidone SJ. (1975). *Physiology of the Nervous System*. Year Book Medical Publishers: Chicago.

Fair DA, Brown TT, Petersen SE, Schlaggar BL. (2006). A comparison of analysis of variance for investigating cognitive development with functional magnetic resonance imaging. *Developmental Neuropsychology*, 30:531-546.

Ferrari M, Quaresima V. (2012). A brief review on the history of human functional near-infrared spectroscopy (fNIRS) development and fields of application. *NeuroImage*, 63:921-935.

Ferrari M, Mottola L, Quaresima V. (2004). Principles, techniques, and limitations of near infrared spectroscopy. *Canadian Journal of Applied Physiology*, 29:463-487.

Fetz EE. (2006). "Motor systems" in *McGraw Hill Concise Encyclopedia of Science and Technology*. McGraw Hill: New York. Retrieved from http://0-literati.credoreference.com.library.unl.edu/content/entry/conscitech/motor_systems/0

Flanagan JR, Johansson RS. (2002). Hand Movements. *Encyclopedia of the Human Brain*, 2:399-414.

French AS. (1992). Mechanotransduction. *Annual Reviews of Physiology*, 54:135-152.

Gagnon L, Cooper RJ, Yücel MA, Perdue KL, Greve DN, Boas DA. (2012). Short separation channel location impacts the performance of short channel regression in NIRS. *NeuroImage*, 59:2518-2528.

Garcia-Larrea L, Lukaszewicz AC, Mauguiere F. (1995). Somatosensory responses during selective spatial attention: The N120-to-N140 transition. *Psychophysiology*, 32:526-537.

Gardner EP, Martin JH. (2000). "Coding of sensory information" in Kandel ER, Schwartz JH, Jessell TM (eds) *Principles of Neural Science*. 4th edition. McGraw Hill: New York.

Garnett RA, O'Donovan MJ, Stephens JA, Taylor A. (1979). Motor unit organization of human medial gastrocnemius. *Journal of Physiology (London)*, 287:33-43.

Ghez C, Krakauer J. (2000). "The organization of movement" in Kandel ER, Schwartz JH, Jessell TM (eds) *Principles of Neural Science*. 4th edition. McGraw Hill: New York.

Gobbele R, Schurmann M, Forss N, Juottonen K, Buchner H, Hari R. (2003). Activation of the human posterior parietal and temporoparietal cortices during audiotactile interaction. *NeuroImage*, 20:503-511.

Godde B, Ehrhardt J, Braun C. (2003). Behavioral significance of input-dependent plasticity of human somatosensory cortex. *NeuroReport*, 14:543-546.

Goffman L, Smith A. (1999). Development and differentiation of speech movement patterns. *Human Perception and Performance*, 25:1-12.

Gogtay N, Giedd JN, Lusk L, Hayashi KM, Greenstein D,…Thompson PM. (2004). Dynamic mapping of human cortical development during childhood through early adulthood. *Proceedings of the National Academy of Sciences*, 101:8174-8179.

Gordon J, Ghez C. (1991). “Muscle receptors and spinal reflexes: the stretch reflex” in Kandel ER, Schwartz JH, Jessell TM (eds) *Principles of Neural Science*. 3rd edition. Elsevier Science: New York.

Green JR, Moore CA, Higashikawa M, Steeve RW. (2000). The physiological development of speech motor control: Lip and jaw coordination. *Journal of Speech, Language, and Hearing Research*, 43:239-255.

Green JR, Moore CA, Reilly KJ. (2002). The sequential development of jaw and lip control for speech. *Journal of Speech, Language, and Hearing Research*, 45:66-79.

Greenlee MW, Georgeson MA, Magnussen S, Harris JP. (1991). The time course of adaptation to spatial contrast. *Vision Research*, 31:223-236.

Gusnard DA, Raichle ME. (2001). Searching for a baseline: Functional imaging and the resting human brain. *Nature Reviews Neuroscience*, 2:685-694.

Gutnisky D, Dragoi V. (2008). Adaptive coding of visual information in neural populations. *Nature*, 452:220-224.

Hamdy S, Rothwell JC, Aziz Q, Singh KD, Thompson DG. (1998). Long-term reorganization of human motor cortex driven by short-term sensory stimulation. *Nature Neuroscience*, 1:64-68.

Hebb DO. (1947). The effects of early experience on problem solving at maturity. *American Psychologist*, 2:306-307.

Hebb DO. (1949). *The Organization of Behavior*. Wiley & Sons: New York.

Hellweg FC, Schultz W, Creutzfeldt OD. (1977). Extracellular and intracellular recordings from cat's cortical whisker projection area: thalamocortical response transformation. *Journal of Neurophysiology*, 40:463-479.

Holland BA, Haas DK, Norman D, Brant-Zawadzki M, Newton TH. (1986). MRI of normal brain maturation. *American Journal of Neuroradiology*, 7:201-208.

Hoshi Y. (2007). Functional near-infrared spectroscopy: current status and future prospects. *Journal of Biomedical Optics*, 12:062106.

Hosoya T, Baccus SA, Meister M. (2005). Dynamic predictive coding by the retina. *Nature*, 436:71-77.

Huttenlocher PR. (1994). “Synaptogenesis in human cerebral cortex”, in Dawson G, Fischer K (eds) *Human behavior and the developing brain*. Guilford Press: New York.

Hsiao S. (2008). Central mechanisms of tactile shape perception. *Current Opinion in Neurobiology*, 18:418-24.

Hu C, Kato Y, Luo Z. (2014). Activation of human prefrontal cortex to pleasant and aversive taste using functional near-infrared spectroscopy. *Food and Nutrition Sciences*, 5:236-244.

Hu L, Zhang ZG, Hu Y. (2012). A time-varying source connectivity approach to reveal human somatosensory information processing. *NeuroImage*, 62:217-228.

Hyvarinen J. (1982). Posterior parietal lobe of the primate brain. *Physiological Reviews*, 62:1060-1129.

Iannetti GD, Porro CA, Pantano P, Romanelli PL, Galeotti F, Cruccu G. (2003). Representation of different trigeminal divisions within the primary and secondary human somatosensory cortex. *NeuroImage*, 19:906-912.

Inui K, Wang X, Tamura Y, Kaneoke Y, Kakigi R. (2004). Serial processing in the human somatosensory system. *Cerebral Cortex*, 14:851-857.
Jansen-Osmann P, Richter S, Konczak J, Kalveram KT. (2002). Force adaptation transfers to untrained workspace regions in children: Evidence for developing inverse dynamic motor models. *Experimental Brain Research*, 143:212-220.
Jasper HH. (1958). The ten-twenty electrode system of the International Federation. *Electroencephalography and Clinical Neurophysiology*, 10:367-380.
Jenkins WM, Merzenich MM, Ochs M, Allard TT, Guic-Robles E. (1990). Functional reorganization of primary somatosensory cortex in adult owl monkeys after behaviourally controlled tactile stimulation. *Journal of Neurophysiology*, 63:82-104.
Jernigan TL, Tallal P. (1990). Late childhood changes in brain morphology observable with MRI. *Developmental Medicine & Child Neurology*, 32:379-385.
Johansson RS, Trulsson M, Olsson KÅ, Westberg K-G. (1988a). Mechanoreceptor activity from the human face and oral mucosa. *Experimental Brain Research*, 72:204-208.
Johansson RS, Vallbo ÅB. (1983). Tactile sensory coding in the glabrous skin of the human hand. *Trends in Neuroscience*, 6:27-32.
Kaas JH. (1991). Plasticity of sensory and motor maps in adult mammals. *Annual Reviews of Neuroscience*, 14:137-167.
Kaas JH, Nelson RJ, Sur M, Dykes RW, Merzenich MM. (1984). The somatic organization of the ventroposterior thalamus of the squirrel monkey. *Journal of Comparative Neurology*, 226:111-140.
Kaas JH, Nelson RJ, Sur M, Lin CS, Merzenich MM. (1979). Multiple representations of the body within the primary somatosensory cortex of primates. *Science*, 204:521-523.
Kaas JH, Nelson RJ, Sur M, Merzenich MM. (1981). "Organization of somatosensory cortex in primates" in Schmitt FO, Worden FG, Adelman G, Dennis SG (eds) *The Organization of the Cerebral Cortex: Proceedings of a Neurosciences Research Program Colloquium*. MIT Press: Cambridge.
Kandel ER. (2000). "From nerve cells to cognition: the internal cellular representation required for perception and action" in Kandel ER, Schwartz JH, Jessell TM (eds) *Principles of Neural Science*. 4th edition. McGraw Hill: New York.
Katz L, Shatz C. (1996). Synaptic activity and the construction of cortical circuits. *Science*, 274:1133-1138.
Keidel WD, Keidel UO, Wigand ME. (1961). "Adaptation: loss or gain of sensory information", in Rosenblith WA (ed) *Sensory Communication*. MIT Press: Cambridge.
Kennerley AJ, Harris S, Bruyns-Haylett M, Boorman L, Zheng Y, Jones M, Berwick J. (2012). Early and late stimulus-evoked cortical hemodynamic responses provide insight into the neurogenic nature of neurovascular coupling. *Journal of Cerebral Blood Flow & Metabolism*, 32:468-480.
Kleim JA, Barbay S, Nudo RJ. (1998). Functional reorganization of the rat motor cortex following motor skill learning. *Journal of Neurophysiology*, 80:3321-3325.

Kleinschmidt A, Obrig H, Requardt M, Merboldt KD, Dirnagl U, Villringer A, Frahm J. (1996). Simultaneous recording of cerebral blood oxygenation changes during human brain activation by magnetic resonance imaging and near-infrared spectroscopy. *Journal of Cerebral Blood Flow and Metabolism*, 16:817-826.

Kocsis L, Herman P, Eke A. (2006). The modified Beer–Lambert law revisited. *Physics in Medicine and Biology*, 51:N91-N98.

Kohn A. (2007). Visual adaptation: Physiology, mechanisms, and functional benefits. *Journal of Neurophysiology*, 97:3155-3164.

Kotilahti K, Nissilä I, Näsi T, Lipiäinen L, Noponen T, Meriläinen P, Huotilainen M, Fellman V. (2010). Hemodynamic responses to speech and music in newborn infants. *Human Brain Mapping*, 31:595-603.

Krubitzer L, Clarey J, Tweedale R, Elston G, Calford M. (1995). A redefinition of somatosensory areas in the lateral sulcus of macaque monkeys. *Journal of Neuroscience*, 15:3821-3839.

Kuhtz-Buschbeck JP, Stolze H, Boczek-Funcke A, Johnk K, Heinrichs H, Illert M. (1998). Kinematic analysis of prehension movements in children. *Behavioral Brain Research*, 93:131-141.

Kurth R, Villringer K, Mackert, B-M, Schwiemann J, Braun J, Curio G, Villringer A, Wolf, K-J. (1998). fMRI assessment of somatotopy in human Brodmann area 3b by electrical finger stimulation. *NeuroReport*, 9:207-209.

Kurz JM, Wilson TW, Arpin DJ. (2014). An fNIRS exploratory investigation of the cortical activity during gait in children with spastic diplegic cerebral palsy. *Brain and Development*, 36:870-877.

Lenz FA, Dostrovsky JO, Tasker RR, Yamashiro K, Kwan HC, Murphy JT. (1988). Single-unit analysis of the human ventral thalamic nuclear group: Somatosensory responses. *Journal of Neurophysiology*, 59:299.

Liddell EGT, Sherrington CS. (1925). Recruitment and some other factors of reflex inhibition. *Proceedings of the Royal Society of London*, B97:488-518.

Liu KR, Borrett DS, Cheng A, Gasparro D, Kwan HC. (2008). Near-infrared spectroscopy study of language activated hyper- and hypo-oxygenation in human prefrontal cortex. *International Journal of Neuroscience*, 118:657-666.

Lloyd-Fox S, Blasi A, Elwell C. (2010). Illuminating the developing brain: the past, present and future of functional near infrared spectroscopy. *Neuroscience & Biobehavioral Reviews*, 34:269-284.

Lloyd-Fox S, Széplaki-Köllod B, Yin J, Csibra G. (2015). Are you talking to me? Neural activations in 6-month-old infants in response to being addressed during natural interactions. *Cortex*, 70:35-48.

Logothetis NK, Pauls J, Augath M, Trinath T, Oeltermann A. (2001). Neurophysiological investigation of the basis of the fMRI signal. *Nature*, 412:150-157.

Lovell M, Sutton D, Lindeman RC. (1977). Muscle spindles in nonhuman primate extrinsic auricular muscles. *Anatomical Record*, 189:519-523.

Lu C-F, Teng S, Wu Y-T. (2013). Dynamics of hemoglobin states in the sensorimotor cortex during motor tasks: a functional near infrared spectroscopy study. *35th Annual International Conference of the IEEE EMBS*, Osaka, Japan, pp. 1803-1806.

Luft AR, Kaelin-Lang A, Hauser T-K, Buitrago MM, Thakor NV, Hanley DF, Cohen LG. (2002). Modulation of rodent cortical motor excitability by somatosensory input. *Experimental Brain Research*, 142:562-569.

Marcar VL, Strässle AE, Loenneker T, Schwarz U, Martin E. (2004). The influence of cortical maturation on the BOLD response: an fMRI study of the visual cortex of children. *Pediatric Research*, 56:967-974.

Matthews PBC. (1972). *Mammalian Muscle Receptors and Their Central Actions*. Edward Arnold: London.

McDonagh JC, Binder MD, Reinking RM, Stuart DG. (1980). Tetrapartite classification of motor units of cat tibialis posterior. *Journal of Neurophysiology*, 44:696-712.

McGlone F, Reilly D. (2010). The cutaneous sensory system. *Neuroscience and Biobehavioral Reviews*, 34:148-159.

Mehagnoul-Schipper DJ, van der Kallen BFW, Collier WNMJ, van der Sluijs MC, van Erning LJTO, Thijseen HOM, et al. (2002). Simultaneous measurements of cerebral oxygenation changes during brain activation by near-infrared spectroscopy and functional magnetic resonance imaging in healthy young and elderly subjects. *Human Brain Mapping*, 16:14-23.

Meier JK, Aflalo TN, Kastner S, Graziano MSA. (2008). Complex organization of human primary motor cortex: a high-resolution fMRI study. *Journal of Neurophysiology*, 100:1800-1812.

Mihara M, Yagura H, Hatakenaka M, Hattori N, Miyai I. (2010). Clinical application of functional near-infrared spectroscopy in rehabilitation medicine. *Brain Nerve*, 62:125-132.

Mink JW. (1996). The basal ganglia: focused selection and inhibition of competing motor programs. *Progress in Neurobiology*, 50:381-425.

Moon H, Kim C, Kwon M, Chen Y-T, Fox E, Christou EA. (2015). High-gain visual feedback exacerbates ankle movement variability in children. *Experimental Brain Research*, 233:1597-1606.

Moses P, DiNino M, Hernandez L, Liu TT. (2014a). Developmental changes in resting and functional cerebral blood flow and their relationship to the BOLD response. *Human Brain Mapping*, 35:3188-3198.

Moses P, Hernandez LM, Orient E. (2014b). Age-related differences in cerebral blood flow underlie the BOLD fMRI signal in childhood. *Frontiers in Psychology*, 5:1-9.

Mountcastle VB, Lynch JC, Georgopoulos A, Sakata H, Acuna C. (1975). Posterior parietal association cortex of the monkey: command functions for operations within extrapersonal space. *Journal of Neurophysiology*, 38:871-908.

Muller JR, Metha AB, Krauskopf J, Lennie P. (1999). Rapid adaptation in visual cortex to the structure of images. *Science*, 285:1405-1408.

Nelson CA. (1999). Neural plasticity and human development. *Current Directions in Psychological Science*, 8:42-45.

Nezu A, Kimura S, Euhara S, Kobayashi T, Tanaka M, Saito K. (1997). Magnetic stimulation of motor cortex in children: maturity of corticospinal pathway and problem of clinical application. *Brain & Development*, 19:176-180.

Nordin M, Hagbarth KE. (1989). Mechanoreceptive units in the human infra-orbital nerve. *Acta Physiologica Scandinavica*, 135:149-161.

Nudo RJ, Milliken GW, Jenkins WM, Merzenich MM. (1996). Use-dependent alterations of movement representations in primary motor cortex of adult squirrel monkeys. *Journal of Neuroscience*, 16:785-807.

Nudo RJ, Plautz EJ, Milliken GW. (1997). Adaptive plasticity in primate motor cortex as a consequence of behavioral experience and neuronal injury. *Seminars in Neuroscience*, 9:13-23.

Obata A, Morimoto K, Sato H, Maki A, Koizumi H. (2003). Acute effects of alcohol on haemodynamic changes during visual stimulation assessed using 24-channel near-infrared spectroscopy *Psychiatry Research: Neuroimaging*, 123**:**145-152.

Obrig H, Israel H, Kohl-Bareis M, Uludag K, Wenzel R, Müller B, Arnold G, Villringer A. (2002). Habituation of the visually evoked potential and its vascular response: implications for neurovascular coupling in the healthy adult. *NeuroImage*, 17:1-18.

Obrig H, Wolf T, Döge C, Hülsing JJ, Dirnagl U, Villringer A. (1996). "Cerebral oxygenation changes during motor and somatosensory stimulation in humans, as measured by near-infrared spectroscopy", in Ince C, Kesecioglu J, Telci L, Akpir K (eds) *Oxygen Transport to Tissue XVII*. Springer US.

Oder A, Custead R, Oh H, and Barlow SM. (2014). Hemodynamic changes in cortical sensorimotor systems following hand and orofacial motor tasks and pulse cutaneous stimulation. *Society for Functional Near Infrared Spectroscopy*, Oct 8-12, Montreal, Quebec Canada.

Offenhauser N, Thomsen K, Caesar K, Lauritzen M. (2005). Activity-induced tissue oxygenation changes in rat cerebellar cortex: interplay of postsynaptic activation and blood flow. *Journal of Physiology*, 565:279-294.

Ohzawa I, Sclar G, Freeman R. (1982). Contrast gain control in the cat visual cortex. *Nature*, 298:266-268.

Okada E, Delpy DT. (2003). Near-infrared light propagation in an adult head model: II. Effect of superficial tissue thickness on the sensitivity of the near-infrared spectroscopy signal. *Applied Optics*, 42**:**2915-2922.

Ou W, Nissilä I, Radhakrishnan H, Boas DA, Hämäläinen MS, Franceschini MA. (2009). Study of neurovascular coupling in humans via simultaneous magnetoencephalography and diffuse optical imaging acquisition. *NeuroImage*, 46:624-632.

Pangelinan MM, Kagerer FA, Momen B, Hatfield BD, Clark JE. (2011). Electrocortical dynamics reflect age-related differences in movement kinematics among children and adults. *Cerebral Cortex*, 21:737-747.

Parks NA. (2013). Concurrent application of TMS and near-infrared optical imaging: methodological considerations and potential artifacts. *Frontiers in Human Neuroscience*, 7, article 592.

Paus T. (2005). Mapping brain maturation and cognitive development during adolescence. *Trends in Cognitive Sciences*, 9:60-68

Peck D, Buxton DF, Nitz A. (1984). A comparison of spindle concentrations in large and small muscles acting in parallel combinations. *Journal of Morphology*, 180:243-252.

Penfield W, Rasmussen T. (1950). *The cerebral cortex of man: a clinical study of localization of function*. The Macmillan Company: New York.

Penn AA, Shatz CJ. (1999). Brain waves and brain wiring: the role of endogenous and sensory-driven neural activity in development. *Pediatric Research*, 45:447-458.
Pons TP, Garraghty PE, Mishkin M. (1992). Serial and parallel processing of tactual information in somatosensory cortex of rhesus monkeys. *Journal of Neurophysiology*, 68:518-527.
Popescu EA, Barlow SM, Venkatesan L, Wang J, Popescu M. (2013). Adaptive changes in the neuromagnetic response of the primary and association somatosensory areas following repetitive tactile hand stimulation in humans. *Human Brain Mapping*, 34:1415-1426.
Purves D, Augustine GJ, Fitzpatrick D, Katz LC, LaMantia A-S, McNamara JO, Williams SM (eds.). (2001). *Neuroscience*. 2nd edition. Sinauer Associates: Sunderland.
Rademacher J, Caviness VS, Steinmetz H, Galabruda AM. (1993). Topographical variation of the human primary cortices: implications for neuroimaging, brain mapping, and neurobiology. *Cerebral Cortex,* 3:313-329.
Rakic P. (1996). "Development of the cerebral cortex in human and nonhuman primates" in Lewis M (ed) *Child and adolescent psychiatry*. Williams and Wilkins: Baltimore.
Richmond FJR, Abrahams VC. (1975). Morphology and distribution of muscle spindles in dorsal muscles of the cat neck. *Journal of Neurophysiology,* 38:1322-1339.
Riecker A, Grodd W, Klose U, Schulz J, Groschel K, …, Kastrup A. (2003). Relation between regional functional MRI activation and vascular reactivity to carbon dioxide during normal aging. *Journal of Cerebral Blood Flow and Metabolism*, 23:565-573.
Roche-Labarbe N, Fenoglio A, Radhakrishnan H, Kocienski-Filip M, Carp SA, Dubb J, Boas DA, Grant PE, Franceschini MA. (2014). Somatosensory evoked changes in cerebral oxygen consumption measured non-invasively in premature infants. *NeuroImage*, 85:279-286.
Romaiguère P, Vedel J-P, Pagni S, Zenatti A. (1989). Physiological properties of the motor units of the wrist extensor muscles in man. *Experimental Brain Research*, 78:51-61.
Rothwell JC. (1994). *Control of Human Voluntary Movement.* 2nd edition. Chapman & Hall: London.
Ruben J, Schwiemann J, Deuchert M, Meyey R, Krause T … Villringer A. (2001). Somatotopic organization of human secondary somatosensory cortex. *Cerebral Cortex*, 11:463-473.
Rumsey JM, Ernst ME. (2009). "Neuroimaging in developmental clinical neuroscience today" in Rumsey JM, Ernst ME (eds) *Neuroimaging in Developmental clinical Neuroscience*. Cambridge University Press: New York.
Sack AT. (2009). Parietal cortex and spatial cognition. *Behavioral Brain Research*, 202:153-161.
Saper CB. (2000). "Brain stem, reflexive behavior, and the cranial nerves" in Kandel ER, Schwartz JH, Jessell TM (eds) *Principles of Neural Science*. 4th edition. McGraw Hill: New York.

Saper CB, Iversen S, Frackowiak R. (2000). “Integration of sensory and motor function” in Kandel ER, Schwartz JH, Jessell TM (eds) *Principles of Neural Science*. 4th edition. McGraw Hill: New York.

Sassaroli A, Tong Y, Frederick BB, Renshaw PF, Ehrenberg BL, Fantini S. (2005). Studying brain function with concurrent near-infrared spectroscopy (NIRS) and functional magnetic resonance imaging (fMRI). *Proceedings in SPIE* 5693, Optical Tomography and Spectroscopy of Tissue VI, 161.

Sato H, Fuchino Y, Kiguchi M, Katura T, Maki A, Yoro T, Koizumi H. (2005). Intersubject variability of near-infrared spectroscopy signals during sensorimotor cortex activation. *Journal of Biomedical Optics*, 10:44001.

Sato H, Kiguchi M, Kawaguchi F, Maki A. (2004). Practicality of wavelength selection to improve signal-to-noise ratio in infrared spectroscopy. *NeuroImage*, 21:1554-1562.

Sato H, Kiguchi M, Maki A, Fuchino Y, Obata A, Yoro T, Koizumi H. (2006). Within-subject reproducibility of near-infrared spectroscopy signals in sensorimotor activation after 6 months. *Journal of Biomedical Optics*, 11**:**014021.

Sato K, Nariai T, Tanaka Y, Maehara T, Miyakawa N, … , Ohno K (2005). Functional representation of the finger and face in the human somatosensory cortex: Intraoperative intrinsic optical imaging. *NeuroImage*, 25:1292-1301.

Schuenke M, Schulte E, Schumacher U, Ross LM, Lamperti ED (eds). (2010). *Thieme Atlas of Anatomy: General Anatomy and Musculoskeletal System*. Thieme: New York.

Schwartz O, Hsu A, Dayan P. (2007). Space and time in visual context. *Nature Reviews. Neuroscience*, 8:522-535.

Schapiro MB, Schmithorst VJ, Wilke M, Byars AW, Strawsburg RH, Holland SK. (2004). BOLD-fMRI signal increases with age in selected brain regions in children. *Neuroreport*, 15:2575-2578.

Seiyama A, Seki J, Tanabe HC, Sase I, Takatsuki A, Miyauchi S, Hayashi S, Imaruoka T, Iwakura T, Yanagida T. (2005). Circulatory basis of fMRI signals: Relationship between changes in the hemodynamic parameters and BOLD signal intensity. *NeuroImage*, 21:1204-1214.

Sharkey SG, Folkins JW. (1985). Variability of lip and jaw movements in children and adults: Implications for the development of speech motor control. *Journal of Speech and Hearing Research*, 28:8-15.

Sharpee TO, Sugihara H, Kurgansky AV, Rebrik SP, Stryker MP, Miller KD. (2006). Adaptive filtering enhances information transmission in visual cortex. *Nature*, 439:936-942.

Sheth SA, Nemoto M, Guiou M, Walker M, Pouratian N, Toga AW. (2004). Linear and nonlinear relationships between neuronal activity, oxygen metabolism, and hemodynamic responses. *Neuron*, 42:347-355.

Shmuel A, Yacoub E, Pfeuffer J, Van de Moortele P-F, Adriany G, Hu X, Ugurbil K. (2002). Sustained negative BOLD, blood flow and oxygen consumption response and its coupling to the positive response in the human brain. *Neuron*, 36:1195-1210.

Shu Z, Swindale N, Cynader M. (1993). Spectral motion produces an auditory after-effect. *Nature,* 364:721-723.
Smith A, Goffman L. (1998). Stability and patterning of speech movement sequences in children and adults. *Journal of Speech, Language, and Hearing Research*, 41:18-30.
Smith A, Zelaznik HN. (2004). Development of functional synergies for speech motor coordination in childhood and adolescence. *Developmental Psychobiology*, 45:22-33.
Sowell ER, Thompson PM, Toga AW. (2004). Mapping changes in the human cortex through the span of life. *Neuroscientist*, 10:372-392.
Stål P. (1994). Characterization of human oro-facial and masticatory muscles with respect to fibre types, myosins and capillaries. Morphological, enzyme-histochemical, immuno-histochemical and biochemical investigations. *Swedish Dental Journal, Supplement*, 98:1-55.
Strangman G, Boas DA, Sutton JP. (2002a). Non-invasive neuroimaging using near-infrared light. *Biological Psychiatry*, 52:679-693.
Strangman G, Culver JP, Thompson JH, Boas DA. (2002b). A quantitative comparison of simultaneous BOLD fMRI and NIRS recordings during functional brain activation. *NeuroImage*, 17:719-731.
Strangman G, Franchescini MA, Boas D. (2003). Factors affecting the accuracy of near-infrared spectroscopy concentration calculations for focal changes in oxygenation parameters. *NeuroImage*, 18:865-879.
Taga G, Homae F, Watanabe H. (2007). Effects of source-detector distance of near infrared spectroscopy on the measurement of the cortical hemodynamic response in infants. *NeuroImage*, 38:452-460.
Tak S, Ye JC. (2014). Statistical analysis of fNIRS data: A comprehensive review. *NeuroImage*, 85:72-91.
Takahashi CD, Nemet D, Rose-Gottron CM, Larson JK, Cooper DM, Reinkensmeyer DJ. (2003). Neuromotor noise limits motor performance, but not motor adaptation, in children. *Journal of Neurophysiology*, 90:703-711.
Toda T, Taoka M. (2004). Converging patterns of inputs from oral structures in the postcentral somatosensory cortex of conscious macaque monkeys, *Experimental Brain Research*, 158:43-49.
Toga AW, Thompson PM, Sowell ER. (2006). Mapping brain maturation. *TRENDS in Neurosciences*, 29:148-159.
Toma S, Nakajima Y. (1995). Response characteristics of cutaneous mechanoreceptors to vibratory stimuli in human glabrous hand. *Neuroscience Letters*, 195:61-63.
Thomas JE, Lambert EH. (1960). Ulnar nerve conduction velocity and H-reflex in infants and children. *Journal of Applied Physiology*, 15:1-9.
Thomason ME, Burrows BE, Gabrieli JDE, Glover GH. (2005). Breath holding reveals differences in fMRI BOLD signal in children and adults. *NeuroImage*, 25:824-837.
Thompson JK, Peterson MR, Freeman RD. (2003). Single-neuron activity and tissue oxygenation in the cerebral cortex. *Science*, 299:1070-1072.
Thompson RA, Nelson CA. (2001). Developmental science and the media. Early brain development. *American Psychologist*, 56:5-15.

Toronov V, Webb A, Choi JH, Wolf M, Michalos A, Gratton E, Hueber D. (2001). Investigation of human brain hemodynamics by simultaneous near-infrared spectroscopy and functional magnetic resonance imaging. *Medical Physics*, 28:521.
Trulsson M, Essick GK. (1997). Low-threshold mechanoreceptive afferents in the human lingual nerve. *Journal of Neurophysiology*, 77:737-748.
Trulsson M, Essick GK. (2004). "Mechanosensation," in Miles TS, Nauntofte B, Svensson P (eds) *Clinical Oral Physiology*. Quintessence Books: Copenhagen.
Trulsson M, Johansson RS. Orofacial mechanoreceptors in humans: encoding characteristics and responses during natural orofacial behaviors. *Behavioral Brain Research*, 135:27-33.
Ulanovsky N, Las L, Nelken I. (2003). Processing of low-probability sounds by cortical neurons. *Nature Neuroscience*, 6:391-398.
Ulanovsky N, Las L, Farkas D, Nelken I. (2004). Multiple time scales of adaptation in auditory cortex neurons. *Journal of Neuroscience*, 24:10440-10453.
Vallbo ÅB, Johansson RS. (1984). Properties of cutaneous mechanoreceptors in the human hand related to touch sensation. *Human Neurobiology*, 3:3-14.
Vallbo ÅB, Wessberg J. (1998). Functions of human muscle spindles in hand muscles as analysed with microneurography. *Current Science*, 75:464-469.
Van Cutsem M, Feiereisen P, Duchateau J, Hainaut K. (1997). Mechanical properties and behaviour of motor units in the tibialis anterior during voluntary contractions. *Canadian Journal of Applied Physiology*, 22:585-597.
van Essen DC, Lewis JC, Drury HA, Hadjikhani N, Tootell RB, Bakircioglu M, Miller MI. (2001). Mapping visual cortex in monkeys and human using surface-based atlases. *Vision Research*, 41:1359-1378.
Venkatesan L, Barlow SM, Popescu M, Popescu A, Auer ET. (2010). TAC-Cell inputs to human hand and lip induce short-term adaptation of the primary somatosensory cortex. *Brain Research*, 1348:63-70.
Venkatesan L, Popescu M, Popescu A, Barlow SM. (2014). Integrated approach for studying adaptation mechanisms in the human somatosensory cortical network. *Experimental Brain Research*, in press.
Villringer A. (1997). Understanding functional neuroimaging methods based on neurovascular coupling. *Advances in Experimental Medicine and Biology*, 413:177-193.
Villringer A, Dirnagl U. (1995). Coupling of brain activity and cerebral blood flow: Basis of functional neuroimaging. *Cerebrovascular and Brain Metabolism Reviews*, 7:240-276.
Villringer A, Planck J, Hock C, Schleinkofer L, Dirnagl U. (1993). Near infrared spectroscopy (NIRS): a new tool to study hemodynamic changes during activation of brain function in human adults. *Neuroscience Letters*, 154:101-104.
Voss H. (1956). Zahl und Anordung der Muskelspindeln in den oberen Zungenbein-muskeln, im M. trapezius and M. latissimus dorsi. *Anals of Anatomy*, 103:443-446.
Walsh B, Smith A. (2002). Articulatory movements in adolescents: Evidence for protracted development of speech motor control processes. *Journal of Speech, Language, and Hearing Research*, 45:1119-1133.

Walsh B, Smith A, Weber-Fox C. (2006). Short-term plasticity in children's speech motor systems. *Developmental Psychobiology*, 48:660-674.

Wang X, Merzenich MM, Sameshima K, Jenkins WM. (1995). Remodeling of hand representation in adult cortex determined by timing of tactile stimulation. *Nature*, 378:71-75.

Wartenburger I, Steinbrink J, Telkemeyer S, Friedrich M, Obrig H. (2007). The processing of prosody: evident of interhemispheric specialization at the age of four. *NeuroImage*, 34:416-425.

Watanabe E, Yamashita Y, Maki A, Ito Y, Koizumi H. (1996). Non-invasive functional mapping with multi-channel near infra-red spectroscopy topography in humans. *Neuroscience Letters*, 205**:**41-44.

Webber RM, Stanley GB. (2006). Transient and steady-state dynamics of cortical adaptation. *Journal of Neurophysiology*, 95:2923-2932.

Webster MA. (2012). Evolving concepts of sensory adaptation. *F100 Reports Biology*, 4:21.

White LE, Andrews TJ, Hulette C, Richards A, Groelle M, Paydarfar J, Purves D. (1998). Structure of the human sensorimotor system. I: Morphology and cytoarchitecture of the central sulcus. *Cerebral Cortex*, 7:18-30.

Wilson DA. (1998). Synaptic correlates of odor habituation in the rat anterior piriform cortex. *Journal of Neurophysiology*, 80:998-1001.

Yakovlev PI, Lecours AR. (1967). "The myelogenetic cycles of regional maturation of the brain", in Minkowski A (ed) *Regional Development of the Brain in Early Life*. Blackwell Scientific: Oxford.

Yamashita Y, Maki A, Koizumi H. (2001). Depth dependence of the precision of noninvasive optical measurement of oxy-, deoxy-, and total-hemoglobin concentration. *Medical Physics*, 28:1108-1114.

Yan JH, Thomas JR, Stelmach GE, Thomas KT. (2000). Developmental features of rapid aiming arm movements across the lifespan. *Journal of Motor Behavior*, 32:121-140.

Young PA, Young PH, Tolbert DL. (2008). *Basic Clinical Neuroscience*. 2nd edition. Lippincott Williams & Williams: Baltimore.

Zaidi Q, Ennis R, Cao D, Lee B. (2012). Neural locus of color afterimages. *Current Biology*, 22:220-224.

Zhu H, Fan Y, Guo H, Huang D, He S. (2014). Reduced interhemispheric functional connectivity of children with autism spectrum disorder: evidence from functional near infrared spectroscopy studies. *Biomedical Optics Express*, 5:1262-1274.

APPENDIX A

Center for Brain, Biology and Behavior

MRI Safety Screening Form

For CB3 MRI Facility Technologist Use Only:

Date of MRI: _____ Appointment Time: _____ SKYRA ID: _____

Research Project Title: _____

Participant Name_____ **Date**_____

(Please print)

Date of Birth: _____ Height: _____ Weight: _____ □ Male □ Female

Please indicate if you have any of the following:

□ Yes	□ No	Have you ever worked with metal?
□ Yes	□ No	Have you ever had metal in your eyes?
□ Yes	□ No	Breathing problems or motion disorder
□ Yes	□ No	Claustrophobia or PTSD
□ Yes	□ No	Any surgery in the last 6 weeks

The following items can interfere with MR imaging and some can be hazardous to your safety.

□ Yes	□ No	Cardiac pacemaker
□ Yes	□ No	Implanted cardioverter defibrillator (ICD)
□ Yes	□ No	Aneurysm clip(s)
□ Yes	□ No	Metallic embolization coils
□ Yes	□ No	Metallic stent or filter for blood clots
□ Yes	□ No	Electronic implant or device
□ Yes	□ No	Magnetically-activated implant or device
□ Yes	□ No	Neurostimulator system or TENS unit or wires
□ Yes	□ No	Spinal cord or brain stimulator
□ Yes	□ No	Internal electrode or wires
□ Yes	□ No	Bone growth stimulator
□ Yes	□ No	Cochlear, otologic, or other ear implant
□ Yes	□ No	Insulin or other infusion pump
□ Yes	□ No	Implanted drug infusion devise
□ Yes	□ No	Heart valve prosthesis
□ Yes	□ No	Any type of prosthesis or artificial device (eye, etc.)
□ Yes	□ No	Artificial or prosthetic limb
□ Yes	□ No	Eyelid spring or wire
□ Yes	□ No	Shunt (spinal or brain-intraventricular)
□ Yes	□ No	Vascular access port and/or catheter or feeding tube
□ Yes	□ No	Swan-Ganz or thermodilution catheter
□ Yes	□ No	Radiation seeds or implants
□ Yes	□ No	Medication patch (Nicotine, Nitroglycerine, etc)
□ Yes	□ No	Wire mesh implant
□ Yes	□ No	Tissue expander (e.g., breast)
□ Yes	□ No	Surgical staples, clips, metallic sutures
□ Yes	□ No	Joint replacement (hip, knee, etc)
□ Yes	□ No	Bone/joint pin, screw, nail, wire, plate, etc
□ Yes	□ No	Any metallic fragment or foreign body

NCB3 Nebraska Lincoln
Center for Brain, Biology and Behavior

☐ Yes	☐ No	Any shrapnel, gun shot or BB gun wounds
☐ Yes	☐ No	Dentures or partial plates
☐ Yes	☐ No	Tattoo or permanent make-up → *(May heat up during MRI scan)*
☐ Yes	☐ No	Body piercing or jewelry → *(Must be removed before entering)*
☐ Yes	☐ No	Hearing aid → *(Must be removed before entering)*
☐ Yes	☐ No	Colored contact lenses → *(Must be removed before entering)*
☐ Yes	☐ No	Hair extensions → *(May heat up during MRI scan)*

For Women

☐Yes	☐ No	Is there a possibility you may be pregnant? Date of last period________________
☐Yes	☐ No	IUD, diaphragm, or pessary

For Men

☐Yes	☐ No	Any type of penile prosthesis or implant

Participant Signature/Date: ______________________________

Parent or Legal Guardian Name: ______________________ **Relationship to Participant:**____________
(Please print)

Parent or Legal Guardian Signature/Date:_________________________

MRI Technologist Signature/Date: __________________________

****

Date of Return________________ ☐ No Changes ☐ Changes Indicated Above

Participant Signature/Date: ______________________________

Parent or Legal Guardian Name: ______________________Relationship to Participant:____________
(Please print)

Parent or Legal Guardian Signature/Date: __________________________

MRI Technologist Signature/Date:__________________________

****

Date of Return________________ ☐ No Changes ☐ Changes Indicated Above

Participant Signature/Date: ______________________________

Parent or Legal Guardian Name: ______________________Relationship to Participant:____________
(Please print)

Parent or Legal Guardian Signature/Date: __________________________

MRI Technologist Signature/Date: __________________________

****

Date of Return________________ ☐ No Changes ☐ Changes Indicated Above

Participant Signature/Date: ______________________________

Parent or Legal Guardian Name: ______________________Relationship to Participant:____________
(Please print)

Parent or Legal Guardian Signature/Date: __________________________

MRI Technologist Signature/Date: __________________________

APPENDIX B

Galileo™ code to run stimulus sequence:

```
<Series>
  <Date>6/4/2014 01:39:07 PM</Date>
  <File>D:\BARLOW\GALILEO\ FACE A_ODER fNIRS v2.xml</File>
  <Description>FACE fNIRS</Description>
  <Continuous>False</Continuous>
  <Runs>10</Runs>
  <Sequence Num="1">
    <On>True</On>
    <Runs>60</Runs>
    <CycleTime>500</CycleTime>
    <Description>All 50ms</Description>
    <Channel Num="1">
      <OnTime>0</OnTime>
      <OffTime>0</OffTime>
    </Channel>
    <Channel Num="2">
      <OnTime>0</OnTime>
      <OffTime>0</OffTime>
    </Channel>
    <Channel Num="3">
      <OnTime>0</OnTime>
      <OffTime>0</OffTime>
    </Channel>
    <Channel Num="4">
      <OnTime>10</OnTime>
      <OffTime>60</OffTime>
    </Channel>
    <Channel Num="5">
      <OnTime>10</OnTime>
      <OffTime>60</OffTime>
    </Channel>
    <Channel Num="6">
      <OnTime>10</OnTime>
      <OffTime>60</OffTime>
    </Channel>
    <Channel Num="7">
      <OnTime>0</OnTime>
      <OffTime>0</OffTime>
    </Channel>
    <Channel Num="8">
      <OnTime>0</OnTime>
```

```
      <OffTime>0</OffTime>
    </Channel>
  </Sequence>
  <Sequence Num="2">
    <On>True</On>
    <Runs>1</Runs>
    <CycleTime>30000</CycleTime>
    <Description>All 50ms</Description>
    <Channel Num="1">
      <OnTime>0</OnTime>
      <OffTime>0</OffTime>
    </Channel>
    <Channel Num="2">
      <OnTime>0</OnTime>
      <OffTime>0</OffTime>
    </Channel>
    <Channel Num="3">
      <OnTime>0</OnTime>
      <OffTime>0</OffTime>
    </Channel>
    <Channel Num="4">
      <OnTime>0</OnTime>
      <OffTime>0</OffTime>
    </Channel>
    <Channel Num="5">
      <OnTime>0</OnTime>
      <OffTime>0</OffTime>
    </Channel>
    <Channel Num="6">
      <OnTime>0</OnTime>
      <OffTime>0</OffTime>
    </Channel>
    <Channel Num="7">
      <OnTime>0</OnTime>
      <OffTime>0</OffTime>
    </Channel>
    <Channel Num="8">
      <OnTime>0</OnTime>
      <OffTime>0</OffTime>
    </Channel>
  </Sequence>
</Series>
```

APPENDIX C

Image reconstruction/co-registration in Mango:

1. Launch Mango application.
2. Open > Open Image> Use drop down menu to locate image file of interest > Open.
3. Viewer will appear with brain slices in 3 orientations (coronal, sagittal, transverse).

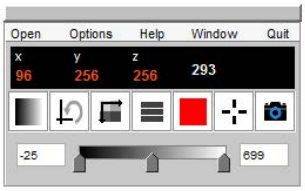

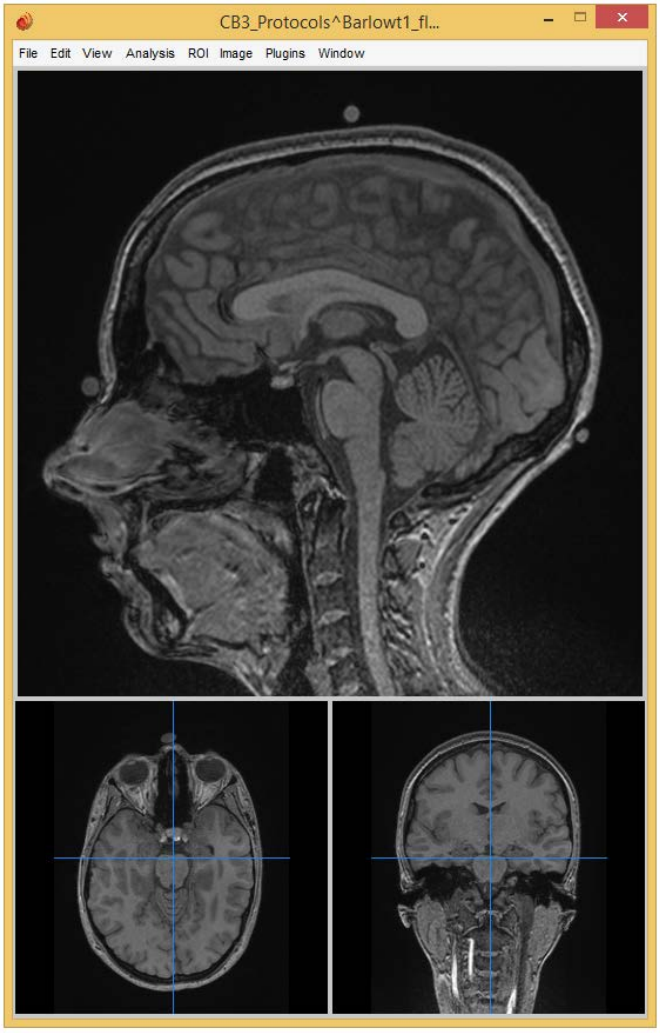

4. Scroll through sagittal view using left/right arrow buttons until you see the 2 short separation Vitamin E capsules.

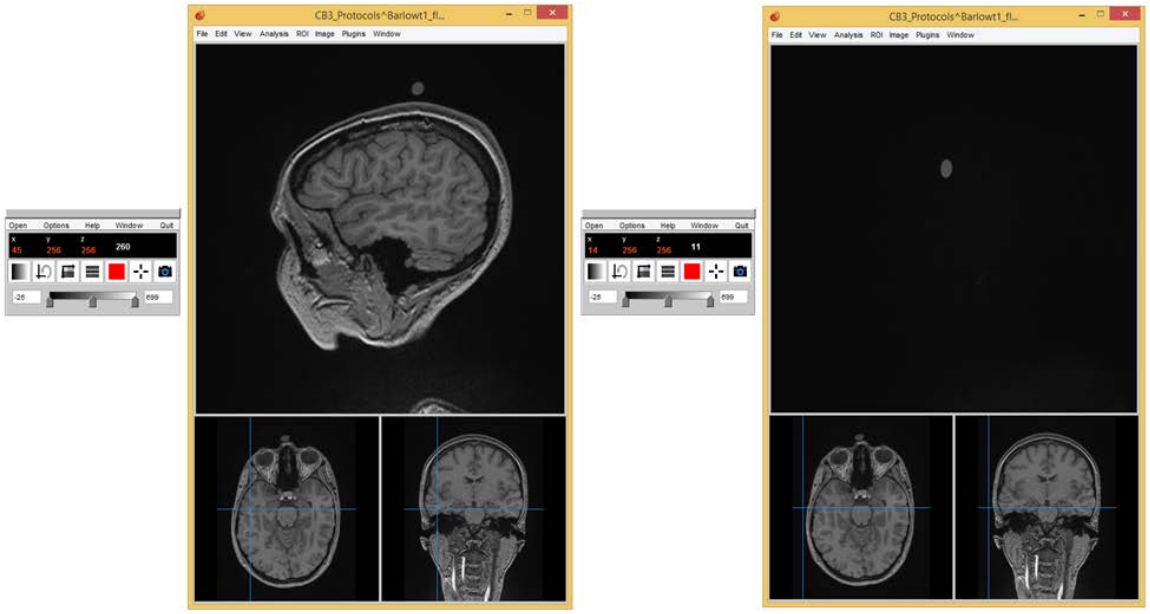

5. Place “points of interest” at the center of each capsule by using SHIFT + left click.

    - To access “points”, click on the crosshair icon in the Toolbox window > click on the square icon in the dropdown list > click on “Add Points” in the dropdown list.
    - If you need to delete a point, navigate to where point is seen in one of the slices, then right click on the point > select Delete.

6. Once both points are placed, do brain extraction by going to Plugins > Extract Brain (BET) > Run.

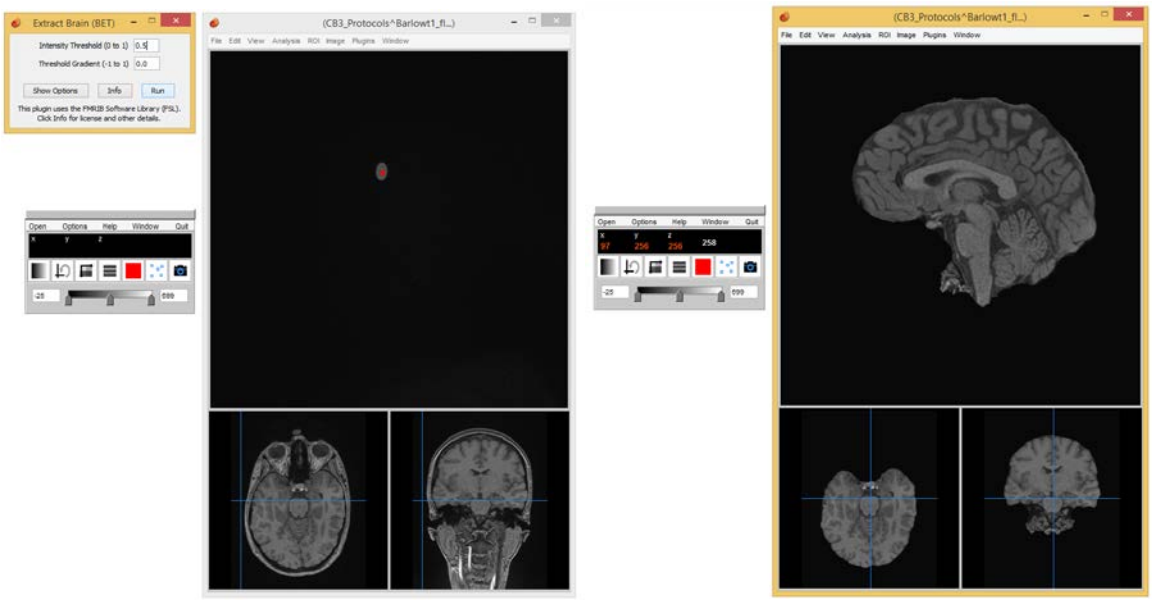

7. Once brain is extracted (see above image on right), go to Image > Build Surface > OK (leave threshold settings for first rendering; if surface rendering is too pixelated or is not clear, try lowering threshold and re-run surface build).

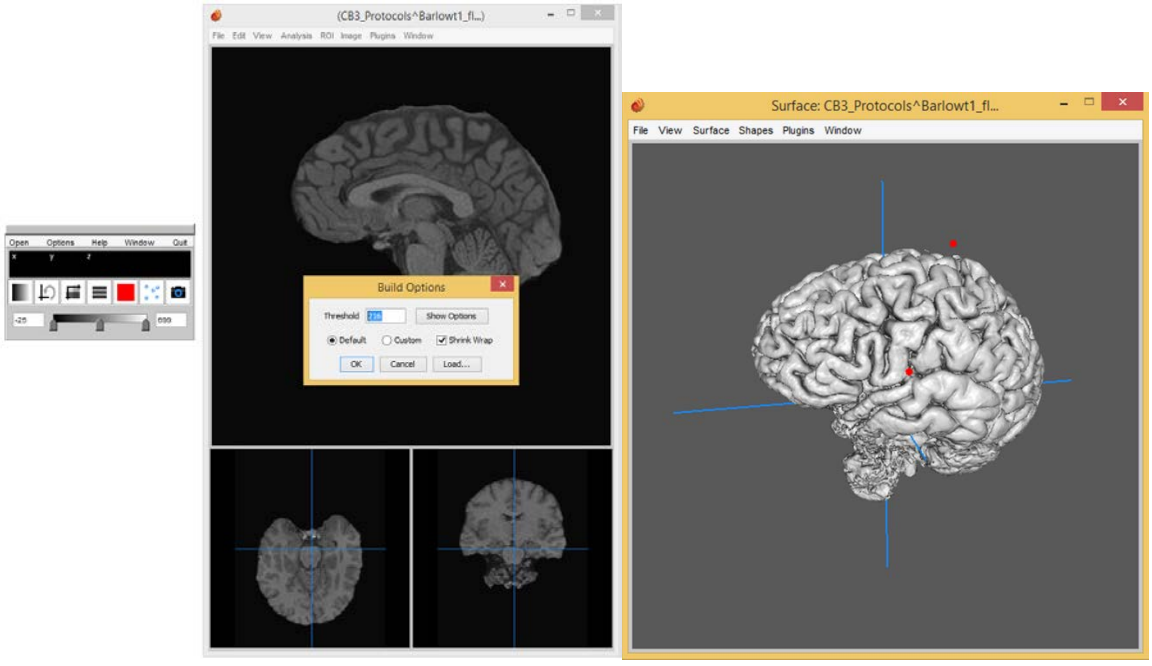

8. Check 3D surface rendering to see if two dots line up along the central sulcus.

    - It can help to draw a line connecting the dots by going to Shapes > Point 1 > Line to > Point 2. Rotate 3D image by left clicking with mouse and dragging to see multiple angles.

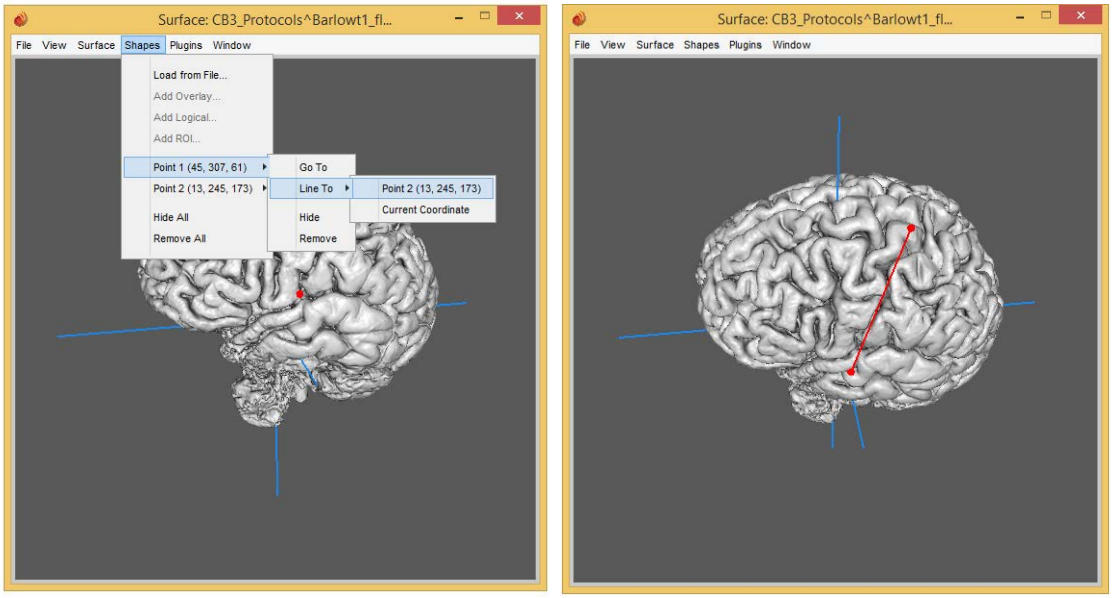

9. If Vitamin-E capsules were not placed approximately on the central sulcus, use 3D rendering to guide placement of new capsules (be sure to mark new locations on the scalp with dry erase marker), and repeat the MRI scan/Mango procedures.

APPENDIX D

Custom MATLAB code to identify peak values in force data:

```
% first download peakfinder.m file from: http://www.mathworks.com/
matlabcentral/fileexchange/25500-peakfinder/content/peakfinder.m

% add file path with peakfinder.m file and all motor data *.mat files
% load hand and face data, examples:
load hand_data_1
load face_data_1

% determine if the hand/face data was first or second motor task by:
figure(); plot (data);

% if first pick the time:
hand_data_1_use = data(1:400000);
face_data_1_use = data(1:400000);
% if second pick the time:
hand_data_1_use = data(400000:end);
face_data_1_use = data(400000:end);

% use peakfinder function on the selected dataset in the format
% (your_data_name, selection, threshold)
%    selection - The amount above surrounding data for a peak to be,
%        identified (default = (max(x0)-min(x0))/4). Larger values mean
%        the algorithm is more selective in finding peaks.
%     threshold - A threshold value which peaks must be larger than to
%     be maxima or smaller than to be minima.
% example for hand:
[peakLoc peakMag] = peakfinder(hand_data_1_use, 1, 5);
% example for face:
[peakLoc peakMag] = peakfinder(face_data_1_use, 0.005, 0.005);

% open peakMag in the Workspace to copy and paste peak values into separate
% spreadsheet (in Excel)

% verify peak values by plotting selected data:
figure(); plot(hand_data_1_use);
```